Tube feet dynamics drive adaptation in sea star locomotion

Dissertation originale pour l'obtention du grade académique de Docteur en Sciences
Dirigée par
Prof. Sylvain GABRIELE et Prof. Patrick FLAMMANG
Année Académique 2025-2026

Amandine DERIDOUX

SYMBIOSE Lab
&
Biology of Marine Organisms and Biomimetics

Thèse soutenue le 17 octobre 2025 devant le jury composé de:

Prof. Mathieu SURIN	Université de Mons, Belgique – President
Prof. Elise HENNEBERT	Université de Mons, Belgique – Secretary
Prof. Romana SANTOS	Universidade de Lisboa, Portugal
Prof. Philippe DUBOIS	Université Libre de Bruxelles, Belgique
Prof. Sylvain GABRIELE	Université de Mons, Belgique - Promoter
Prof. Patrick FLAMMANG	Université de Mons, Belgique - Co-promoter

Amandine DERIDOUX
SYMBIOSE Lab,
Département de Chimie,
Université de Mons,
20, Place du Parc B-7000 Mons (Belgique).
Octobre 2025
Email: Amandine.DERIDOUX@umons.ac.be

Ce travail de recherche a bénéficié du support financier du Fond pour la Formation et la Recherche dans l'Industrie et dans l'Agriculture (FRIA).

ABSTRACT

Sea stars use hundreds of tube feet on their oral surface to crawl, climb, and navigate complex environments, all without the coordination of a central brain. While the morphology of tube feet and their role as muscular hydrostats are well described, the dynamics underlying their locomotion remain poorly understood.

To investigate these dynamics, we employed an optical imaging method based on frustrated total internal reflection to visualize and quantify tube foot adhesion in real-time across individuals of *Asterias rubens* and *Marthasterias glacialis* spanning a wide size range. Our results reveal an inverse relationship between crawling speed and the duration of tube foot contact with the substrate. This suggests that sea stars regulate locomotion by modulating their "foot-substrate" interaction time in response to body load. To test this, we conducted perturbation experiments on *A. rubens* using 3D-printed backpacks that increased body mass by 25% and 50%, along with numerical simulations based on a mechanistic model incorporating decentralized feedback control of the tube feet. The added load significantly increased adhesion time, supporting the role of a load-dependent mechanical adaptation. We further investigated inverted locomotion, both experimentally and through simulation, and found that tube feet adjust their contact behavior when the animal is oriented upside

down relative to gravity.

Together, our findings demonstrate that sea stars adapt their locomotion to changing mechanical demands by modulating tube foot-substrate interactions, revealing a robust, decentralized strategy for navigating diverse and challenging terrains.

REMERCIEMENTS

Tout d'abord, je tiens à adresser un immense merci à Sylvain Gabriele, mon promoteur tout au long de cette thèse, pour m'avoir offert cette magnifique opportunité mais également pour son engagement sans faille pendant plus de quatre années. Depuis la genèse de ce projet, qui s'éloignait de ton domaine de prédilection, lors de ma première année de Master jusqu'à son aboutissement, tu as toujours cru en moi, même dans les moments où je doutais de moi-même. Tu n'as jamais remis en question ma capacité à mener ce projet à bien et tu m'as constamment encouragée à donner le meilleur de moi-même. Malgré ton emploi du temps très chargé, la porte de ton bureau était toujours ouverte quand j'arrivais paniquée car je pensais aller droit dans le mur. Il est évident que je ne suis jamais allée dans ce mur.

Je souhaite ensuite remercier mon co-promoteur de thèse, Patrick Flammang, qui m'a également accompagnée tout au long de ces quatre années. Merci pour votre investissement dans ce projet et pour vos précieux conseils, qui en ont sans cesse amélioré la qualité. Je vous suis particulièrement reconnaissante d'avoir enrichi ce travail par sa dimension biologique, grâce à votre expertise sur les étoiles de mer.

J'aimerais également remercier mes rapporteurs, Romana Santos et Philippe Dubois, ainsi que les autres membres du jury, Mathieu Surin et Élise Hennebert, d'avoir accepté d'évaluer mon travail et pour le temps précieux qu'ils ont consacré à sa lecture et à son évaluation.

Je remercie chaleureusement Renaud Hébert et Denis Tirmarche pour leur accueil au sein du département d'Aquariologie de Nausicaá. Je garde un excellent souvenir de ce séjour parmi vous et je suis reconnaissante pour votre disponibilité et votre aide dans la réalisation de mes mesures sur vos étoiles de mer.

Je remercie Eva Kanso et son ancien doctorant Sina Heydary, nos collaborateurs pour la partie théorique de ce travail. Ils ont développé la théorie présentée dans cette thèse ; leur travail et leurs idées ont été déterminants pour en compléter la portée.

Je remercie Martial et Vladimir, véritables experts de la TFM, pour leur aide précieuse dans la mise en place du dispositif sur l'étoile de mer. Un grand merci à toi, Vladimir, pour ta patience et ton aide dans l'utilisation du programme. Merci aussi à toi, Martial : ta passion pour la « belle science » est une vraie source d'inspiration. J'espère que nous aurons encore l'occasion de filmer des escargots en montagne.

Travailler à l'interface de deux laboratoires m'a permis de rencontrer et de côtoyer de nombreuses personnes. Je remercie tout d'abord l'ensemble des membres de la Team Biomar. Merci à Antoine B. pour ton aide dans le bon fonctionnement du laboratoire et, surtout, pour le maintien des aquariums. Merci également à Guillaume, Jérôme, Alexia, Noé, Émilie, Antoine F., Youri, Lisa, Estelle, Killian, Wendy, Némo et Leandro. Merci pour tous vos conseils et pour les bons moments.

Je tiens ensuite à remercier l'ensemble des membres des équipes InFluX et Symbiose, anciens comme nouveaux : sans vous, cette thèse n'aurait absolument pas eu la même saveur. J'ai eu l'immense joie d'évoluer dans un environnement si agréable, et cela grâce aux personnes qui le composent. Vous avez

été des collègues formidables, toujours présents et attentifs. Je chéris tous les moments que nous avons partagés, de La Rochelle jusqu'aux bords du canal. Vous êtes devenus au fil des années bien plus que de simples collègues.

Merci à Pascal de m'avoir accueillie au sein d'InFluX et pour toutes nos discussions qui m'ont accompagnées tout au long de mon parcours. Merci à Serge pour ton aide précieuse lorsqu'il s'agissait de matériel, mais aussi pour ton enthousiasme et tous les instants de rire partagés au laboratoire. Merci à Marie pour ta bienveillance légendaire, et à Marine, femme forte et inspirante. Votre détermination et énergie ont été pour moi une véritable source de motivation. Merci aussi à Yohalie, qui m'accompagne depuis la première année de bachelier. C'est une immense joie de te voir évoluer et t'épanouir comme tu le fais aujourd'hui. Enfin, merci à Lucie et Zoé, toujours présentes pour discuter, rire.

Que seraient les journées au laboratoire sans les « Zinzins », alias la bande de Klettes ? Merci à Guillaume et Quentin T. d'avoir été pendant si longtemps de super voisins de bureaux. Merci à Roxane et Mary de toujours avoir été là dans les moments où cela comptait vraiment. Enfin, merci à Rémi et Marco, les "petits" nouveaux. Merci pour votre soutien, vos fous rires, les notes dans le carnet, les verres en terrasse après de longues journées, etc... Je ne sais pas comment j'aurais géré ma fin de thèse sans vous. Vous avez tous rendu ce parcours tellement précieux.

Je souhaite également remercier les Calciters, Benjamin, Lia (et Coco). Merci d'être les si belles personnes que vous êtes, et merci d'avoir toujours été présents pour veiller sur notre petit Calcifer lorsque nous étions en déplacement.

Un grand merci aussi à la Bande à Pierrot : David, Pierre, Quentin C., Nathan et Clara. Merci d'avoir été présents et d'avoir contribué à tant de moments de joie, de rires et de partage (autour d'un bon burger de la Taverne). Merci de m'avoir accompagnée durant ces dernières années et d'avoir rendu le quotidien plus léger (sauf durant les parties de Galérapagos).

Je remercie également Darla et Louise. Il y a des amitiés qui ressemblent à des phares dans la nuit : toujours là, qu'il fasse beau ou que les tempêtes se lèvent. Pour moi, vous êtes de celles-là. Depuis le secondaire jusqu'à nos premiers vrais emplois d'adultes, vous avez été et êtes toujours présentes.

Je remercie également ma famille et ma belle-famille pour leur soutien permanent. Papa, maman, un immense merci pour tout ce que vous m'avez apporté, sans vous, je ne serais pas là aujourd'hui. Je suis profondément reconnaissante pour tout ce que vous avez fait au fil des années. Vous m'avez toujours encouragée dans chacun de mes projets et nouveaux défis. Votre soutien sans faille m'a permis d'accomplir tant de choses.

Enfin, je remercie mon fiancé Louis, qui est à mes côtés depuis presque six ans. Merci pour ton soutien sans limite. Tu m'as accompagnée dans les moments de joie comme dans les moments de fragilité. Tu m'as encouragée lorsque j'avais envie de baisser les bras et tu as toujours écouté mes plaintes avec beaucoup de patience lorsque les choses se compliquaient. Je ne pourrais imaginer ce parcours sans toi, et je suis infiniment reconnaissante d'avoir ton amour et ta présence à mes côtés.

LIST OF ABBREVIATIONS

2D	Two-dimensional
3D	Three-dimensional
ABS	Acrylonitrile butadiene styrene
AC1	Type 1 adhesive cell
AC2	Type 2 adhesive cell
AE	Adhesive epidermis
C	Cilia
CI	Circularity index
CL	Connective tissue radial lamellae
CT	Connective tissue
CTL	Connective tissue layer
CU	Cuticle
D	Disc
DA	Displacement advantage
DAC	De-adhesive cell
Di	Diaphragm
DP	Distal pad
E	Epidermis
FC	Fuzzy coat

Fi	Fibrocyte
FPS	Frame per second
FTIR	Frustrated total internal reflection
HF	Homogeneous film
JC	Juxtaligamental cell
K	Knob
L	Water-vascular lumen
LN	Longitudinal nerve
M	Mesothelium
MA	Mechanical advantage
MG	Mucus gland
Mw	Meshwork
My	Myocyte
NE	Non-adhesive epidermis
NP	Nerve plexus
P	Peritoneocyte
PC	Polycarbonate
PDMS	Polydimethylsiloxane
PLA	Polylactic acid
PMMA	Polymethyl methacrylate
Po	Pore
PP	Polypropylene
RPM	Rotation per minute
S	Stem
SC	Secretory cell
Se	Sensory cell
Sfp1	Sea Star Footprint protein 1
Su	Support cell
TFM	Traction force microscopy
TIR	Total internal reflection
TP	Terminal plate

TABLE OF CONTENTS

CHAPTER 1

INTRODUCTION

1.1 From echinoderms to sea stars

Echinoderms (phylum Echinodermata) are exclusively marine invertebrate organisms. They occupy a wide range of diverse benthic habitats, spanning from intertidal to deep-sea environments [1]. The first fossils trace date back to the Cambrian period, a geological period extending from approximately 541 to 485 million years ago [2]. The organisms that are part of this phylum are grouped into five classes: sea urchins (Echinoidea), sea cucumbers (Holothuroidea), crinoids (Crinoidea), brittle stars and basket stars (Ophiuroidea), and sea stars (Asteroidea) (Fig. 1.1).

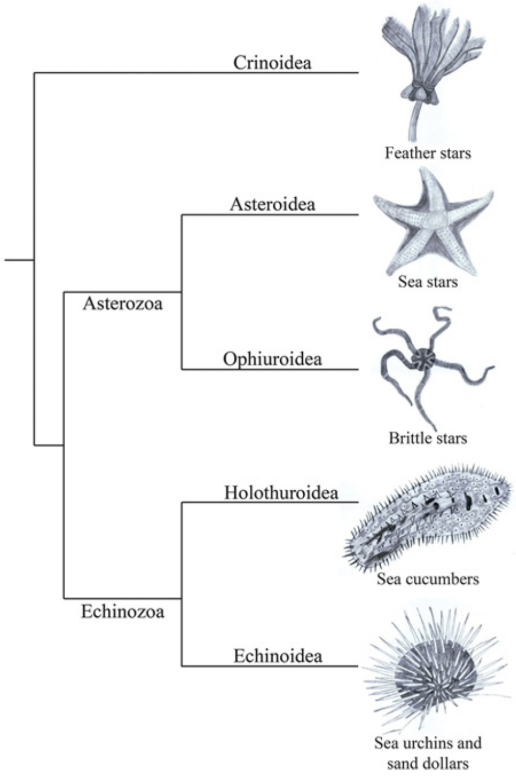

Figure 1.1: *Phylogenetic relationships among the five extant classes of echinoderms. Adapted from [1].*

The phylum Echinodermata groups together invertebrates with morphological similarities. Adult echinoderms have an ambulacral system with external tube feet and a calcareous endoskeleton consisting of ossicles connected by a meshwork of collagen fibers [3]. Adult echinoderms are also recognized by their pentaradial symmetry, which is a central symmetry of order five [4]. In sea stars, this characteristic is not always true, as some species possess more than five arms. For example, the species *Luidia ciliaris* possesses seven arms, indicating that it exhibits heptaradial symmetry. One consistent feature is their radial symmetry, with body parts arranged around a central axis [5]. Here, we will go into further details about sea star morphology and locomotion in the following sections and the following chapter, respectively.

1.2 The Asteroidea in focus

Sea stars (Asteroidea) constitute a large and iconic group of echinoderms. The scientific term Asteroidea, meaning "star-shaped", was introduced in 1830 by Henri Marie Ducrotay de Blainville, a French zoologist, to designate this group [6]. There are currently approximately 1,500 species of sea stars (Fig. 1.2) distributed throughout the world's oceans and seas. They exhibit a remarkable ability to adapt to a variety of habitats, from intertidal zones to great abyssal depths sometimes exceeding 6,000 meters [7].

Figure 1.2: *Diversity of sea stars in the marine ecosystem.*

During this thesis, two species of sea stars were studied:

- *Asterias rubens* as a model species;
- *Marthasterias glacialis* as a confirmation species for our locomotion experiments.

Previous studies have compared these two species, focusing on the adhesive secretions of their tube feet, as well as their morphology and mechanical properties [8, 9]. These aspects will be discussed in detail later in this thesis chapter. Both of these species exhibit the classical pentaradial symmetry of Asteroidea and share similar external morphologies, making them suitable for comparison in functional and ecological studies. Generally, *Asterias rubens* has a mean diameter from 10 to 30 cm, while *Marthasterias glacialis* is a bit larger with a mean diameter ranging from 25 to 30 cm.

	Asterias rubens	*Marthasterias glacialis*
Mean diameter	10 cm - 30 cm	25 - 30 cm
Larger specimen	Up to 52 cm in diameter	Up to 70 cm in diameter
Global distribution	Throughout the northeast Atlantic, from Arctic Norway, along Atlantic coasts to Senegal	From northern Norway to the Mediterranean and West Africa
Habitat	Upon a variety of substrata that include coarse and shelly gravel and rock	From sheltered muddy sites to wave-exposed rock
Depth range	Intertidal to depths of 650 m	Intertidal to depths of 200m
Morphology		

Table 1.1: *Comparative table between Asterias rubens [10] and Marthasterias glacialis [11].*

Both species are distributed throughout the Northeast Atlantic, and their habitats overlap considerably in the coastal region. The overlapping geographic distribution, habitat types, and similar ecological roles as benthic predators make these two species excellent candidates for comparative studies (Table 1.1).

While living in a wide range of marine habitats, sea stars are osmoconformers, meaning their internal salinity mirrors that of the external environment. Their inability to actively regulate internal electrolyte concentrations renders them incapable of surviving in freshwater, where osmotic imbalance becomes rapidly fatal. To maintain osmotic equilibrium, sea stars rely on the accumulation of compatible organic osmolytes (Fig. 1.3) [12] to adjust cellular osmolality, while intracellular ion concentrations remain relatively stable [13].

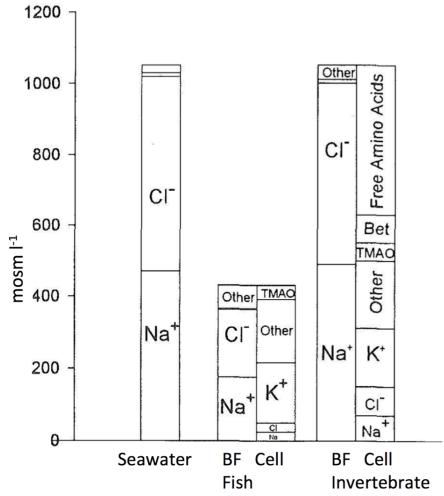

Figure 1.3: *Composition of osmotically active substances in seawater, osmoregulating fish, and osmoconforming invertebrates. BF = body fluid. Adapted from [12].*

Sea stars are distinguished by a wide variety of sizes, shapes, and colors (Fig. 1.2). Most species have five arms radiating from a central disc, but some may have a different number, either due to species variation or abnormal development [7]. Despite this morphological variability, they share a relatively conserved internal organization (Fig. 1.4). Their main anatomical features

include a calcareous endoskeleton, a digestive system, a nervous and sensory system, a reproductive system, and an ambulacral system. This thesis will primarily explore the locomotion of sea stars, focusing on the mechanics of their tube feet and the nervous system that controls them [14]. In the following, we will thus first describe the nervous system, then the ambulacral system, and the morphology and functions of the tube feet.

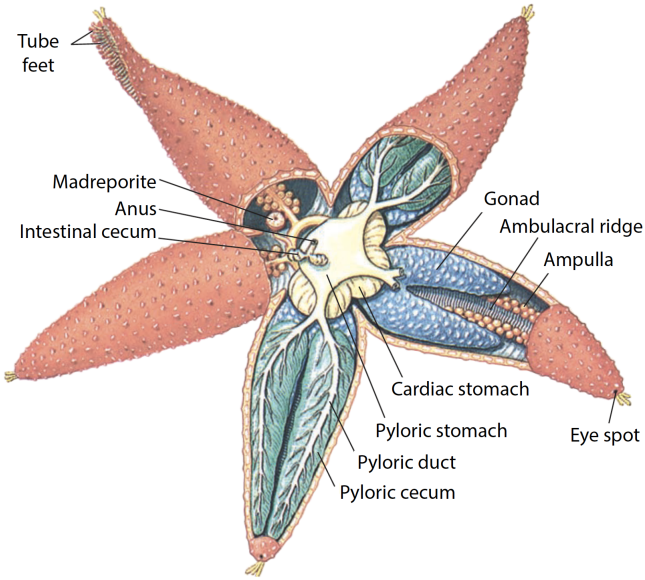

Figure 1.4: *Internal organization of partially dissected sea star. Adapted from [5].*

1.2.1 The nervous system in sea stars

Unlike many other animals, sea stars lack a central brain to process information and coordinate their actions. However, despite this absence, they possess a remarkably complex nervous system that controls hundreds of hydraulically powered tube feet to navigate their environment [15]. Their nervous system comprises a nerve ring encircling the mouth and five radial nerve cords, one extending into each arm (Fig. 1.5). These cords run along the ambulacral regions and are positioned parallel to the radial canals, coordinating both sensory input and motor output [16, 17, 18]. The peripheral nervous system consists of two distinct networks: a sensory system located below the epidermis and a motor

system within the wall of the coelomic cavity[1], interconnected by neurons that traverse the dermis [16]. Marginal and interradial nerves branch laterally at each tube feet. This morphology is revealed by immunolabeling the nervous system with antibodies against α-acetylated tubulin (AcTub) (Fig. 1.5) [19].

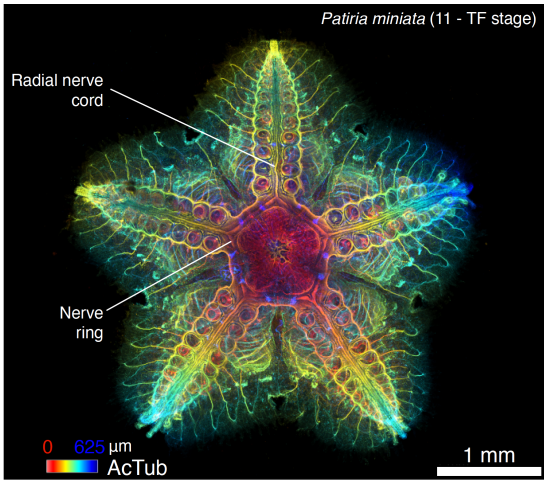

Figure 1.5: *Visualization of the nervous system in a juvenile Patiria miniata at the 11-tube feet (TF) stage, labeling of α-acetylated tubulin. Pseudo-color coloration indicates optical depth, ranging from surface (red) to deeper planes (blue), up to 625 µm thick. Scale bar = 1 mm. Adapted from [19].*

In addition, sea stars are capable of sensing light through photoreceptor cells grouped into ocelli, located at the tips of their arms, forming what are known as eye spots [16]. These structures enable them to orient themselves and move in a directed manner in response to visual cues, such as the presence of a coral reef, to ensure they do not stray from their natural habitat, despite their low-resolution vision [20]. Although sea stars lack a central brain, they remain responsive to a variety of environmental stimuli, including touch, light, temperature, gravity, and the physical and chemical properties of the surrounding water. This sensitivity is largely mediated by their tube feet, which can detect both tactile stimuli and chemical substances, allowing sea stars to perceive odors, through the presence of cilia on their adhesive pad [21] (c.f.

[1] A fluid-filled body cavity found in many animals, located between the body wall and the digestive tract.

Section1.3.2). Sea stars possess specialized tube feet at the tips of their arms, known as terminal tube feet, which are often longer and more flexible than other tube feet. These structures serve various functions, including sensing the environment (Fig. 1.6) [22].

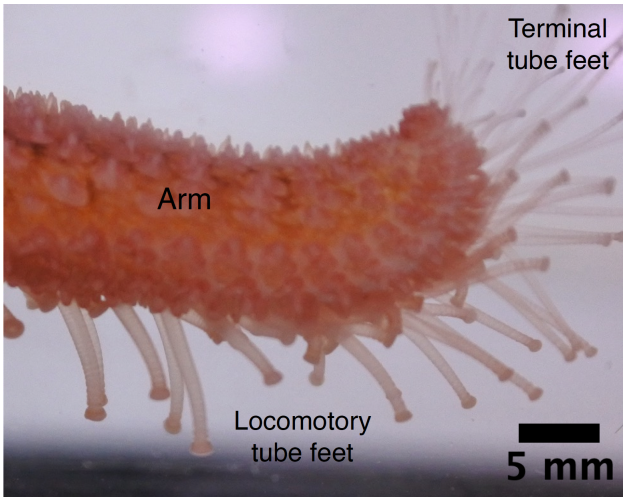

Figure 1.6: *Photography showing terminal tube feet of Asterias rubens.*

1.2.2 The ambulacral system in sea stars

The tube feet, also called podia, are the external appendages of the ambulacral system, a hydraulic structure specific to echinoderms (Fig. 1.7). This system plays a central role in various physiological functions such as locomotion, substrate adhesion, food particle manipulation, and gas exchange [7]. The ambulacral system in sea stars consists of a network of canals filled with a fluid that closely resembles seawater but is characterized by a higher potassium concentration, increased osmolarity, the presence of coelomocytes, and trace amounts of proteins. This fluid generates the hydrostatic pressure required for the operation of tube feet [23, 24, 25].

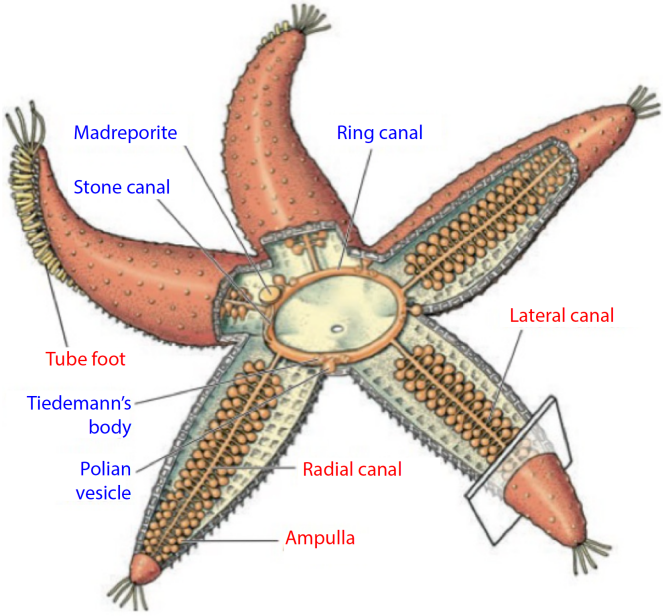

Figure 1.7: *Schematic representation of the sea star ambulacral system. The central parts are highlighted in blue and the peripheral parts in red. Adapted from [5].*

The hydrostatic pressure required for the proper functioning of the ambulacral system (slightly above the surrounding seawater pressure) is provided by a slight difference in ionic concentration between the ambulacral fluid and the surrounding seawater, thus promoting continuous water diffusion through the tissues thanks to osmosis. The ambulacral system is divided into two main parts: the central and the peripheral parts (Fig. 1.7). The central part consists of several key components, including the madreporite, which helps regulate internal pressure as the animal experiences variations in depth. This plate is connected to the ring canal by the stone canal. Then it is followed by the peripheral parts. It is made of five radial canals that branch off this ring, extending along each arm of the sea star. These canals give rise to numerous lateral canals, each opening into an individual tube foot, generally associated with a contractile ampulla [26]. Depending on the size and the species, there are hundreds to thousands of tube feet in the ambulacral groove of the sea stars. The arrangement of the tube feet also varies among sea star families. In *Asterias rubens*, four rows of tube feet are typically observed, arranged along

the oral surface of each arm within the ambulacral groove [27] (Fig. 1.8A). In contrast, *Luidia ciliaris* exhibits two rows of tube feet on the oral surface (Fig. 1.8B).

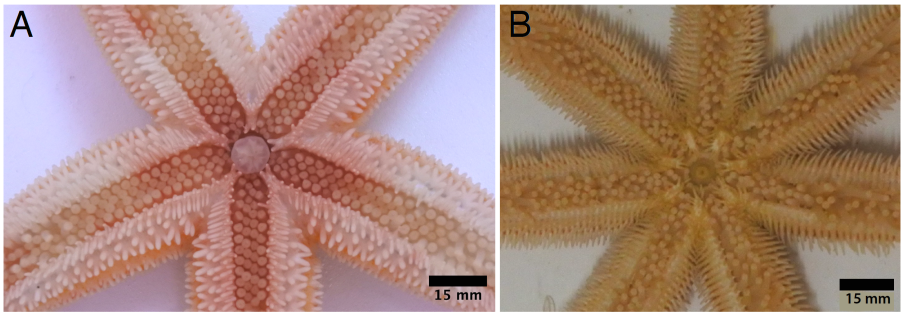

Figure 1.8: *Photography showing the ambulacral groove of two sea star species: (A) Asterias rubens and (B) Luidia ciliaris.*

Additionally, there are two types of accessory structures on the ring canal (Fig. 1.7):

- **the Polian Vesicles**: are muscular sacs presumed to serve primarily as low-pressure reservoirs for fluid within the ambulacral system [28]. They are not present in all asteroids [29].
- **the Tiedemann's body**: may play a role in the formation of coelomocytes and are always found in asteroids [28, 30, 31].

1.3 Structure and role of tube feet

Many activities and adaptations of sea stars in their natural habitats are correlated with their interactions with substrates, including the sea bottom. All these activities rely on specialized organs, the tube feet, which are involved in nearly all actions sea stars perform, including locomotion, righting, foraging, and food manipulation. The coordinated movement of tube feet imparts direction, purpose, and rhythm to these behaviors. When the tube feet coordination is incomplete or absent, actions may be delayed, imprecise, or entirely fail [32].

Although the general structure of a tube foot appears relatively simple, consisting of a flexible stem terminating in a disc, it is a highly specialized organ. Tube feet perform diverse functions, and this functional diversity is often reflected in variations in their morphology. Based on the organization of their constituent tissues, tube feet can be classified into three main morphological categories: knob-ending (Fig. 1.9A and D), simple disc- ending (Fig. 1.9B and E), and reinforced disc- ending tube feet (Fig. 1.9C and F) [24, 26].

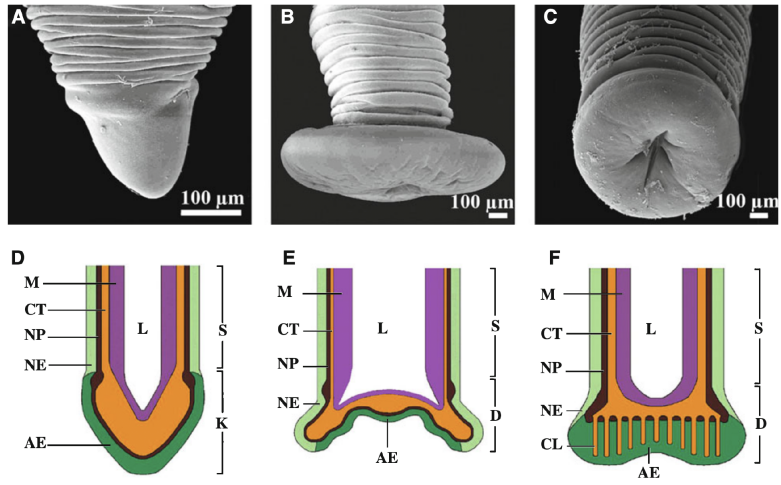

Figure 1.9: *External morphology and histological organization of the three tube feet morphotypes described in sea stars. (A–C) Scanning electron microscopy views of a knob-ending tube foot (Astropecten irregularis, A), of a simple disc-ending tube foot (Mithrodia clavigera, B) and a reinforced disc-ending tube foot (Asterias rubens, C). (D, E) Schematic drawings of a knob-ending tube foot (D), of a simple disc-ending tube foot (E), and a reinforced disc-ending tube foot (F). Abbreviations: AE, adhesive epidermis; CL, connective tissue radial lamellae; CT, connective tissue; D, disc; K, knob; L, water-vascular lumen; M, mesothelium; NE, non-adhesive epidermis; NP, nerve plexus; S, stem. Images adapted from [24, 26].*

1.3.1 The stem functions and mechanical properties

As illustrated in the figure 1.9, the three tube feet morphotypes present a comparable histological organisation [26]. The wall of the stem is made up of four main tissue layers (Fig. 1.10), from the outside to the inside:

- **An external epidermis**, covered with a thin cuticle, a glycocalyx composed of glycoproteins and proteoglycans;
- **An underlying nerve plexus**;
- **A connective tissue**, subdivided into two layers, external and internal, characterized by a different orientation of the collagen fibers, longitudinal in the external layer and helical in the internal layer [32]. The external layer also contains neurosecretory cells, called juxtaligamentous cells, rich in granules and organized around a microfibrillar network surrounding the collagen fibers. The connective tissue layer can undergo rapid changes in its passive mechanical properties under nervous control via these juxtaligamental cells. The connective tissue layer exhibits the ability to transition between a flexible state, which facilitates extension and retraction, and a rigid state, which ensures positional stability [9, 33]. Its mechanical properties are modulated by Ca^{2+}, and K^{+} [34];
- **An internal myomesothelium**, which constitutes the retractor muscle and lines the ambulacral lumen [24, 26, 35].

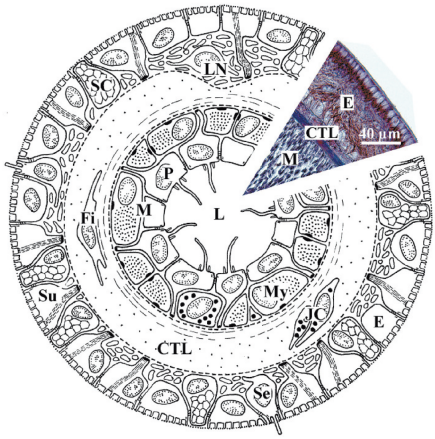

Figure 1.10: *Schematic representation of a transverse section through a typical stem of asteroid disc-ending tube foot. The inset is a light micrograph of a histological section through the stem wall in the sea star Asterias rubens. Abbreviations: CTL, connective tissue layer; E, epidermis; Fi, fibrocyte; JC, juxtaligamental cell; L, ambulacral lumen; LN, longitudinal nerve; M, mesothelium; My, myocyte; P, peritoneocyte; SC, secretory cell; Se, sensory cell; Su, support cell. Adapted from [25].*

The tube feet stem plays a dual role in sea star locomotion by integrating both movement, using its retractor muscle, and tension-bearing capacities, with the combined action of the connective tissue layer and the juxtaligamental cell [9, 25]. Structurally, it is a hollow, extensible cylinder capable of considerable flexibility and mobility, allowing dynamic interaction with the substrate. Internally, the retractor muscle is responsible for contractile movements, facilitating extension, retraction, and flexion of the stem [32, 36].

Regarding locomotion, the stem enables movement through a process driven by the ambulacral system [32]. When internal pressure increases, typically around 48–62kPa for *Asterias rubens*, due to the contraction of ampulla muscles [9, 37], the tube foot can elongate up to 200% of its original length [8, 24]. Then it makes contact with the substrate and adheres temporarily to it. The antagonistic action of the retractor muscle and ampulla muscle bends the tube foot. After detachment, muscle contraction shortens the stem, forcing the fluid back into the ampulla [36, 38] (Fig. 1.11).

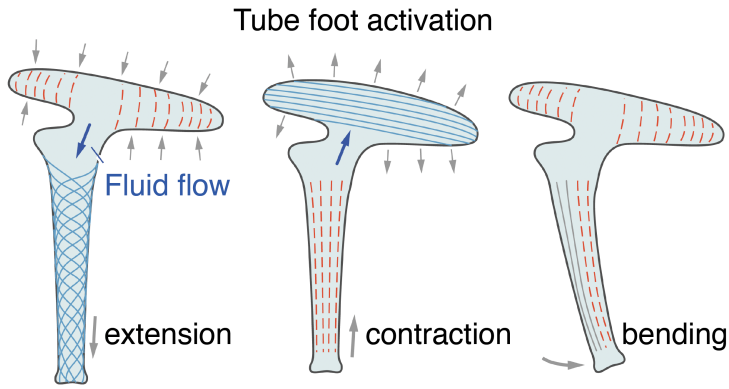

Figure 1.11: *Schematic explaining how the antagonistic action of tube foot stem and ampulla muscles lead to contraction, extension, and bending of the tube feet. Adapted from [38].*

To characterize the mechanical properties of the stem, tensile testing was performed, and different parameters were measured (Fig. 1.12A) [9]:

- **the extensibility**: the ability to stretch without breaking
- **the strength**: the resistance to failure by permanent deformation
- **the elasticity**: the ability to return to its original form after being subjected to a force
- **the toughness**: the ability to absorb energy and plastically deform without fracturing. Toughness refers to the amount of energy a material can absorb per cubic meter before it fractures. Here, true stress is defined as the applied force divided by the instantaneous cross-sectional area, while true strain is the natural logarithm of the ratio of the instantaneous length to the original length.

$$\text{Toughness} = \int \text{True stress} \times d(\text{ True strain }) \tag{1.1}$$

The stem of sea star tube feet exhibits mechanical properties characteristic of a shock-absorbing material, notably displaying a non-linear stress-strain response (Fig. 1.12A). In this case, the curve represents true stress (Pa) versus true strain (dimensionless), which provides a more accurate description of material behavior under large deformations. This approach avoids underestimating stress and overestimating strain in materials that experience significant stretching [9].

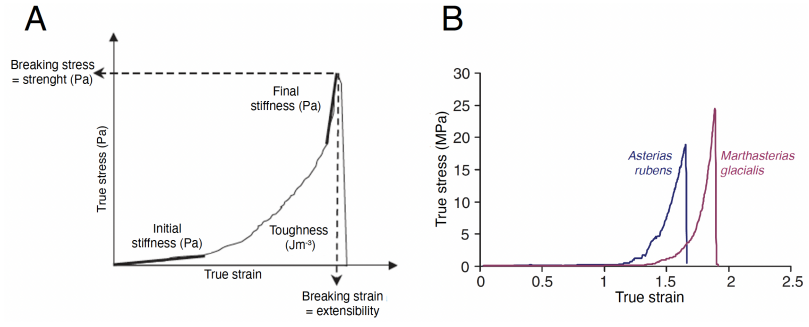

Figure 1.12: *(A) Typical non-linear "J-shaped" stress–strain curves. (B) Stress–strain curves obtained for the tube feet of Asterias rubens and Marthasterias glacialis in artificial seawater. Adapted from [9].*

Initially, stress increases gradually with increasing strain, indicating low initial stiffness. Beyond a certain threshold, however, stress rises sharply, reflecting a rapid stiffening of the material before failure occurs at a high final stiffness. This curve is typical of biological tissues designed to endure deformation while retaining resilience (Fig. 1.12A). This behavior is supported by the stem's flexible and elastic structural organization, which enables the tube foot to recover its shape after mechanical stress. Here, *Asterias rubens* tube feet exhibit lower strength of 20.71±12.79 MPa but break sooner (strain ≈ 1.6) while *Marthasterias glacialis* tube feet have higher strength of 23.06±6.28 MPa and are more extensible (strain ≈ 2.0) (Fig. 1.12B). There is no significant difference between the two species [9]. Such elasticity is crucial for withstanding repeated compressive and tensile forces encountered in dynamic marine environments. Furthermore, the stem's ability to distribute loads and maintain stable attachment to substrates contributes significantly to the animal's overall structural stability [9]. These features collectively serve to minimize the impact of external forces, such as wave-induced hydrodynamic stresses, thereby protecting the organism and enabling effective locomotion and adhesion under challenging environmental conditions.

1.3.2 The disc functions and mechanical properties

In *A. rubens*, tube feet have the morphotype called reinforced disc-ending tube feet. Here, the disc is composed of a thick adhesive epidermal layer overlying a connective tissue layer. From this underlying layer, fine connective tissue branches extend and intercalate between the epidermal cells (Fig. 1.13). In its reinforced form, the disc exhibits well-developed supportive structures composed of connective tissue, along with a distinct differentiation of the musculature [21].

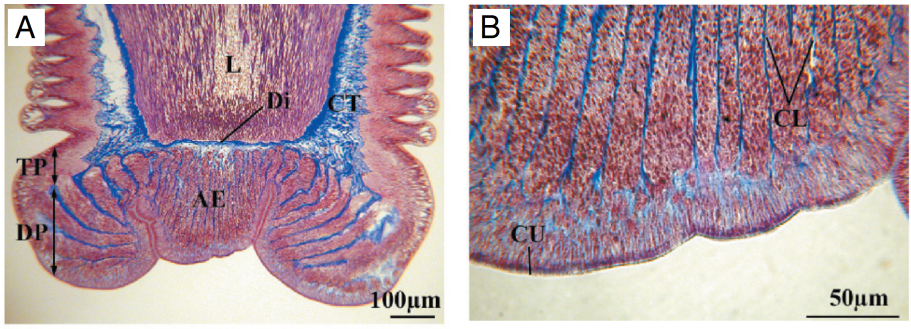

Figure 1.13: *Longitudinal histological section through the disc of the tube foot of the asteroid Asterias rubens. (A, B) The section goes through the margin of the disc to show the connective tissue radial lamellae. Abbreviations: AE, adhesive epidermis; CL, connective tissue radial lamellae; CT, connective tissue layer; CU, cuticle; Di, diaphragm; DP, distal pad; L, lumen; TP, terminal plate. Adapted from [21].*

The tube foot disc plays a crucial role in both temporary adhesion and mechanical plasticity, enabling sea stars to efficiently adhere to and release from a variety of surfaces [25]. It mediates the adhesion with the substratum through a duo-glandular system and the presence of secretory pores (c.f. Section 1.4) [35].

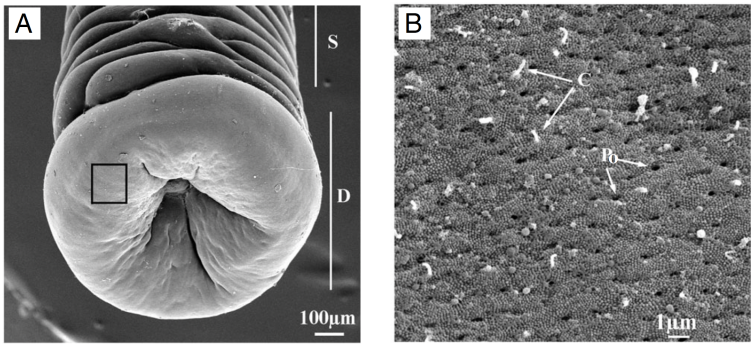

Figure 1.14: *(A, B) External morphology of non-attached tube feet of Asterias rubens. Boxed area in A is magnified in B. Abbreviations: C, cilia; D, disc; Po, pore; S, stem. Adapted from [21].*

The tube foot can also perceive different types of sensations, such as mechanical and chemical stimuli, through the presence of 1 μm-long cilia (Fig. 1.14). The identification of G-protein-coupled receptors (GPCRs), commonly

associated with olfaction, and putative olfactory receptors on the tube foot epidermis strongly suggests a chemosensory role for these organs [39]. The mechano-sensation is the transduction of mechanical stimuli into neural signals [21]. In sea stars, cilia are presumably involved in substratum sensing [35].

The adhesive pad in *A. rubens* is made of a very soft material with an elastic modulus around 6 kPa. The tube foot adhesive pad behaves like a viscoelastic material [21]. It is elastically deformed under rapidly applied forces and behaves viscously under slowly acting forces [21]. Surface irregularities can induce microscopic shape changes of the tube foot depending on their amplitude. The adhesive secretion fills surface irregularities in the nanometer range, thereby enhancing its adhesive tenacity (Fig. 1.15).

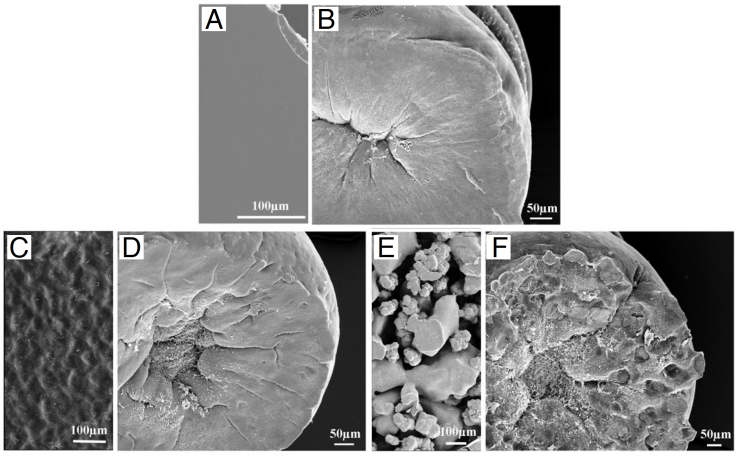

Figure 1.15: *Scanning electron microscopy images of the surface of smooth PMMA (A), rough PMMA (C), and rough PP (E) samples and of the distal surfaces of tube foot discs from Asterias rubens attached to each of these substrata (B; D and F; respectively). Adapted from [21].*

1.4 Underwater temporary adhesion

1.4.1 Adhesion mechanism

Sea stars can remain firmly attached to their substrate, with the species *A. rubens* exhibiting a measured tenacity of 0.2 MPa [40]. This strong yet reversible attachment is enabled by a temporary adhesion mechanism, allowing sea stars to resist hydrodynamic forces and maintain their position, an essential feature for their locomotion and interaction with the environment. Tube feet attach to the substrate and then detach voluntarily and quickly, before initiating another cycle of attachment/detachment thanks to a duo-glandular system. This process relies on the action of the tube feet, whose terminal disc ensures direct contact with the surface [8].

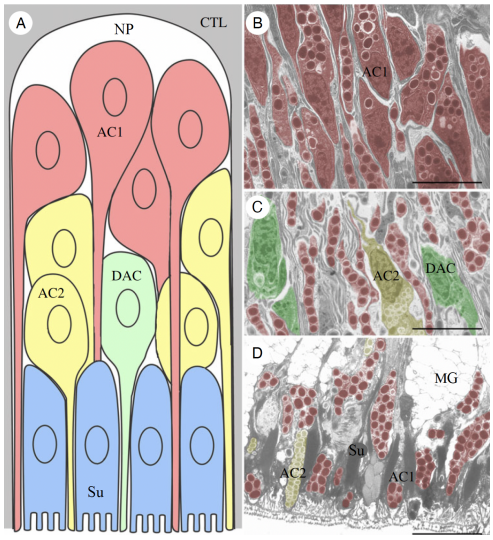

Figure 1.16: *(A) Schematic representation of a longitudinal section through a radial epidermal strip located between two adjacent connective tissue laminae. The distal surface of the tube foot is at the bottom of the drawing. (B-D) Transmission electron microscopy images taken at the same magnification and showing different areas of the adhesive epidermis corresponding to the areas illustrated in the drawing. Secretory cells are false colored according to the schematic representation. (B) Proximal part showing cell bodies of AC1. (C) Middle part showing cell bodies of AC2 and DAC. (D) Distal part showing support cells and the apical processes of duo-gland cells (AC1, AC2 and DAC). Abbreviations: AC1, type 1 adhesive cell; AC2, type 2 adhesive cell; CTL, connective tissue layer; DAC, de-adhesive cell; MG, mucus gland; NP, nerve plexus; Su, support cell. Adapted from [41].*

This disc is held against the substrate by adhesive secretions produced by a specialized epidermis (Fig. 1.16). During adhesion, the tensions generated within the epidermis are transferred to the connective tissue plate, which relays them to the connective tissue of the stem. The tube foot adhesive epidermis has a stratified organization of glandular cells. They comprise four distinct cell types: support cells (Su), sensory cells (SC), two types of adhesive cells (AC1 and AC2), rich in secretory granules, and (DAC) de-adhesive cells, also filled with granules (Fig. 1.16) [8].

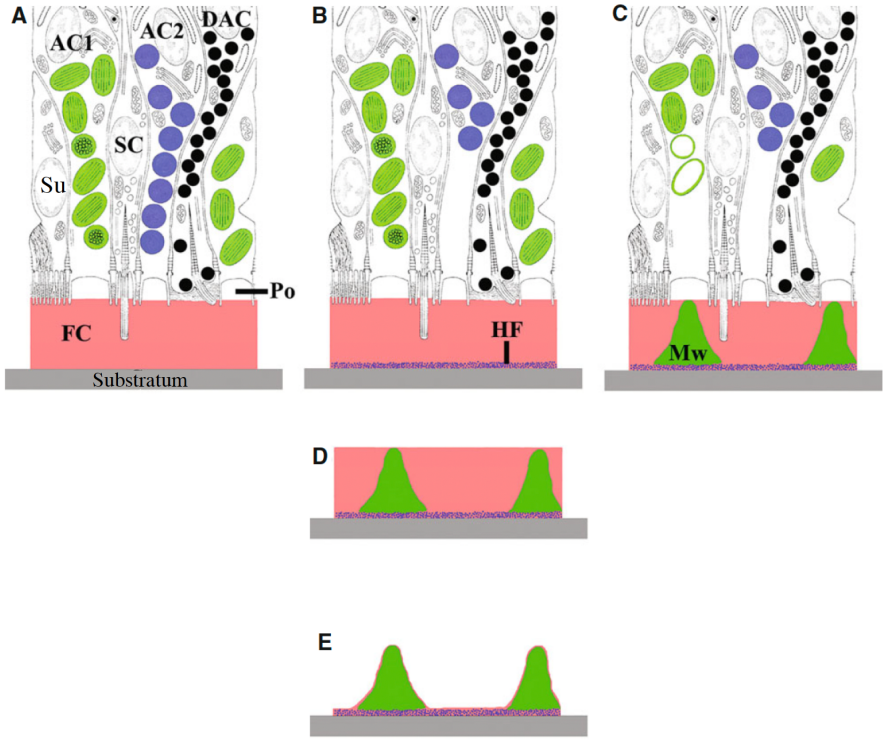

Figure 1.17: *Schematic representation for the formation of the adhesive material microstructure in the footprints of Asterias rubens. Diagrammatic representations (not to scale) of longitudinal sections through the disc epidermis of a tube foot illustrating the proposed successive steps in the secretion (A–C), deposition (D), and drying (E) of a footprint. Adapted from [42].*

All of these cells participate in a coordinated manner in the reversible adhesion of the tube feet to the substrate. The adhesion process consists of two main phases: anchoring (or attachment) and detachment. The attachment phase, shown in Figure 1.17, involves a sequence of simple, coordinated steps. First, the distal part of the terminal disc makes contact with the surface, adapting to its topography (Fig. 1.17A). Sensory cells detect the substratum, triggering the controlled release of adhesive substances through the nerve plexus [8]. Two types of adhesive cells are involved: AC2 cells secrete a uniform adhesive film (HF) (Fig. 1.17B), while AC1 cells produce a mesh-like reinforcement (Mw) (Fig. 1.17C) [25]. Detachment occurs through the action of de-adhesive cells (DAC), which release substances that disrupt the adhesive interface (Fig. 1.17D) [26].

1.4.2 Composition of tube foot adhesive

The reversible adhesion of sea star tube feet leaves characteristic footprints on the substrate (Fig. 1.18), illustrating the temporary yet effective nature of the mechanism. The adhesive material secreted by the tube feet of sea stars is a complex, multifunctional substance composed of various proteins and carbohydrates that act synergistically to enable strong and reversible adhesion to surfaces [42].

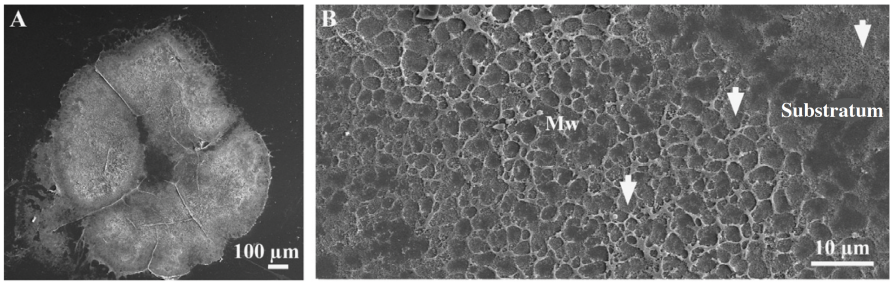

Figure 1.18: *Scanning electron microscopy photographs of a footprint deposited by a tube foot of Asterias rubens on pieces of glass. (A) Low magnification view of a complete footprint. (B) Views of footprint thin areas where the adhesive material forms a meshwork (Mw) deposited on a thin homogeneous film. The arrows indicate the thin homogeneous film covering the substratum. Adapted from [42].*

In terms of dry weight (Fig. 1.19) [43], the footprints are primarily composed of proteins (20.6%) and carbohydrates (8%). A significant inorganic fraction (approximately 40%) was also detected [26]. This fraction is made of sulfate SO_4^{2-} and seawater ionic components such as Na^+, Ca^{2+}, Mg^{2+}, K^+ and Cl^-. A minor lipid component (5.6%) has also been detected. However, lipids were not detected in secretory granules of adhesive cells, suggesting that they might come from membranes of these granules or result from contamination by epidermal cell membranes of the tube feet [43]. However, lipids could also play a functional role by maximizing adhesion in aquatic environments when secreted before the adhesive material, as observed in barnacle larvae [44]. The composition of the adhesive material secreted by *A. rubens* tube feet was extensively investigated.

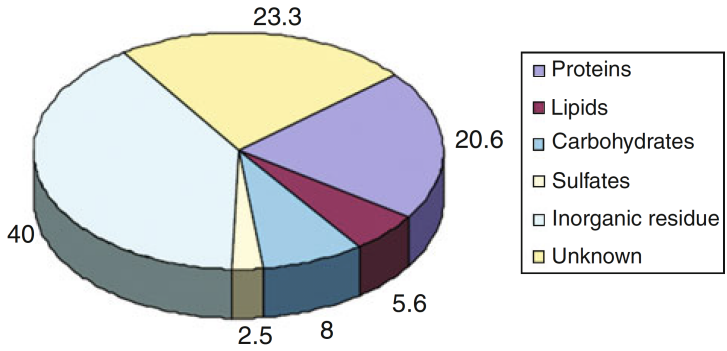

Figure 1.19: *Diagram illustrating the biochemical composition of the footprint material of Asterias rubens. Values are expressed as percentages of dry mass. The unknown fraction reflects the incomplete recovery when all fractions are added and can be explained by losses or incomplete hydrolysis in the chemical analyses. Images from [43].*

Proteins, also called sea star footprint proteins (Sfps), constitute a major component of the adhesive. Sixteen distinct Sfps have been identified in the sea star *A. rubens* and are involved in temporary underwater adhesion [41]. One key protein, the Sea star footprint protein 1 (Sfp1), is a large protein composed of 3,853 amino acids, with a calculated molecular weight of 426 kDa [45]. Sfp1 is organized into four subunits (α, β, γ, and δ) that display specific protein-, carbohydrate-, and metal-binding domains. It is stabilized by intermolecular disulfide bridges, which enhance the cohesion of the adhesive matrix. Sfp proteins interact with the substrate through electrostatic and polar

interactions involving the side chains of amino acids. Such interactions are essential not only for the cohesive properties of the adhesive but also for its ability to anchor effectively to surfaces.

In addition to proteins, the adhesive contains substantial carbohydrate components, including glycoproteins and sialylated proteoglycans. The glycan chains in these molecules mediate polar and hydrogen-bonding interactions through functional groups such as hydroxyls, carboxylates, and amines. Sulfate groups, potentially linked to either protein or carbohydrate residues, may further modulate the adhesive's properties and functionality [46].

Concerning the de-adhesive secretion, the ultrastructural and immunocytochemical data suggest that it might function enzymatically to leave the fuzzy coat, thereby allowing the tube foot to detach [8, 43]. A protease named Astacin-like Sfp has been identified, which is exclusively expressed in the de-adhesive cells [41].

Overall, the specific biochemical composition and the organized structural integration of proteins, carbohydrates, and lipids provide the tube feet with an effective adhesion mechanism, particularly suited for the challenges of attachment and detachment in marine environments.

BIBLIOGRAPHY

[1] A. REICH *et al.* Phylogenomic Analyses of Echinodermata Support the Sister Groups of Asterozoa and Echinozoa, *PLOS ONE* **10**, e0119627, 2015.

[2] E. SWEET. Fossil Groups: Modern forms: Asteroids: Extant Orders of the Asteroidea, *University of Bristol*, 2005.

[3] G.A. WRAY. Echinodermata. Spiny-skinned animals: sea urchins, starfish, and their allies, *Tree of Life*, 1999.

[4] R. FOX. Invertebrate anatomy online, *Zoobotryon verticillatum*, 2001.

[5] C. P. Hickman *et al. Integrated Principles of Zoology*, 14th ed., McGraw-Hill, 2008.

[6] H. M. D. de BLAINVILLE. Zoophytes, *Dictionnaire des Sciences Naturelles etc.*, **60**, 1830.

[7] M. RAHMAN *et al.* The Sea Stars (Echinodermata: Asteroidea): Their Biology, Ecology, Evolution and Utilization, *SF Journal of Biotechnology and Biomedical Engineering* **1007**, 2018.

[8] P. FLAMMANG *et al.* The Role of Podial Secretions in Adhesion in Two Species of Sea Stars (Echinodermata), *The Biological Bulletin* **187**, 35-47, 1994.

[9] E. HENNEBERT *et al.* Evaluation of the different forces brought into play during tube foot activities in sea stars, *Journal of Experimental Biology* **213**, 1162-1174, 2010.

[10] MarLIN. *Asterias rubens.* Accédé le 6 avril 2025.https://www.marlin.ac.uk/species/detail/1194.

[11] MarLIN. *Marthasterias glacialis.* Accédé le 6 avril 2025. https://www.marlin.ac.uk/species/detail/1688.

[12] P.W. HOCHACHKA & G.N. SOMERO, Biochemical Adaptation: Mechanism and Process in Physiological Evolution, *Oxford University Press.*, 2002.

[13] L. SCHMITTMANN, Local adaptation of the common sea star *Asterias rubens* to different salinities, *Doctoral dissertation* **Christian-Albrechts-Universität Kiel**, 2017.

[14] T. PO *et al.* The directional control of phototaxis in sea stars (*Protoreaster nodosus*), *Journal of Experimental Biology* **228**, jeb249293, 2025.

[15] G.A. KERKUT, The Mechanisms of Coordination of the Starfish Tube Feet, *Behaviour* **6**, 206-232, 1954.

[16] J. E. SMITH & H. G. CANNON, On the nervous system of the starfish *Mathasterias glacialis* (L.), *Philosophical Transactions of the Royal Society of London. Series B, Biological Sciences* **227**, 111-173, 1937.

[17] J. L. S. COBB & T. R. STUBBS, The giant neurone system in ophiuroids, *Cell and Tissue Research* **226**, 675, 1982.

[18] R. D. BURKE *et al.* A genomic view of the sea urchin nervous system, *Developmental Biology* **300**, 434-460, 2006.

[19] D. N. CLARKE *et al.* See-Star: a versatile hydrogel-based protocol for clearing large, opaque and calcified marine invertebrates, *EvoDevo* **15**, 8, 2024.

[20] A. GARM & D.-E. NILSSON, Visual navigation in starfish: first evidence for the use of vision and eyes in starfish, *Proceedings of the Royal Society B: Biological Sciences* **281**, 20133011, 2014.

[21] R. SANTOS *et al.* Adhesion of echinoderm tube feet to rough surfaces, *SF Journal of Experimental Biology* **208**, 2555-2567, 2005.

[22] J.B. MCCLINTOCK *et al.* Chemotactic tube-foot responses of a spongivorous sea star *Perknaster fuscus* to organic extracts from antarctic sponges, *Journal of Chemical Ecology* **20**, 859-870, 1994.

[23] C. O. HERMANS, The duo-gland adhesive system, *Oceanography and Marine Biology* **21**, 283-339, 1983.

[24] R. SANTOS *et al.* Comparative histological and immunohistochemical study of sea star tube feet (Echinodermata, Asteroidea), *Journal of Morphology* **263**, 259-269, 2005.

[25] R. SANTOS *et al.* The echinoderm tube foot and its role in temporary underwater adhesion, *Functional surfaces in biology* Springer, 9-41, 2009.

[26] E. HENNEBERT *et al.* Adhesion Mechanisms Developed by Sea Stars: A Review of the Ultrastructure and Composition of Tube Feet and Their Secretion, *Biological Adhesive Systems: From Nature to Technical and Medical Application* Springer, 99-109, 2010.

[27] J. M. LAWRENCE, A functional biology of echinoderms, *Croom Helm. London. GB*, 1987.

[28] D. NICHOLS, Functional morphology of the water-vascular system, *Physiology of echinodermata*, Wiley Interscience, 219-244, 1966.

[29] L. CUENOT, Études morphologiques sur les Echinodermes, *Arch. Bio. (Paris)* **11**, 313-680, 1891.

[30] L. CUENOT, Anatomie, éthologie et systématique des échinodermes, *Traité de zoologie* **11**, 3-275, 1948.

[31] W. BARGMANN & B. BEHRENS, Über die Tiedemannschen organe des seesterns (*Asterias rubens* L.), *Zeitschrift für Zellforschung und Mikroskopische Anatomie* **63**, 120-133, 1964.

[32] J.E. SMITH, The mechanics and innervation of the starfish tube foot-ampulla system, *Philosophical Transactions of the Royal Society of London. Series B, Biological Sciences* **232**, 279-310, 1946.

[33] R. SANTOS, The tube feet of sea urchins and sea stars contain functionally different mutable collagenous tissues, *Journal of Experimental Biology* **208**, 2277-2288, 2005.

[34] M. BONNEEL *et al.* Chapter 36 - Mutable collagenous tissues in sea cucumbers, *The world of sea cucumbers.* **Academic Press**, 573-584, 2024.

[35] P. FLAMMANG, Adhesion in echinoderms, *Echinoderm studies* **CRC Press**, 1-60, 1996.

[36] J.E. SMITH, The Activities of the Tube Feet of *Asterias Rubens* L : I. The Mechanics of Movement and of Posture, *Journal of Cell Science* **88**, 1-14, 1947.

[37] T. PO *et al.* Gearing in a hydrostatic skeleton: the tube feet of juvenile sea stars (*Leptasterias sp.*), *Journal of Experimental Biology* **227**, jeb247804, 2024.

[38] S. HEYDARY *et al.* Sea star inspired crawling and bouncing, *Journal of The Royal Society Interface* **17**, 20190700, 2020.

[39] R.E. ROBERT *et al.* Putative chemosensory receptors are differentially expressed in the sensory organs of male and female crown-of-thorns starfish, *Acanthaster planci*, *BMC Genomics* **19**, 853, 2018.

[40] P. FLAMMANG & G. WALKER, Measurement of the Adhesion of the Podia in the Asteroid *Asterias Rubens*(Echinodermata), *Journal of the Marine Biological Association of the United Kingdom* **77**, 1251-1254, 1997.

[41] M. ALGRAIN. *et al.* In the footsteps of sea stars: deciphering the catalogue of proteins involved in underwater temporary adhesion, *Open Biology* **12**, 220103, 2022.

[42] E. HENNEBERT *et al.* Micro- and nanostructure of the adhesive material secreted by the tube feet of the sea star *Asterias rubens*, *Journal of Structural Biology* **164**, 108-118, 2008.

[43] P. FLAMMANG *et al.* A study of the temporary adhesion of the podia in the sea star *Asterias rubens* (Echinodermata, asteroidea) through their footprints, *Journal of Experimental Biology* **201**, 2383–2395, 1998.

[44] A. B. YULE & G. WALKER, Adhesion in barnacles, *Barnacle Biology* **5**, 389–402, 1987.

[45] E. HENNEBERT *et al.* Sea star tenacity mediated by a protein that fragments, then aggregates, *Proceedings of the National Academy of Sciences* **111**, 6317-6322, 2014.

[46] E. HENNEBERT *et al.* Characterisation of the Carbohydrate Fraction of the Temporary Adhesive Secreted by the Tube Feet of the Sea Star *Asterias rubens*, *Marine Biotechnology* **13**, 484-495, 2011.

CHAPTER 2

STATE OF THE ART

Sea star locomotion has long captivated the interest of researchers. Although observational records of sea stars date back to the 18^{th} century, Romanes's 1887 publication is considered the first major scientific work specifically dedicated to their locomotion [1]. In the early 20th century, more systematic investigations emerged on the locomotion of sea stars. For example, Cole's 1913 on the directionality of movement in *Asterias forbesi* provided detailed experimental insights on their locomotor and righting behavior, when the animal flips itself upright after being turned over (Fig. 2.1) [2]. For many decades, studies have primarily focused on how sea stars respond to environmental and physiological factors that influence their locomotion and behavior, often across multiple species. The next chapter of this thesis will present and discuss recent studies that have advanced our understanding of these processes.

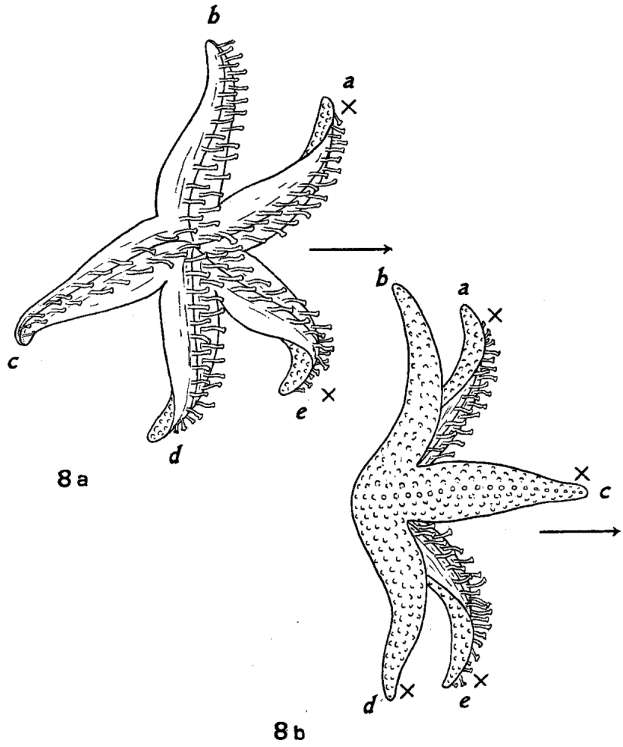

Figure 2.1: *Original schematic illustration drawn by hand showing a sea star righting itself. The arrow indicates the direction of turning. Note that all tube feet are extended in that direction. Arms attached to substratum are indicated by X. Adapted from [2].*

2.1 What factor influences sea star locomotion speed?

2.1.1 Influence of size and body shape

McMahon demonstrated that size influences the structure and function across animal species. Changes in size alter the relative impact of physical forces, which in turn shape the design of organisms [3, 4].

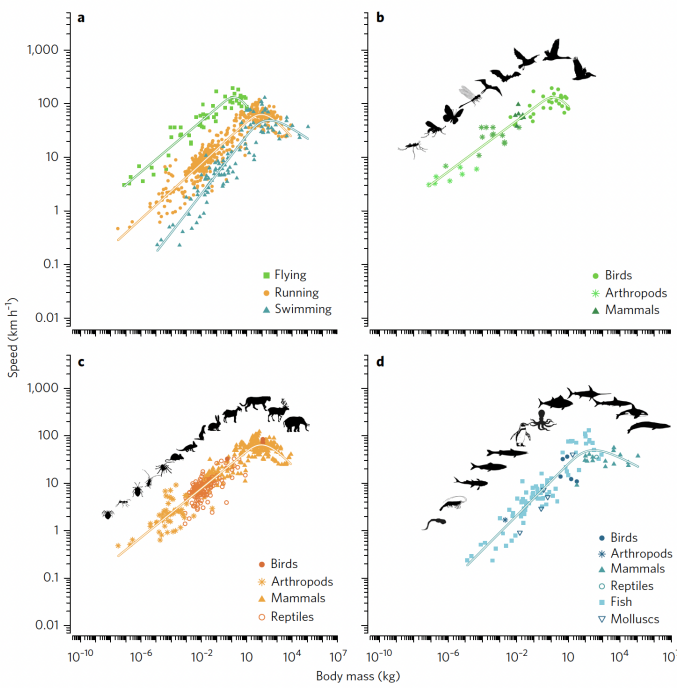

Figure 2.2: *Empirical data for the allometric scaling of maximum speed in animals. a, Comparison of scaling for the different locomotion modes (flying, running, swimming). b–d, Taxonomic differences are illustrated separately for flying (b; n = 55), running (c; n = 458) and swimming (d; n = 109) animals. Overall model fit:* $R^2 = 0.893$. *Adapted from [5].*

Similar principles have been observed for the locomotion speed. It generally scales with body size or mass (Fig. 2.2), following allometric principles like to those observed in other morphological and physiological traits [5]. In 2017, Hirt *et al.* highlighted that across all locomotion types (flying, running, swim-

ming), speed increases with body mass up to a certain point and then declines. The proposed hypothesis is that larger animals tend to be faster, except for a drop-off in speed at the largest body masses, likely reflecting biomechanical and physiological constraints, such as muscle efficiency, drag, and the cost of locomotion, which scale non-linearly with mass.

In their 2014 study, Montgomery *et al.* demonstrated that, for four Northeast Pacific sea star species, morphological traits exhibit an allometric relationship with wet mass [6]. Both arm length and disc area increase as the sea star's wet mass increases (Fig. 2.3A and C). Additionally, arm length scales positively with disc area, indicating a proportional relationship between these two morphological traits during growth (Fig. 2.3B). These data support the hypothesis that morphological traits follow predictable scaling laws but also reveal some interspecific variations.

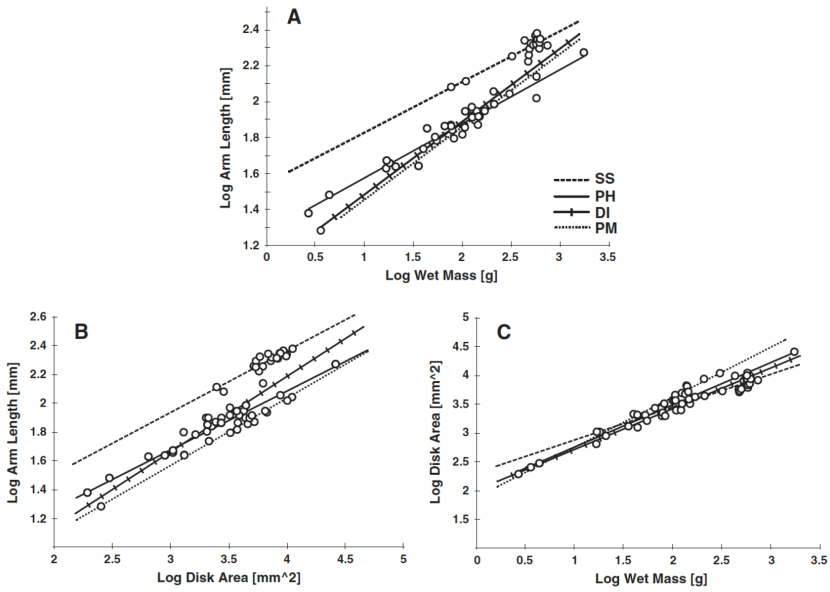

Figure 2.3: *(A–C) Scaling relations among three species of Northeast Pacific sea stars: Solaster stimpsoni (SS), Pycnopodia helianthoides (PH), Dermasterias imbricata (DI), and Patiria miniata (PM). Adapted from [6].*

However, the relationships between body size and locomotion speed appear to be less predictable and exhibit considerable inter- and intraspecific variation. Studies by Montgomery *et al.* demonstrated that in the species *Patiria miniata*, body size significantly influences crawling speed, despite intraspecific morphological variation, as some individuals possess five arms while others have six [6, 7]. In this species, both instantaneous and maximum crawling speeds, as well as size-specific crawling speed, decrease with increasing body size, regardless of arm number (Fig. 2.4) [7].

This finding is somewhat counterintuitive, as the presence of a sixth arm might be expected to enhance locomotion by increasing the number of tube feet available for movement [8]. Furthermore, in many animal species, higher locomotion speeds are typically associated with the use of fewer limbs [9, 10], while a greater number of limbs is generally correlated with enhanced adhesion capabilities [11].

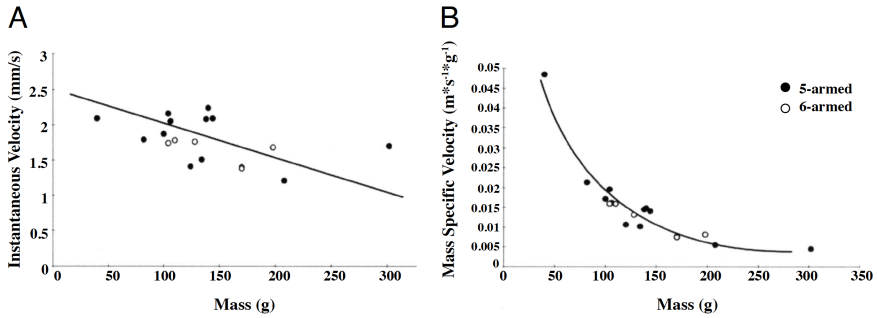

Figure 2.4: *Absolute and size-specific crawling velocities of various sizes of Patiria miniata individuals: (A) instantaneous crawling velocity versus body mass, (B) mass-specific velocity versus mass. Velocities were mean values from the plateau phase of instantaneous velocity curves. Data were log_{10} transformed before statistical analysis. (A) y = 2.02 - 0.003x (n = 18, P = 0.03). (B) y = 0.82 - 1.29x (n = 18, P < 0.01). Adapted from [7].*

Numerous studies have demonstrated that the relationship between body size and crawling speed is inconsistent across sea star species. In 2011, Mueller *et al.* investigated the locomotion of four Indo-Pacific sea star species (Fig. 2.5), highlighting this variability. Their results revealed a positive linear relationship between arm length and crawling speed in *Archaster typicus*, suggesting a proportional increase in speed with body size (Fig. 2.5B). Interestingly,

despite exhibiting the highest locomotion speed, *A. typicus* was the smallest species examined, with an average radius of approximately 3.2 cm. In contrast, Mueller *et al.* found no significant relationship between body size and locomotion speed in the three other species studied, *A. planci*, *L. laevigata*, and *P. nodosus*, respectively (Fig. 2.5A, C, and D).

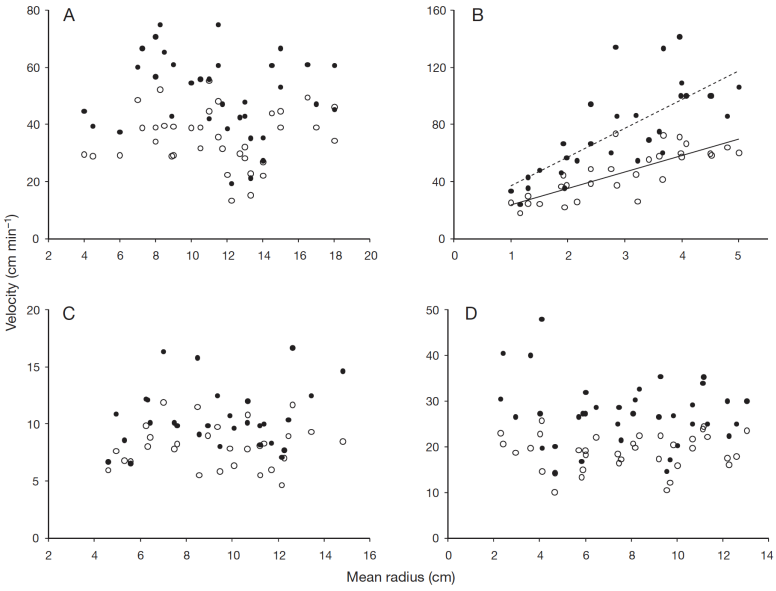

Figure 2.5: *Velocity as a function of mean radius (R) in (A) Acanthaster planci (n = 38), (B) Archaster typicus (n = 29), (C) Linckia laevigata (n = 29), and (D) Protoreaster nodosus (n = 38). Locomotion rate (empty circle) and maximum speed (dark circle) are shown. Linear regression of locomotion rate (continuous line) ($r^2 = 0.633$, $p < 0.001$, $y = 11.466 \times R + 12.207$) and of maximum speed (dashed line) ($r^2 = 0.548$, $p < 0.001$, $y = 20.091 \times R + 17.102$) for A. typicus are also shown. Note the differences in scale of the vertical axes. Adapted from [12].*

Similarly, a study by Pratchett *et al.* (2017) reported that in *Acanthaster solaris*, maximum crawling speed increases with body size (Fig. 2.6) [13]. However, research on *Echinaster graminicola* found no apparent effect on crawling speed in this species [14].

These findings collectively suggest that the influence of body size on locomotion in sea stars is species-specific and likely modulated by ecological, anatom-

ical, or biomechanical factors unique to each species. Several hypotheses have been proposed to explain the marked inconsistency in the relationship between body size and crawling speed across different sea star species. One possibility is that this relationship is species-specific, with interspecific differences in morphology accounting for variation in locomotor performance [12]. Morphological ratios, such as aspect ratio (relates arm length to arm width), disc ratio (relates arm length to oral disc diameter), and tube foot coverage, have been shown to explain differences in crawling speed partially. These parameters serve as useful predictors of locomotor capacity relative to body mass [6].

One suggested mechanism is that, in larger individuals, body mass increases disproportionately relative to the total surface area of the tube feet, potentially reducing locomotor efficiency [7]. Conversely, in some species, crawling performance may improve with size, possibly due to a higher number or increased size of tube feet, which could enhance traction and force generation [12].

Interestingly, this variability in sea stars challenges general patterns observed in other animals, where increased speed is often associated with a reduction in the number of limbs involved in locomotion, while additional limbs tend to contribute more to stability, and adhesion [15, 16]. In sea stars, however, the relationship between limb number, body size, and crawling speed remains variable across species. This highlights the need for a deeper understanding of biomechanics and coordination of tube feet, which may hold the key to explaining these interspecific differences [7, 12].

2.1.2 Influence of the substrate

Living in marine environments, sea stars encounter a wide range of substrate types over which they must navigate. These different substrates might significantly influence their crawling speed. In their 2017 study, Pratchett *et al.* reported that *Acanthaster solaris* exhibits higher mean (Fig. 2.6A) and maximum crawling speeds (Fig. 2.6B) as the diameter of the sea star increases. They also found that both parameters were elevated on sandy substrates (white circles) compared to rubble substrates (grey circles) (Fig. 2.6), implying that uneven or irregular surfaces may impede their mobility [13].

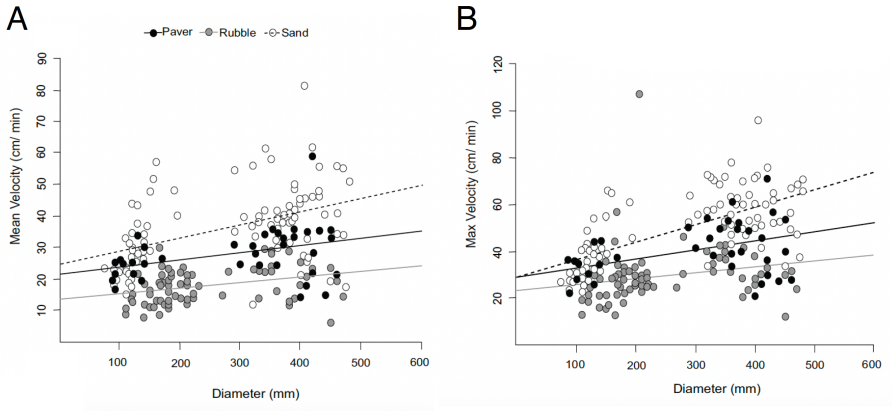

Figure 2.6: *Relationships between (A) mean velocity or (B) maximum velocity and diameter for the crown-of-thorns sea star Acanthaster solaris (n = 42). Movement rates were quantified for three different substrate types: paver (black circles), rubble (grey circles), and sand (white circles). Lines indicate the best fit for each different substrate type (paver: black line, rubble: grey line, sand: dashed line). Adapted from [13].*

This observation may be attributed to an increase in tenacity[1] of the tube foot disc when locomotion occurs on rough substrates [17]. The findings of Santos *et al.* in 2005 indicated that increased surface irregularities of the substrate induce the tube foot disc to undergo microscopic shape changes, thereby increasing its geometrical contact area and, consequently, its adhesive tenacity (Fig. 2.7). They hypothesized that the resulting stronger adhesion likely requires a greater force to detach the tube foot disc from the substrate, potentially reducing locomotion speed. This mechanism may also account for the more pronounced substrate effect observed in larger individuals, which possess a higher number of tube feet [13]. However, this hypothesis remains speculative, as detachment is believed to occur through the secretion of a de-adhesive substance [18, 19].

[1] Attachment force divided by the area of the imprint left by the tube foot.

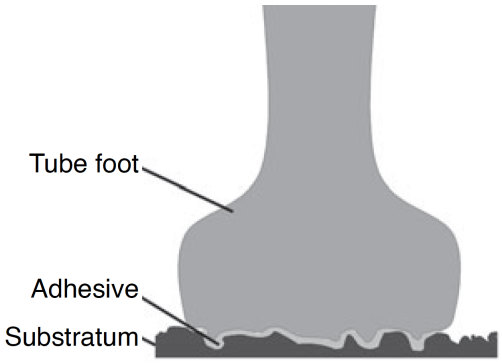

Figure 2.7: *Schematic representation of a tube foot adhesion to rough surfaces. The disc deforms to match the substratum profile, and the adhesive is released as an even thin film. Adapted from [17].*

2.1.3 Response to environmental changes

Understanding the factors that govern locomotion is therefore crucial for understanding the sea star responses to environmental changes. Studies on the impact of climate change, particularly rising temperatures, salinity changes, or pH variation, highlight the potential vulnerability of these organisms.

Influence of temperature

Sea stars are found in various oceans around the world, each characterized by a specific temperature depending on its geographical location [20]. Temperature variations appear to influence the maximum crawling speed of sea stars. Indeed, species native to tropical waters tend to exhibit higher crawling speeds than many species from temperate regions (Fig. 2.8). However, this trend is not universal and may be modulated by other factors, such as morphological traits, including a greater number of arms, or behavioral adaptations like active predation, which could favor increased locomotor performance [7].

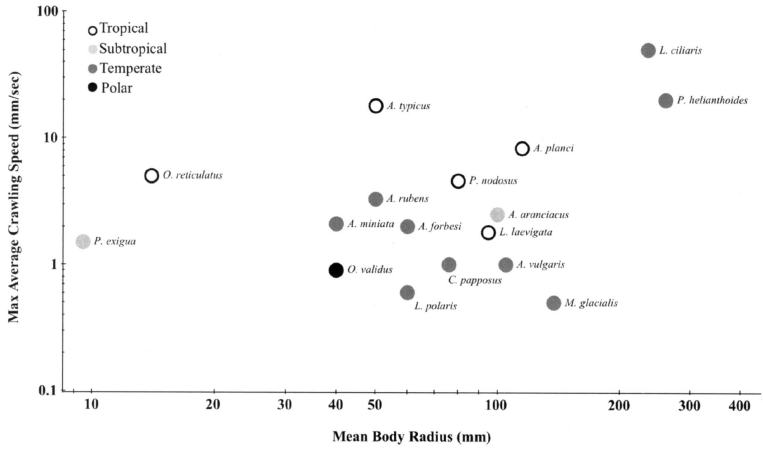

Figure 2.8: *Body size versus crawling speed in various sea star species from different geographic regions. Each point represents the maximum reported crawling speed at a mean radius (arm tip to centre of aboral disc) for each species. Water temperature was defined by latitude: tropical (<20°C), subtropical (20-40°C), temperate (40-60°C), and polar (>60°C). "Warm water" contained tropical and subtropical, while "cold water" included temperate and polar. Adapted from [7].*

Earlier studies on ectothermic taxa, including arthropods, echinoderms, and molluscs, have reported that locomotion speed tends to increase with temperature. This effect is likely linked to temperature-dependent changes in muscle kinetics, affecting contraction speed, power output, and coordination [21, 22, 23, 24]. While the precise mechanisms in sea stars remain to be fully elucidated, these observations suggest that the thermal environment may contribute, directly or indirectly, to interspecific differences in crawling speed.

Each species, regardless of its habitat, has a thermal optimum (Fig. 2.8), and any deviation from this optimum leads to a decline in metabolic rate and locomotor performance. Studies were carried out across a broad thermal range, from tropical species such as *Acanthaster solaris* (Fig. 2.9) [25] to cold-water species such as *Odontaster validus* (Fig. 2.10) [26]. In the study conducted by Lang *et al.* to assess the average movement rate of *A. solaris*, experiments were carried out on days 1, 8, 15, and 22 during a temperature ramping period (symbols with colored fill in Fig. 2.9A). Increasing the temperature to 32°C, the predicted summer maximum by 2100 in the Pacific Ocean [27, 28, 29], will

negatively affects locomotor performance, leading to a measurable decrease in crawling speed (Fig. 2.9B) [25].

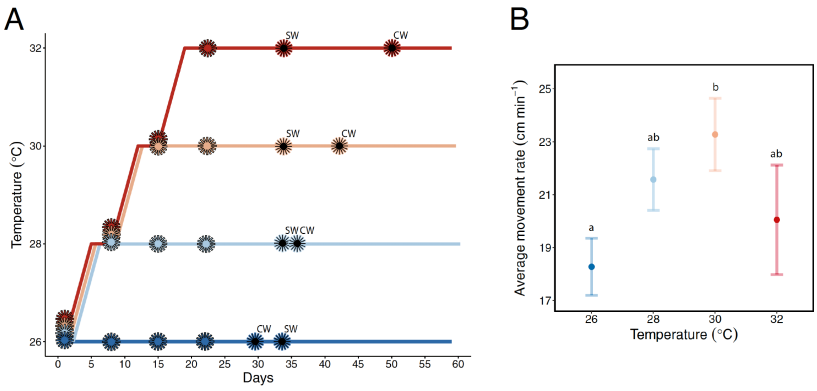

Figure 2.9: *(A)Experimental design timeline. The figure indicates the temperature profiles for the 26 °C (dark blue), 28 °C (light blue), 30 °C (orange), and 32 °C (red) treatments, from day 1 of the study until day 59. (B) Average movement rate (cm/min) in Acanthaster solaris (n = 48 individuals, n = 188 average movement rate observations). Estimated marginal means are provided (± SE). Letters represent significant differences between temperatures (Tukey method, $p < 0.05$). Abbreviations: SW, same week; CW, consecutive week. Adapted from [25].*

For Antarctic species, such as *O. validus*, an increase in ambient temperature of as little as 5°C has been shown to reduce the rate of key physiological processes, including locomotor performance, as well as the proportion of sea stars capable of movement (Fig. 2.10). This phenomenon may be related to their adaptation to low and stable temperatures, and possibly to oxygen limitation at higher temperatures [30, 31, 32]. For tropical species, although they tolerate higher temperatures, exceeding their thermal optimum can result in metabolic depression, likely due to oxygen limitation and increased anaerobic dependence, as well as cellular damage, ultimately impairing their ability to maintain life functions and survival [31, 33, 34, 35, 36].

Temperature	n1	Sea stars capable of locomotion (%)	n2	Locomotion speed (cm/min)	
				mean	SE
0°C	75	100.0	75	$0.85^{b,c,d}$	0.045
1°C	75	100.0	75	$1.21^{a,c}$	0.051
2°C	75	100.0	75	$0.99^{a,b,c}$	0.045
3°C	72	87.5*	63	$0.89^{b,c,d}$	0.061
4°C	50	70.0*	35	$0.78^{b,c,d}$	0.051
5°C	22	40.9*	9	$0.55^{b,d}$	0.037

Figure 2.10: *The effect of temperature on the proportion of Odontaster validus capable of locomotion and their speed of movement. Each variant of the experiment was replicated 15 times, with a different sea star used in each trial. As there were no statistically significant differences between movement speed for successive trials, data for each temperature were pooled together. n1 – number of sea stars capable of righting, n2 – number of sea stars capable of locomotion. Adapted from [26].*

Influence of salinity

Another consequence of climate change on the marine environment is the reduction in salinity, which leads to osmotic stress associated with low-salinity conditions (hyposalinity) [37]. This shift has detrimental effects on stenohaline[2] organisms, such as echinoderms, and particularly affects sea stars, which are highly sensitive to salinity fluctuations [38].

The 2025 study by Shellem *et al.* demonstrated that salinity exerts a greater influence on the righting response, a behavioral proxy for fitness, of the sea star species *Coscinasterias muricata* than temperature. While a 5°C increase in temperature did not significantly alter righting time in *Acanthaster solaris* and *Odontaster validus* [25, 26], a reduction in salinity had a marked effect on *C. muricata* [39]. Over one week, individuals exposed to low-salinity conditions exhibited significantly slower righting responses. Specifically, sea stars maintained at ambient salinity righted themselves approximately 47% faster than those subjected to hyposaline treatments ($\approx$ 26‰), indicating a substantial impairment of locomotor ability under osmotic stress (Fig. 2.11).

[2]Species that can only survive within narrow salinity ranges.

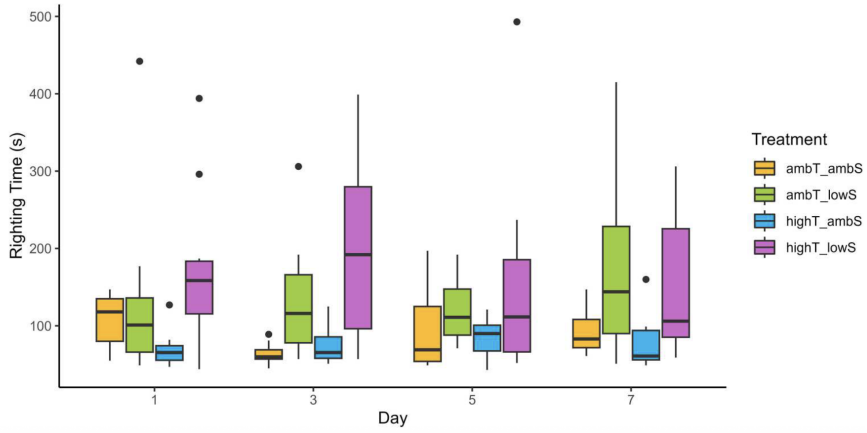

Figure 2.11: *Righting time for each treatment and day of the experiment is plotted, depicting the mean righting time and interquartile ranges with color corresponding to treatment. ambT ≈ 17°C; highT ≈ 22°C; ambS ≈ 33‰ and lowS ≈ 26‰. Adapted from [39].*

These findings align with the work of Moura *et al.* (2023), who investigated the effects of salinity on the sea urchin *Strongylocentrotus droebachiensis*, another echinoderm closely related to sea stars [40]. Their study demonstrated that reduced salinity negatively affected the locomotor capacity of this species, as maximum locomotor speed declined with decreasing salinity. This finding further supports the sensitivity of sea stars to hyposaline conditions, especially given that sea stars and sea urchins share a homologous ambulacral system and tube feet.

The decrease in locomotor capacity was linked to a decrease in tube foot disc tenacity as salinity declined [40]. They hypothesized that decreased salinity impairs both maximum locomotor speed and tube foot disc tenacity, primarily due to the dilution of essential ions (Na^+, Ca^{2+}, and K^+) involved in neuromuscular function [41, 42] and biochemical adhesion mechanisms [43]. This should explain why complex and coordinated behaviors such as locomotion and righting in sea star, as shown in Shellem *et al.* 2025 work [39], are disrupted at lower salinity levels (hyposalinity).

Influence of pH

Ocean acidification, like rising temperatures, impacts the vital functions of sea stars. In the study of McLaren *et al.*, acidification was simulated by a decrease in pH to 7.8 and 7.6 compared to the ambient pH of 8.05 [44]. The influence of this pH decrease was tested on the escape response of *Parvulastra exigua* after contact with its predator *Meridiastra calcar*. A decrease in pH resulted in a significant increase in the latency before the onset of this behavioral response. This response time was, on average, 2.8 times longer at pH 7.6 than at ambient pH (Fig. 2.12A). This decrease in pH also results in a slightly modified crawling speed for the escape response of *P.exigua* initiated by contact with its predator *M. calcar* (Fig. 2.12B). This slowdown could increase the vulnerability of *P. exigua* to predation. The mechanisms underlying this increase in latency are not yet fully understood, but could involve physiological stress, hypercapnia (excessive concentration of carbon dioxide (CO_2) in the ambulacral fluid or body tissues) affecting locomotor abilities [45], or an alteration of sensory pathways such as chemoreception [46] or mechanoreception [47].

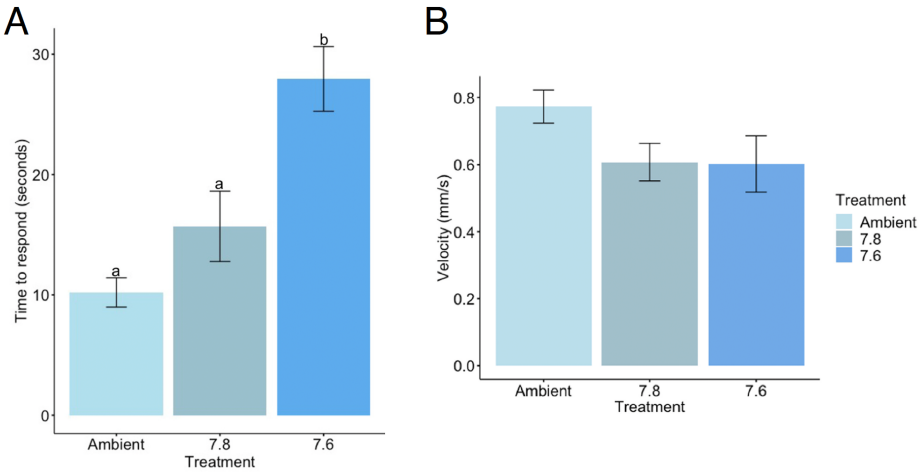

Figure 2.12: *(A)Average time taken (seconds) (± standard error of the mean) for Parvulastra exigua to initiate an escape response after contact with Meridiastra calcar (n = 20). (B) Average velocity (mm/s) (± standard error of the mean) of Parvulastra exigua after contact with Meridiastra calcar following conditioning to ambient pH_T (n = 20), 7.8 (n = 18) or 7.6 (n = 20). Adapted from [44].*

However, the direction of locomotion was not affected by the pH decrease, as there was no significant difference in the mean vectors of each treatment (Fig. 2.13), although other factors, such as water current force or light [48, 49], may influence this parameter.

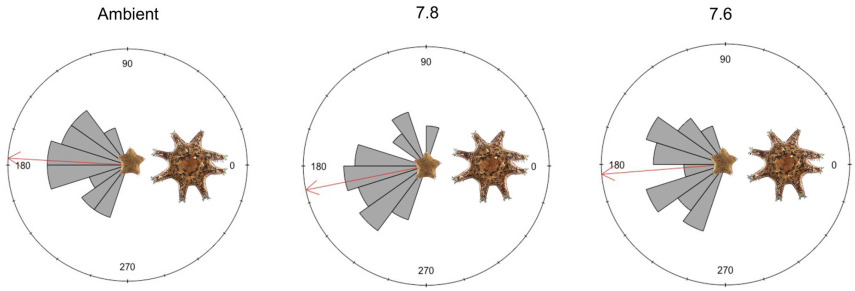

Figure 2.13: *Trajectories of movement of P. exigua from the point of stimulation for animals conditioned to ambient (pH_T8.05), pH_T7.8, and pH_T7.6 treatments (from left to right). The angle of stimulation was always 0°. Adapted from [44].*

2.2 Directionnal locomotion

Directional locomotion refers to the guided movement of an organism along a preferred axis, where directionality arises from the spontaneous or stimulus-induced breaking of spatial symmetry within the organism [50]. Despite their apparent radial symmetry and decentralized nervous system, sea stars exhibit directional locomotion. Typically, one arm, referred to as the 'leading arm', or a pair of adjacent arms near the madreporite, exhibits a greater tendency to position itself at the front during locomotion (Fig. 2.14) [14]. This arm guides the trajectory, while the lateral arms contribute to propulsion and stabilization. As a result, the body orientation temporarily aligns with the leading arm. Radially symmetrical animals, which lack a defined anterior-posterior or left-right axis, have traditionally been assumed to exhibit limited directional behavior [51, 52]. However, the following observations (Fig. 2.14) challenge these assumptions by revealing complex patterns of movement and coordination [53, 54]. Although lacking a defined head or centralized brain, sea star can coordinate their tube feet and arms to generate coherent and goal-directed movements.

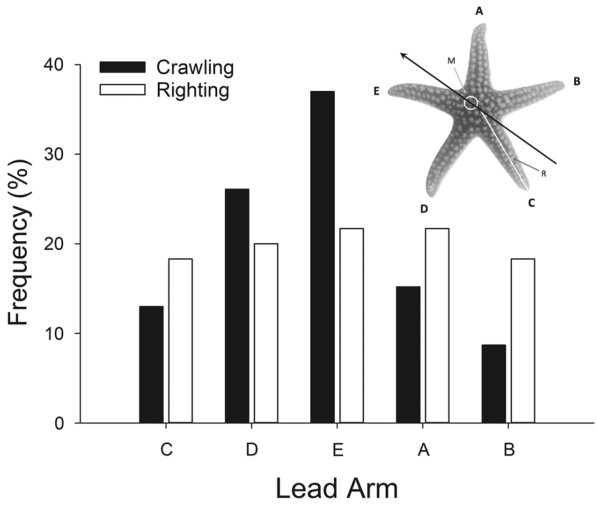

Figure 2.14: *Frequency (%) of lead arm usage during crawling (black bars) and righting (open bars) by Echinaster graminicola (n = 30). The behavioral plane of symmetry for crawling in E. graminicola is illustrated, with the arrow pointing toward the anterior end. Arms are labeled A through E, clockwise from the madreporite (M). Radius is indicated as R. Adapted from [14].*

Observations across sea star species remain inconsistent, offering no definitive explanation regarding the existence, or not, of a leading arm during locomotion [14, 54]. Recent studies have therefore turned to external environmental factors to elucidate the mechanisms that govern directional locomotion in sea stars.

2.2.1 Influence of currents and gravity

As sea stars inhabit marine environments such as coral reefs or rocky shores, they are continuously exposed to wave-induced water movements and varying substrate orientations. In 2021, Meretta *et al.* analyzed the role of body directionality during crawling and righting by recording these behaviors in an experimental set-up allowing for measuring the reaction of sea stars to the water current (rheotaxis) and substrate orientation (gravitaxis) [49]. The presence of water current has been observed to lead to increased locomotion speed (Fig. 2.15A, green box) and more linear trajectories (Fig. 2.15B, green box) in the species *Asterina stellifera*. However, this response did not exhibit a preferential

direction relative to the current, indicating the absence of rheotaxis in this species, despite its faster and more linear locomotion. On the other hand, an increase in the crawling speed of sea stars going downward a vertical surface (red box) was observed compared to the ones going upward (aquamarine box) (Fig. 2.15A and B).

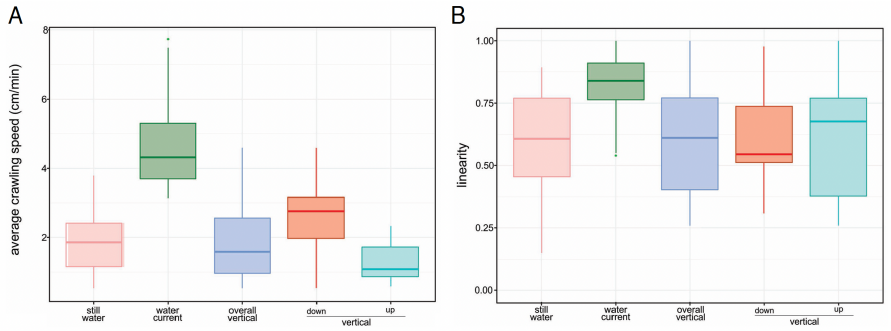

Figure 2.15: *(A) Average crawling speed (cm/min) and (B) linearity regarding two water-flow regimes (still water, pink; water current, green) and the angle of substrata (90° vertical plane, blue) going downwards (red) and upwards (aquamarine). N = 120 sea stars/trial. Adapted from [49].*

This suggests a key role of the inclination of the surface. The proposed hypothesis is that gravitational force facilitates an increased locomotion speed in sea stars when moving down a vertical surface. This leads to gravitaxis as the orientation and the movement are influenced by gravity [49].

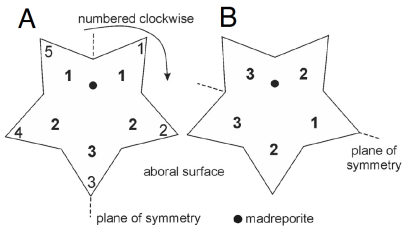

C

Arm classes	Arm numbering					G-test	
	1	2	3	4	5	G	P
Crawling Trials							
arms individually numbered	0.17	0.22	0.24	0.22	0.15	2.983	0.561
madreporite axis	0.45	0.39	0.16	–	–	1.485	0.476
arm 2 to inter-radius 4-5 axis	0.27	0.39	0.34	–	–	3.180	0.204
Righting Trials							
arms individually numbered	0.23	0.20	0.24	0.15	0.18	2.757	0.599
madreporite axis	0.41	0.35	0.24	–	–	1.429	0.489
arm 2 to inter-radius 4-5 axis	0.20	0.47	0.33	–	–	2.463	0.292

Figure 2.16: *Aboral view of three arm-numbering systems for describing sea star bilateral behavior. Arms are numbered clockwise (1–5) from the madreporite. (A) Bold numbering based on equivalent positions across the madreporite symmetry plane [7]. (B) Numbering relative to a symmetry plane from arm 2 to the 4–5 interradius [54]. (C) Bilateral-like movement: arm preference in locomotion (N = 120) and righting (N = 100) trials. Adapted from [49].*

Meretta and his colleague also evaluated bilaterally symmetrical behavior, using three different arm-numbering systems to test the existence of a plane of symmetry during both locomotion and righting (Fig. 2.16A and B). During locomotion, the sea stars used two arms at the front, two on the sides, and one at the back. However, no significant preference for a particular arm was observed during locomotion and righting trials (Fig. 2.16C). This means that the species does not exhibit an anterior/posterior plane of symmetry during locomotion or positioning, indicating a lack of bilaterality.

2.2.2 Influence of the light

A complementary perspective was provided in 2025 by Po *et al.* using *Protreaster nodosus*. The directional control of this species was investigated during free-moving (Fig. 2.17A) and inverted experiments (Fig. 2.17B), in which a white LED was directed to a single eye spot.

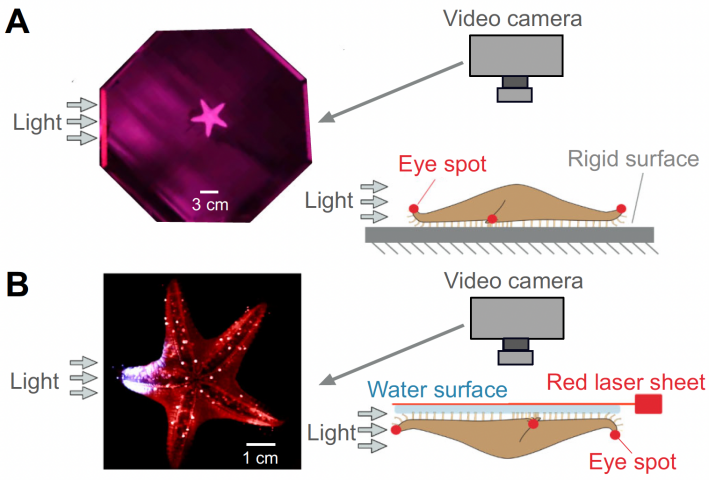

Figure 2.17: *(A) The trajectory of sea stars was captured by a camera above an arena made up of an acrylic tank with walls in an octagonal arrangement, with one illuminated wall. (B) In inverted experiments, sea stars were placed in an upside-down position with the water level lowered to the tips of the sea star's tube feet. We illuminated the tube feet with four red laser sheets at the water's surface, and a white LED was directed at a single eye spot. Some inverted experiments additionally featured a glass plate placed atop the tube feet. Adapted from [48].*

In this work, Po *et al.* (2025) investigated sea star ability to exhibit phototaxis, which defines the ability to move directionally toward or away from a light source [48]. The study finds that *P. nodosus* were approximately twice as likely to initiate movement under light conditions than under dark conditions (Fig. 2.18A). Also, in the presence of light, individuals exhibited rapid movements generally along straighter trajectories (Fig. 2.18B), suggesting that light must be considered as an important stimulus promoting locomotion in this species, consistent with observations reported in the literature [55, 56, 57]. In contrast, movements were slower and followed sinuous and randomly oriented trajectories when there was no light. The results of the Rayleigh test confirm the absence of significant directionality in movements under dark conditions (Fig. 2.18C), indicating disorganized exploratory behavior.

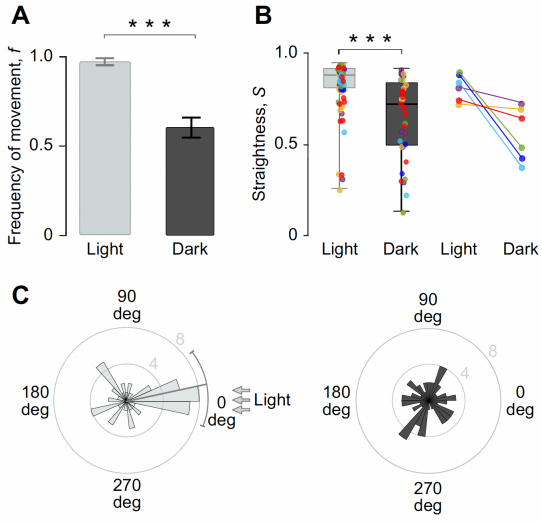

Figure 2.18: *(A) The proportion of sequences where sea stars moved (>0.5 cm in net distance of entire experiment), with 95% confidence intervals (error bars, ***P<0.001). (B) The straightness of locomotion is shown by the median (central line), first and third quartiles (top and bottom boundaries of boxes), and the range of values (error bars, ***P<0.001). The individual sequences are overlaid, and mean values for each individual are plotted to the right. (C) Polar histograms of the number of trials directed towards an angle (in deg) relative to the light (at 0 deg; left) or in the dark (right) for 98 trials for all individuals. The significant trend (P<0.05) in direction under illumination (left plot) shows the mean direction (radial line) and 95% confidence intervals. Adapted from [48].*

Inverted trials offered insight into the role of tube feet and nervous control. Tube feet directional coordination varies greatly depending on environmental conditions. In the absence of light, the power strokes, when tube feet push against the substrate to drive movement, showed high directional variability, reflected by low polarization (Fig. 2.19 A, B, and C in dark blue). The polarization parameter (ρ) expresses the degree of directional coordination among the tube feet. It is determined using the following equation [58]:

$$\rho = \frac{1}{n}\sqrt{\left(\sum_{i=1}^{n}\sin\theta_i\right)^2 + \left(\sum_{i=1}^{n}\cos\theta_i\right)^2} \tag{2.1}$$

where θ is the angular direction of the displacement vector of the ith foot in the power stroke, and n is the number of tube feet.

Conversely, in the presence of light, tube feet adopt a consistent orientation across the whole body, exhibiting a high degree of polarization (Fig. 2.19A, B and C in light blue). In addition, mechanical coupling with a rigid surface (e.g., a glass plate) induces a similarly consistent orientation of movements, independent of light conditions (Fig. 2.19D and E in magenta). Tube feet in contact with the rigid surface show significantly greater polarization ($0.98 < \rho < 0.99$) than those not in contact ($0.13 < \rho < 0.68$), with a highly significant statistical difference (Fig. 2.19F).

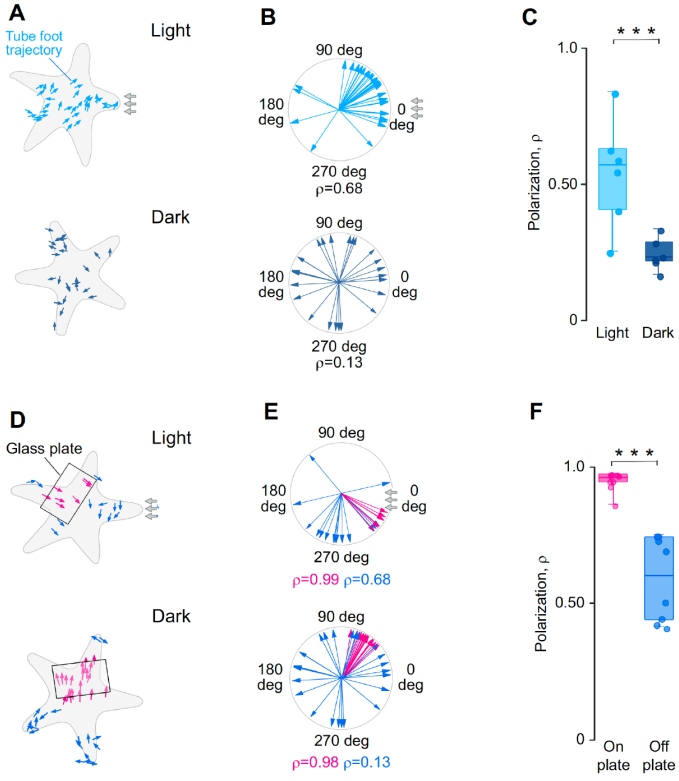

Figure 2.19: *For measurements employing the inverted preparation, results are presented for (A–C) sea stars in the light (in light blue) and in the dark (in dark blue), and (D–F) experiments that introduced a glass plate in contact with some tube feet (in magenta), but not others (in blue). Representative sequences for (A, D) the displacement of tube feet during the power stroke and (B, E) their corresponding angular direction. (C, F) Values of the polarization parameter are shown for all sequences. Highly significant differences are highlighted with asterisks (***P<0.001). Adapted from [48].*

These results suggest that both light signals and mechanical interactions with the environment play key roles in modulating the motor coordination of tube feet during locomotion. Data from the inverted experiments support the hypothesis of a centralized motor control, wherein a single directional command is transmitted to the tube feet of all arms [59]. The consistent orientation of power strokes observed under illuminated conditions, which is difficult to explain solely through local mechanical interactions, suggests the presence of a global coordination mechanism involving a shared directional motor signal In contrast, locomotion in the absence of light, characterized by frequent changes in direction, may result from mechanical conflicts between tube feet attempting to simultaneously propel the animal in divergent directions [48].

2.3 Biomechanics of tube feet and sea star locomotion

In recent years, mathematical and computational approaches have been developed to better understand the mechanical principles underlying sea star locomotion based on the coordination of their tube feet. These models aim to depict the interactions between tube feet, the sea star body, and the surrounding environment at various levels. Beyond advancing our understanding of echinoderm biomechanics, such models offer valuable insights for the design of flexible, stable, and adaptive soft robotic systems [60]. The following chapter will present some of the most recent models focused on the biomechanics of tube feet and sea star locomotion.

2.3.1 Tube feet as soft actuators

In 2020, Eva Kanso and her team developed a mechanical model characterizing tube foot function, treating the ampulla/tube foot unit as a hydrostatic actuator [61]. In this model, tube feet are conceptualized as soft actuators capable of generating active force (F_a) for both pushing and pulling actions (Fig. 2.20). The active force follows a linear force–length relationship, inspired by the classical Hill model of muscle mechanics [62, 63].

In addition to active force generation, the model incorporates passive components (F_p), which represent restoring elastic forces elements, such as elastic forces arising from the connective tissue, as well as a viscous damping element (F_d) accounting for internal resistance due to displacement of the ambulacral fluid. Together, these elements reproduce the overall mechanical behavior of the tube foot during both the power stroke and the recovery phase, without explicitly modeling underlying neuromuscular control mechanisms [61].

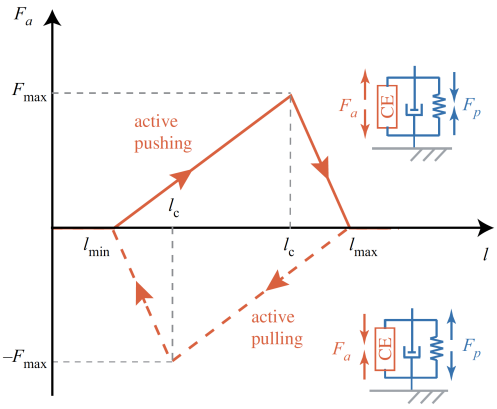

Figure 2.20: *Tube foot inspired soft actuator: when attached to a substrate, a tube foot generates either a pushing or a pulling force on the body it is attached to. These active forces act longitudinally along the tube foot direction, and their magnitude depends on the tube foot length l. Adapted from [61].*

2.3.2 Tube foot as hydrostatic skeleton

In 2024, both Ellers *et al.* and Po *et al.* establish sea star tube feet as classic hydrostatic skeletons, a fluid-filled structure where muscular contraction (especially of the ampulla) drives shape change and movement [64, 65]. In this context, sea star tube feet are fluid-filled structures where muscular contraction (especially of the ampulla) drives shape change and movement. These structures operate similarly to the body of worms or the human tongue, transmitting force without rigid joints [66, 67]. Comparative modeling approaches have examined several mechanical analogues, including a hydraulic press (fixed transmission), a McKibben actuator (variable transmission based on fiber angle), and a fiberless cylindrical hydrostat (shape-dependent transmission). The

tube foot is typically represented as a two-chamber system comprising the ampulla and the stem (Fig. 2.21A), with the stem modeled analogously to a McKibben actuator and the ampulla considered a more compliant structure. The overall architecture includes a stem inflated by the ampulla and reinforced by musculature and a cross-helical arrangement of elastic fibers [68]. Extension of the tube foot occurs through contraction of the ampullar muscles [69], which increases the internal pressure and drives fluid into the stem, resulting in elongation [70, 71, 72, 73] (Fig. 2.21B).

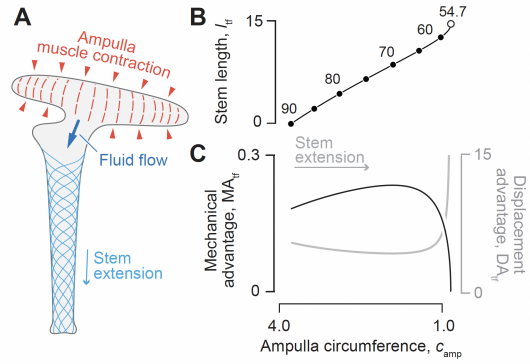

Figure 2.21: *(A) Schematic representation of tube foot extension. Parametric plots illustrate the change in (B) tube foot length and fiber helix angle (intervals of 5 deg, filled circles, and at 54.7 deg, open circle) during extension (for n = 8). The associated changes in (C) MA_{tf} (black) and DA_{tf} (grey) are shown with consideration to that reduction in ampullar circumference c_{amp}, which drives tube foot extension. All curves were plotted as parametric functions of θ versus c_{amp}, all in arbitrary units. Adapted from [64].*

Ellers *et al.* develop a general theoretical framework for gearing in soft actuators. As tube feet extend, the displacement advantage (DA, the ratio of output to input) increases while the mechanical advantage (MA, the ratio of output to input force) declines [64]. Unlike rigid levers, sea star tube feet exhibit variable gearing, where mechanical advantage (MA) and displacement advantage (DA) shift with deformation. Here, the mechanical advantage is not always the inverse of the displacement advantage [74]. This decoupling, largely due to energy storage and dissipation in tissues such as muscle or connective tissue, plays a crucial role in determining movement efficiency. In particular, the tube foot model suggests that the MA can reach a maximum at an inter-

mediate length during extension (Fig. 2.21C). The addition of a parallel elastic element, simulating longitudinal muscles, may reduce overall transmission efficiency (MA $\times$ DA < 1), but potentially contributes to fine control of posture or lengthening.

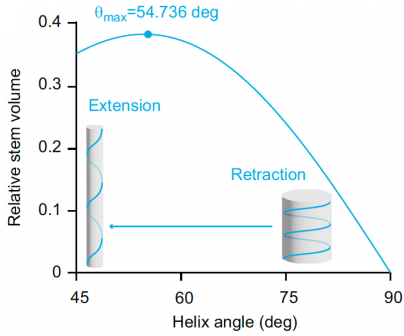

Figure 2.22: *The relationship between the relative stem volume (v) and pitch angle of the helical winding (θ), with the maximum volume highlighted (filled circle). Arrows denote the changes in stem length that generate alterations in pitch angle. Adapted from [65].*

Po *et al.* extended their mathematical model to more accurately represent the biomechanics of sea star tube feet by incorporating key anatomical features such as the substantial longitudinal muscle volume, the terminal disc, and the ellipsoidal shape of the ampulla. Their refined model revealed that peak mechanical advantage (MA) can occur at mid-extension, a phenomenon shaped by both geometry and the internal arrangement of muscle fiber [65].

Both of their studies also highlight the critical role of helically wound collagen fibers in the tube foot stem. These fibers constrain deformation, resist internal pressure, and store elastic energy. A central finding is the importance of the so-called "magic angle", a helix angle θ of approximately 54.7°, at which volume conservation and force transmission are simultaneously optimized (Fig. 2.22).

Together, these studies highlight that sea star locomotion results from the interplay between active neuromuscular control and the passive mechanical properties embedded within the tissue architecture.

2.3.3 Sea star as a rigid body coupled to a network of actuators

In addition to their previous model of the tube foot, Kanso and her team modeled the sea star's body during locomotion. They designed it as a rigid body of mass m connected to a series of N soft actuators that correspond to their tube feet. Tube feet are separated by a constant distance d, with (x, y) representing the position of the sea star's centre of mass and indicating its tilt angle (β) measured counterclockwise from the x-axis (Fig. 2.23A). The figure 2.23B schematically illustrates the hierarchical motor control of the tube feet, which consists of:

- a global directionality command, originating from the nerve ring and radial nerves, responsible for communicating the step direction to all tube feet;
- a local sensory-motor feedback loop at each tube foot that dictates tube foot power and recovery, i.e., the decisions to push or pull and attach or detach.

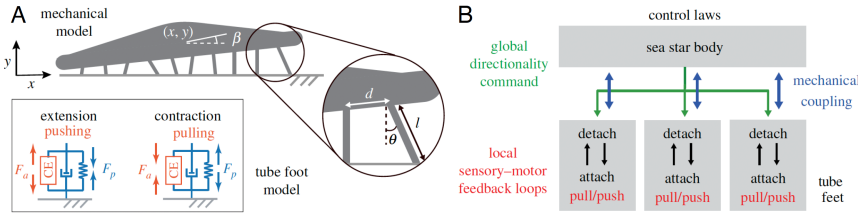

Figure 2.23: *(A) Schematic of the mechanical model of the sea star and tube feet inspired actuators, with inset showing contractile, passive, and dissipative force elements along each tube foot. (B) Hierarchical motor control of the tube feet consists of global directionality commands issued by the radial nerves and nerve ring and local sensory–motor feedback loops at the tube foot level. Adapted from [61].*

Here, they consider that the only connection that exists between the tube feet is through their structural attachment to the sea star body (Fig. 2.23B). This model facilitates the investigation of how coordination among tube feet arises from mechanical coupling with the body, revealing collective dynamics that contribute to the generation of a stable and robust global movement.

2.3.4 Tube feet coordination and cooperative transport

In 2024, Kanso and Po introduced novel computational models to investigate how tube foot recruitment adapts to increasing mechanical load, notably without relying on assumptions of centralized control [75]. Drawing inspiration from collective transport in foraging ants [76, 77, 78], the authors proposed that tube feet coordinate locomotion in a similarly decentralized manner. In their models, tube feet are represented as mechanically coupled agents that can act independently in response to local mechanical cues. These agents were modeled either as linear and torsion springs in two dimensions or as stochastically recruited actuators in one dimension. Using this framework, the authors demonstrated that increased tube foot recruitment under higher load conditions can emerge spontaneously through local mechanical interactions between the feet and the body, without the need for explicit neural coordination. This work offers new insight into how distributed mechanical feedback may underlie robust and adaptive locomotion in echinoderms.

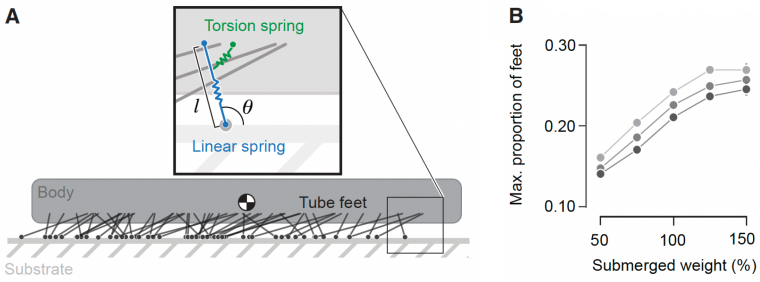

Figure 2.24: *(A) The submerged weight of the body (in grey) resists the forces generated by the tube feet to move. (B) Each point shows the mean value (± 1 SE, with error flags that are smaller than the point diameter) from batches of 10 simulations conducted over varying values for the submerged weight for models with 225, 250, or 275 tube feet. Adapted from [75].*

Each tube foot (inset in Fig. 2.24A) is modeled as generating force based on its length (l) and angle (θ), following the dynamics of a linear spring (in blue) and a torsional spring (in green) (Fig. 2.24A). The model accurately predicts a comparable proportion of tube feet engaged in the power stroke, in agreement with experimental observations. When subjected to increased load, sea stars compensate by recruiting a greater number of tube feet (Fig. 2.24B).

BIBLIOGRAPHY

[1] G. J. ROMANES, The Locomotor System of Star-Fish, *Nature* **36**, 20-21, 1887.

[2] L. J. COLE, Direction of locomotion of the starfish, *Journal of Experimental Zoology* **14**, 1-32, 1913.

[3] T.A. MCMAHON, Size and shape in biology: elastic criteria impose limits on biological proportions, and consequently on metabolic rates, *Science* **179**,1201-1204, 1973.

[4] T.A. MCMAHON, On size and life, *New York: Scientific American Library*, 1983.

[5] M.R. HIRT *et al.* A general scaling law reveals why the largest animals are not the fastest, *Nature Ecology & Evolution* **1**, 1116-1122, 2017.

[6] E. MONTGOMERY, Predicting crawling speed relative to mass in sea stars, *Journal of Experimental Marine Biology and Ecology* **458**, 27-33, 2014.

[7] E. MONTGOMERY *et al.* Effects of Body Size and Shape on Locomotion in the Bat Star (*Patiria miniata*), *Biological Bulletin* **222**, 222-232, 2012.

[8] F.H.C. HOTCHKISS, On the Number of Rays in Starfish, *American Zoologist* **40**, 340–354, 2000.

[9] R.J. FULL *et al.* Mechanics of A Rapid Running Insect: Two-, Four-and Six-Legged Locomotion, *Journal of Experimental Biology* **156**, 215-231, 1991.

[10] T. WEIHMANN, The Smooth Transition From Many-Legged to Bipedal Locomotion—Gradual Leg Force Reduction and its Impact on Total Ground Reaction Forces, Body Dynamics and Gait Transitions, *Frontiers in Bioengineering and Biotechnology* **9**, 769684, 2022.

[11] D. LABONTE & W. FEDERLE, Scaling and biomechanics of surface attachment in climbing animals, *Philosophical Transactions of the Royal Society B: Biological Sciences* **370**, 20140027, 2015.

[12] B. MUELLER *et al.* Size-specific locomotion rate and movement pattern of four common Indo-Pacific sea stars (Echinodermata; Asteroidea), *Aquatic Biology* **12**, 157-164, 2011.

[13] M.S. PRATCHETT *et al.* Body size and substrate type modulate movement by the western Pacific crown-of-thorns starfish, *Acanthaster solaris*, *PLOS ONE* **12**, 1-14, 2017.

[14] L.M. ARDOR BELLUCCI *et al.* Crawling and righting behavior of the subtropical sea star *Echinaster (Othilia) graminicola*: effects of elevated temperature, *Marine Biology* **166**, 1-9, 2019.

[15] T. WEIHMANN, Leg force interference in polypedal locomotion, *Science Advances* **4**, eaat3721, 2018.

[16] W. FEDERLE *et al.* Dynamic biological adhesion: mechanisms for controlling attachment during locomotion, *Philosophical Transactions of the Royal Society B: Biological Sciences* **374**, 20190199, 2019.

[17] R. SANTOS *et al.* Adhesion of echinoderm tube feet to rough surfaces, *SF Journal of Experimental Biology* **208**, 2555-2567, 2005.

[18] P. FLAMMANG *et al.* The Role of Podial Secretions in Adhesion in Two Species of Sea Stars (Echinodermata), *The Biological Bulletin* **187**, 35-47, 1994.

[19] P. FLAMMANG *et al.* A study of the temporary adhesion of the podia in the sea star *Asterias rubens* (Echinodermata, asteroidea) through their footprints, *Journal of Experimental Biology* **201**, 2383–2395, 1998.

[20] M. RAHMAN *et al.* The Sea Stars (Echinodermata: Asteroidea): Their Biology, Ecology, Evolution and Utilization, *SF Journal of Biotechnology and Biomedical Engineering* **169**, 1007, 2018.

[21] A.F. BENNETT, Thermal dependence of locomotor capacity, *American Journal of Physiology-Regulatory, Integrative and Comparative Physiology* **259**, R253-R258, 1990.

[22] R.L. MARSH, Deactivation rate and shortening velocity as determinants of contractile frequency, *American Journal of Physiology-Regulatory, Integrative and Comparative Physiology* **259**, R223-R230, 1990.

[23] J.S. YOUNG *et al.* The effects of temperature on peripheral neuronal function in eurythermal and stenothermal crustaceans, *Journal of Experimental Biology* **209**, 1976-1987, 2006.

[24] A.H. HULBERT *et al.* Shaking a leg and hot to trot: the effects of body size and temperature on running speed in ants, *Ecological Entomology* **33**, 144-154, 2008.

[25] B.J. LANG *et al.* Effects of elevated temperature on the performance and survival of pacific crown-of-thorns starfish (*Acanthaster cf. solaris*), *Marine Biology* **169**, 43, 2022.

[26] A. KIDAWA *et al.* The effects of temperature on the behaviour of the Antarctic sea star *Odontaster validus*, *Polish Polar Research* **31**, 273-284, 2010.

[27] T.F. STOCKER *et al.* Summary for policymakers , *Climate change 2013* **Cambridge University Press**, 159-204, 2013.

[28] V. MASSON-DELMOTTE *et al.* Summary for policymakers, *Climate change 2021* **Cambridge University Press** , 3-32, 2021.

[29] O. HOEGH-GULDBERG *et al.* Impacts of 1.5°C Global Warming on Natural and Human Systems, *Global warming of 1.5°C* **IPCC Secretariat**, 175-311, 2018.

[30] L.S. PECK, Prospects for survival in the Southern Ocean: vulnerability of benthic species to temperature change, *Antarctic Science* **17**, 497-507, 2005.

[31] H.O. PÖRTNER, Climate variations and the physiological basis of temperature dependent biogeography: systemic to molecular hierarchy of thermal tolerance in animals, *Comparative Biochemistry and Physiology Part A: Molecular & Integrative Physiology* **132**, 739-761, 2002.

[32] H.O. PÖRTNER *et al.* Thermal limits and adaptation in marine Antarctic ectotherms: an integrative view, *Philosophical Transactions of the Royal Society B: Biological Sciences* **362**, 2233-2258, 2007.

[33] C.-P. CHEN *et al.* The effect of temperature-salinity combinations on survival and growth of juvenile *Patiriella pseudoexigua* (Echinodermata: Asteroidea), *Marine Biology* **115**, 119-122, 1993.

[34] H.O. PÖRTNER, Climate change and temperature-dependent biogeography: oxygen limitation of thermal tolerance in animals, *Naturwissenschaften* **88**, 137-146, 2001.

[35] A.B. CHRISTENSEN *et al.* Effects of CO2, pH and temperature on respiration and regeneration in the burrowing brittle stars *Hemipholis cordifera* and *Microphiopholis gracillima*, *Journal of Experimental Marine Biology and Ecology* **495**, 13-23, 2017.

[36] J. HARIANTO *et al.* The effect of warming on mortality, metabolic rate, heat-shock protein response and gonad growth in thermally acclimated sea urchins (*Heliocidaris erythrogramma*), *Marine Biology* **165**, 1-12, 2018.

[37] B.S. CHENG *et al.* Atmospheric rivers and the mass mortality of wild oysters: insight into an extreme future?, Proceedings of the Royal Society B: Biological Sciences **283**, 201614620, 2016.

[38] L. SCHMITTMANN, Local adaptation of the common sea star Asterias rubens to different salinities, *Doctoral dissertation* **Christian-Albrechts-Universität Kiel**, 2017.

[39] C.T. SHELLEM *et al.* Salinity has a greater effect on sea star righting time than temperature, New Zealand Journal of Marine and Freshwater Research, 1-15, 2025.

[40] A.J. MOURA *et al.* Hyposalinity reduces coordination and adhesion of sea urchin tube feet, Journal of Experimental Biology **226**, jeb245750, 2023.

[41] E. CARAFOLI, Calcium – a universal carrier of biological signals, *The FEBS Journal* **272**, 1073-1089, 2005.

[42] R.W. HILL *et al.* Animal Physiology, *Sunderland, MA: Sinauer Associate* **5th edn.**, 2012.

[43] E. HENNEBERT *et al.* Adhesion Mechanisms Developed by Sea Stars: A Review of the Ultrastructure and Composition of Tube Feet and Their Secretion, *Biological Adhesive Systems: From Nature to Technical and Medical Application* Springer, 99-109, 2010.

[44] E.J. MCLAREN & M. BYRNE, The effect of ocean acidification on the escape behaviour of the sea star *Parvulastra exigua* to its sea star predator *Meridiastra calcar*, *Experimental Marine Biology and Ecology* **555**, 151779, 2022.

[45] S.-A. WATSON *et al.* Marine mollusc predator-escape behaviour altered by near-future carbon dioxide levels, *Proceedings of the Royal Society B: Biological Sciences* **281**, 20132377, 2014.

[46] C.A. MOTTO *et al.* Chemical Ecology of Chemosensation in Asteroidea: Insights Towards Management Strategies of Pest Species, *Journal of Chemical Ecology* **44**, 147-177, 2018.

[47] A. GARM, Sensory Biology of Starfish—With Emphasis on Recent Discoveries in their Visual Ecology, *Integrative and Comparative Biology* **57**, 1082-1092, 2017.

[48] T. PO *et al.* The directional control of phototaxis in sea stars (*Protoreaster nodosus*), *Journal of Experimental Biology* **228**, jeb249293, 2025.

[49] P.-E. MERETTA *et al.* Locomotion and righting behavior of sea stars: a study case on the bat star *Asterina stellifera* (Asterinidae), *Revista de Biología Tropical* **69**, 501-513, 2021.

[50] C.GÄHRS *et al.* Locomotion, Encyclopedia of Animal Cognition and Behavior **Cham: Springer International Publishing**, 3986-4001, 2022.

[51] G. HOLLÓ & M. NOVÁK, The manoeuvrability hypothesis to explain the maintenance of bilateral symmetry in animal evolution, Biology Direct **7**, 22, 2012.

[52] G. HOLLÓ, Demystification of animal symmetry: symmetry is a response to mechanical forces, Biology Direct **12**, 11, 2017.

[53] I.I. ARSHAVSKII *et al.* Coordination of arm movement during locomotion in Ophiuroidea, *Neirofiziologiia = Neurophysiology* **8**, 529-537, 1976.

[54] C. JI *et al.* Echinoderms Have Bilateral Tendencies, *PLOS ONE* **7**, e28978, 2012.

[55] A. GARM *et al.* Visual navigation in starfish: first evidence for the use of vision and eyes in starfish, Proceedings of the Royal Society B: Biological Sciences **281**, 20133011, 2014.

[56] M. YOSHIDA *et al.* The phototactic behavior of the starfish, *Asterias amurensis* lütken, The Biological Bulletin **134**, 516-532, 1968.

[57] J.E SMITH & H.G. CANNON, On the nervous system of the starfish *Mathasterias glacialis* (L.), Philosophical Transactions of the Royal Society of London. Series B, Biological Sciences **227**, 111-173, 1937.

[58] J.W. JOLLES *et al.* Consistent Individual Differences Drive Collective Behavior and Group Functioning of Schooling Fish, *Current Biology* **27**, 2862-2868, 2017.

[59] J.E. SMITH, The Role of the Nervous System in Some Activities of Starfishes, *Biological Reviews* **20**, 29-43, 1945.

[60] D. RUS & M.T. TOLLEY, Design, fabrication and control of soft robots, *Nature* **521**, 467-475, 2015.

[61] S. HEYDARY *et al.* Sea star inspired crawling and bouncing, *Journal of The Royal Society Interface* **17**, 20190700, 2020.

[62] A. V. HILL, The heat of shortening and the dynamic constants of muscle, *Proceedings of the Royal Society of London. Series B - Biological Sciences* **126**, 136-195, 1997.

[63] Y.C. FUNG *et al.* Biomechanics. Mechanical Properties of Living Tissues, *Journal of Applied Mechanics* **49**, 464-465, 1982.

[64] O. ELLERS *et al.* Soft skeletons transmit force with variable gearing, *Journal of Experimental Biology* **227**, jeb246901, 2024.

[65] T. PO *et al.* Gearing in a hydrostatic skeleton: the tube feet of juvenile sea stars (*Leptasterias sp.*), *Journal of Experimental Biology* **227**, jeb247804, 2024.

[66] G. CHAPMAN, The Hydrostatic Skeleton in the Invertebrates, *Biological Reviews* **33**, 338-371, 1958.

[67] W.M. KIER, The diversity of hydrostatic skeletons, *Journal of Experimental Biology* **215**, 1247-1257, 2012.

[68] J.E. SMITH, The mechanics and innervation of the starfish tube foot-ampulla system, *Philosophical Transactions of the Royal Society of London. Series B, Biological Sciences* **232**, 279-310, 1946.

[69] E. HENNEBERT *et al.* Evaluation of the different forces brought into play during tube foot activities in sea stars, *Journal of Experimental Biology* **213**, 1162-1174, 2010.

[70] J.E. SMITH, The Activities of the Tube Feet of *Asterias Rubens* L : I. The Mechanics of Movement and of Posture, *Journal of Cell Science* **88**, 1-14, 1947.

[71] R.S. MCCURLEY & W.M. KIER, The functional morphology of starfish tube feet: the role of a crossed-fiber helical array in movement, *The Biological Bulletin* **188**,197-209, 1995.

[72] H. LEDDY & A. JOHNSON, Walking versus breathing: mechanical differentiation of sea urchin podia corresponds to functional specialization, *The Biological Bulletin* **198**,88-93, 2000.

[73] O. ELLERS *et al.* Kinematics of sea star legged locomotion, *Journal of Experimental Biology* **224**, jeb242813, 2021.

[74] J.M. SMITH & R.J.G. SAVAGE, Some locomotory adaptations in mammals, *Zoological Journal of the Linnean Society* **42**, 603–622, 1956.

[75] T. PO *et al.* Cooperative transport in sea star locomotion, *Current Biology* **34**, 2551-2557.e4, 2024.

[76] S. GRILLNER & P. WALLEN, Central Pattern Generators for Locomotion, with Special Reference to Vertebrates, *Annual Review of Neuroscience* **8**, 233-261, 1985.

[77] A.E. HOPKINS, On the physiology of the central nervous system in the starfish, *Asterias tenuispina*, *Journal of Experimental Zoology* **46**, 263-275, 1926.

[78] M.W. MOFFETT, Cooperative food transport by an Asiatic ant, *National Geographic Research* **4**, 386-394, 1988.

CHAPTER 3

GOALS AND STRATEGIES

Sea stars exhibit remarkable mobility, engaging in behaviors such as foraging and climbing over rocky substrates. This locomotion is powered by numerous tubular adhesive structures, known as tube feet or podia, distributed across the oral surface and connected to the water vascular system. Their motion, achieved through the sequential extension, flexion, and retraction of their stem, occurs in the absence of a centralized brain. Although the morphology and internal architecture of sea star tube feet are well described, the biomechanical principles and control mechanisms underlying their role in locomotion remain incompletely understood.

This PhD Thesis aims to elucidate the dynamic principles governing the biomechanics and control of tube feet in the sea star species *Asterias rubens* and *Marthasterias glacialis*. Specifically, it investigates how tube feet adhesion time regulates crawling speed in response to varying mechanical demands, including changes in body size, external loading, and orientation relative to gravity, in the absence of a centralized nervous system.

In this context, we developed a high-resolution optical imaging technique based on frustrated total internal reflection (FTIR), allowing real-time visualization and quantification of tube feet adhesion. Coupled with image thresholding analysis, this approach enabled precise tracking of the timing, spatial position, and contact area of individual tube feet during locomotion across a range of body sizes in both species.

In contrast to many other animal groups, sea stars exhibit considerable interspecific and intraspecific variability in the relationship between body size and locomotor speed. However, morphological traits such as arm length and disc surface area exhibit consistent allometric scaling with body mass. The first section of this thesis focuses on quantifying these scaling relationships to elucidate the biomechanical and morphological factors underlying sea star locomotion. Specifically, we investigate which morphological parameters influence crawling speed and characterize the dynamics of tube feet function. To this end, we conducted comprehensive morphometric and functional scaling analyses to examine how body mass and arm length relate to tube feet number, contact area, and adhesion time.

We examined individuals across a broad size range to establish scaling laws to inform how mechanical output scales with morphology. To further investigate adhesion dynamics, high magnification videos of the ambulacral groove were recorded.

Recent studies have explored how external environmental factors, such as water currents, light, and body orientation, affect sea star locomotion, offering a deeper understanding of the mechanisms that control their locomotion. In the second part of this thesis, we investigated the adaptive responses of sea stars to controlled external perturbations, intending to quantify their effects on adhesion dynamics and overall locomotor performance. Two experimental perturbations were implemented. First, we assessed the impact of increased body mass by attaching custom-designed 3D-printed backpacks that augmented the animal's mass by 25% and 50%. Second, we evaluated locomotor behavior under gravitational inversion by placing individuals in an upside-down orientation. These experiments were designed to determine how such perturbations affect key locomotor parameters, including crawling speed, the percentage of tube feet in adhesion, and the adhesion time.

Finally, due to the interdisciplinary nature of this work, we wanted to integrate a biomechanical model to corroborate the locomotion mechanisms we observed in the perturbation experiments. To this end, we collaborated with Professor Eva Kanso from the University of Southern California, who adapted a previously established decentralized tube feet control model to simulate crawling dynamics under both normal and perturbed conditions. The model treats the sea star as a rigid body propelled by individual tube feet that follow local feedback rules based on shear force direction and tube feet stretch.

CHAPTER 4

MATERIAL AND METHODS

4.1 Sea stars collection and maintenance

Specimens of *Asterias rubens* Linnaeus, were collected manually during low tide from the wave breakers at Knokke-Heist, Belgium (Fig. 4.1). *Marthasterias glacialis* specimens were hand-collected at the Concarneau marine station, France, during low tide.

Figure 4.1: *The rocky wave breakers at Knokke-Heist (Belgium) during low tide. Asterias rubens are attached strongly to the mussel colony on the wave breakers.*

Upon collection, specimens were transported to the University of Mons, where they were maintained in 1500-litre recirculating seawater aquaria located in the Biomarine Laboratory. The aquaria conditions were regulated at 13-15°C and salinity around 30-33 psu. Salinity levels were monitored and adjusted using a precision refractometer (ATC-S/Mill-E, accuracy ± 0.2%). The sea stars received fresh mussels (*Mytilus edulis* L.) as weekly food. To minimize stress

and allow for acclimatization, all individuals were kept in these conditions for at least two weeks before performing locomotion trials [1]. Locomotion trials were conducted in an experimental glass aquarium, where seawater temperature was maintained at 15°C and salinity was set to 33 psu.

It is important to note that different cohorts of animals were used throughout the study to avoid potential artifacts due to long-term aquarium maintenance. Sea stars were hand-collected at multiple time points during the course of the thesis. After each collection, individuals were weighed, measured, and their tube feet counted. They were then maintained in aquaria for a short acclimation period of two weeks prior to experimentation, ensuring comparable physiological conditions across specimens.

In total:

- 25 *Asterias rubens* collected in March 2021 were used for locomotion experiments.
- To complement these, 15 *A. rubens* collected in February 2022 were added.
- A combined dataset of 74 *A. rubens* (March 2021 + February 2022) was analyzed to establish the relationship between mass and arm length.
- Specimens collected in October 2023 were divided into two groups: 5 for mass-addition ("backpack") experiments and 6 for inverted locomotion trials.
- 15 *Marthasterias glacialis* collected in March 2023 were used to compare locomotion performance with *A. rubens.*
- An additional 10 *M. glacialis* collected in March 2024 were used for traction force microscopy (TFM) experiments.

Thus, each experimental dataset was obtained from freshly collected individuals, not from animals kept in aquaria for extended periods. This strategy eliminates the risk of artifacts linked to long-term captivity, such as reduced tenacity or depletion of adhesive secretions.

All *Asterias rubens* specimens used to determine the relationship between body mass and arm length were collected in February and March, which corresponds to the same stage of gonadal maturation and gamete accumulation prior to spawning (see [2]). Specimens collected in October, corresponding to the post-spawning recovery phase, were not included in this dataset. Therefore, variation in gonadal development did not confound our morphometric analyses.

The six additional species (*Asterina gibbosa*, *Echinaster sepositus*, *Linckia laevigata*, *Patiria miniata*, *Dermasterias imbricata*, and *Pentaceraster mammillatus*) were obtained from the aquariology department of the Nausicaá Aquarium. For these specimens, we recorded only morphometric data (mass and arm length); locomotion experiments were not conducted. Consequently, the duration of aquarium maintenance is not relevant to our analyses. All animals were kept under professional husbandry conditions with appropriate water flow, aeration, and diet.

4.2 Frustrated Total Internal Reflection

Frustrated total internal reflection (FTIR) has been a subject of scientific investigation since the early work of Newton and Fresnel [4]. Before delving into the principles and mechanisms underlying FTIR, it is essential first to discuss the fundamental phenomena of refraction and total internal reflection (TIR). Refraction is an optical phenomenon that occurs when light passes from one medium to another at an oblique angle, provided the two media have different refractive indices or optical densities. The change in the propagation speed of light between the two materials results in a bending of the light path at the interface (Fig. 4.2). According to the Snell-Descartes law, this relationship is described as:

$$n_1 sin\theta_1 = n_2 sin\theta_2 \tag{4.1}$$

where n_1 and n_2 are the refractive indices of the first and second medium, respectively, and θ_1 is the angle of incidence and θ_2 the angle of refraction.

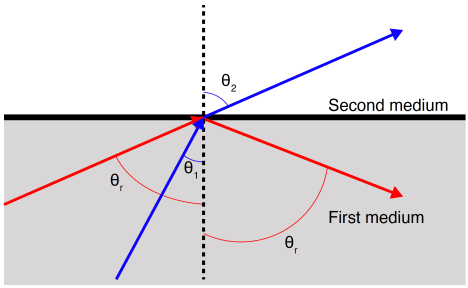

Figure 4.2: *Schematic representation of refraction (in blue) and total internal reflection (in red). Adapted from [5].*

When the incidence angle (θ_1) exceeds a critical angle ($\theta_c = arcsin(n_2/n_1)$), total internal reflection occurs: light is no longer transmitted into the second medium but is instead entirely reflected into the first medium, preserving the angle of incidence. During TIR, a phenomenon known as evanescent wave generation occurs. These non-propagating waves are formed at the interface between two media where TIR occurs. When an object is positioned nearby, it results in the transmission of light energy. Depending on the optical properties of the object, this transmitted light may be absorbed, reflected, refracted, or scattered [5]. The intensity of evanescent waves decreases exponentially with the distance z from the interface:

$$I_z = I_0 \exp\left(-\frac{z}{d}\right) \tag{4.2}$$

Where I_z is the intensity at distance z of the interface, I_0 is the intensity at the interface (z=0), and d is the penetration depth of the evanescent waves.

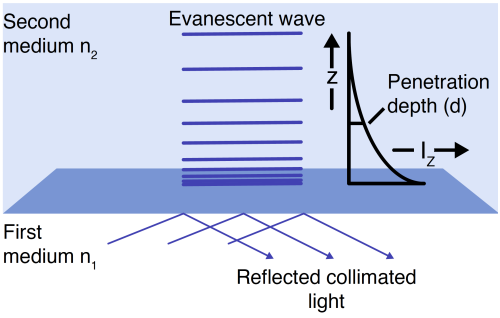

Figure 4.3: *Schematic representation of an evanescent field intensity decays exponentially with increasing distance from the interface. Adapted from [6].*

The penetration depth (Fig. 4.3), characteristic of the decrease in intensity, is influenced by several factors, including the wavelength of the incident light (λ_0), the angle of incidence (θ_1), and the refractive indices of both media (n_1 and n_2) [7]:

$$d = \frac{\lambda_0}{4\pi\sqrt{n_1^2 \sin\theta_1 - n_2^2}} \tag{4.3}$$

FTIR-based imaging has been developed to measure the contact areas of adhesive pads during locomotion, but its use has mainly focused on mammalian cells, tree frog climbing, stress distribution in gecko toes, and various insect species [8, 9, 10, 11, 12]. In this thesis, to visualize the contact between sea star tube feet and the substrate, we utilized a custom aquarium made of high refractive index glass ($n_1 = 1.52$) equipped with an LED strip at its base (Fig. 4.4) to reproduce the principle of frustrated total internal reflection. Under normal conditions, light traveling through the glass undergoes total internal reflection when it reaches the glass-seawater interface ($n_2 = 1.34$) at an angle exceeding the critical value, effectively "trapping" the light within the glass. However, when an object comes into close contact with this surface, it alters the local refractive index, allowing light to escape and diffuse into the second medium (Fig. 4.5).

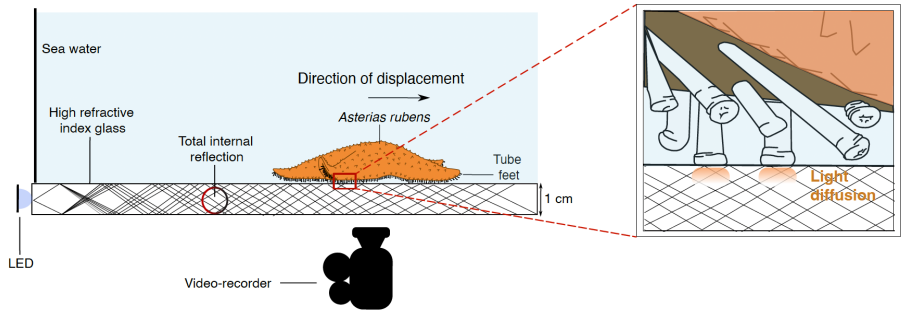

Figure 4.4: *(A)Schematic representation of the experimental device employing the principle of frustrated total internal reflection (FTIR). Sea stars are allowed to crawl, and their movements are recorded using a camera placed beneath the aquarium. The inset provides a close-up view of an Asterias rubens arm, where contact points of individual tube feet with the substrate are visible during locomotion (arrow).*

As shown in (Fig. 4.5) for fingerprints, when a tube feet makes close contact with the glass, the local interaction between the evanescent waves and the adjacent tube feet illuminates only the tube feet in contact with the interface, while the other zones remain dark. This TIRF-based setup enabled illumination of the tube feet contact area, resulting in bright spots at sites of adhesion.

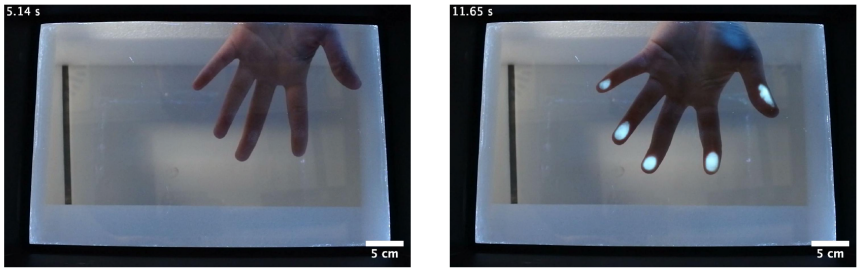

Figure 4.5: *Demonstration of our total internal reflection-based system using human fingertips. Bright contact points appear where fingers touch the surface, illustrating the principle of frustrated total internal reflection.*

In the inverted locomotion experiments, individuals of *A. rubens* were allowed to walk upside down on a high refractive index glass plate equipped with an FTIR-based system. Locomotion was recorded using a Nikon 1 J5 camera with a 1 Nikkor 10-30 VR lens positioned above the plate to visualize their altered movement during inverted locomotion (Fig. 4.6).

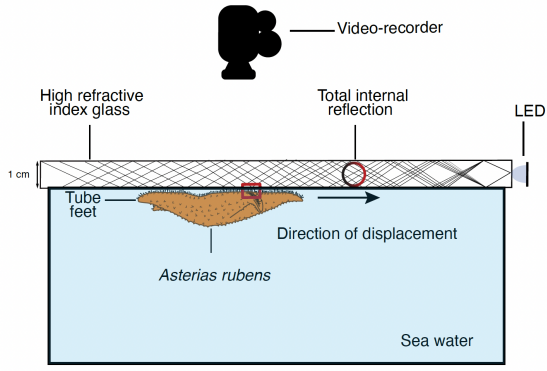

Figure 4.6: *(A) Schematic of the experimental setup used to assess inverted locomotion. (B) Photography of our inverted set-up. Sea stars were allowed to crawl upside down, with their oral surface recorded from above using a camera positioned over the aquarium.*

The glass experimental aquarium and the glass plate were custom-built by Poisson d'Or (Estaimpuis, Belgium), and the slate plate was purchased from Brico Planit. As expected, a thin biofilm formed upon immersion in seawater [13]. To prevent the development of thick biofilms that could affect adhesion or optical clarity, seawater was replaced daily with fresh, aerated water from the housing aquaria which were maintained in a temperature-controlled room at 15 °C, ensuring stable experimental conditions throughout.

4.3 3D-printed backpack

In order to carry out perturbation experiments to modulate the mass of starfish, we used 3D printers. 3D printing, also known as additive manufacturing (AM), was first described by Charles Hull in 1986 [14]. This method is used to make a 3D solid object, often with a complex shape. These objects are typically constructed layer by layer from a 3D digital model using a 3D printer [15]. To begin, a 3D computer model of the mesh is created using computer-aided design (CAD) software [16]. This model is converted into an STL (Surface Tessellation Language) file. The mesh data will be converted into a build file composed of 2D layers, which will then be sent to the 3D printer for fabrication [17].

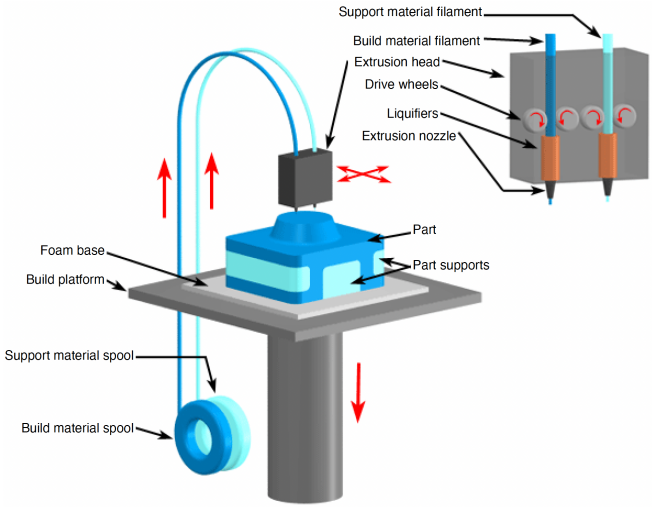

Figure 4.7: *Schematic of the fused deposition modeling [3].*

There are several categories of 3D printing devices, but the most common is fused deposition modeling (FDM for short, Fig. 4.7). Due to their low melting temperature, thermoplastics such as PC, ABS resin, and PLA are widely used. The melting temperatures of various polymers are available in the printer program. This type of 3D printer controls the amount of material extruded from the nozzle. The built platform is movable and will go down the z-axis as the object is created. The extrusion nozzle, on the other hand, moves along the x and y axes.

In this thesis, backpack 3D meshes were designed using Autodesk Fusion 360 for added mass locomotion experiments. They were 3D printed using an Ultimaker S5 3D printer with PLA filament. They were securely attached to the sea stars using veterinary glue (Vetbond, 3M Deutschland GmbH). Locomotion was recorded under three conditions: with an empty backpack and with additional mass equivalent to 25% and 50% of the sea star's body mass. Stainless steel marbles were used to provide the additional mass (Fig. 4.8). For each condition, movements were recorded for 20 seconds in the same setup as the experiments without backpacks.

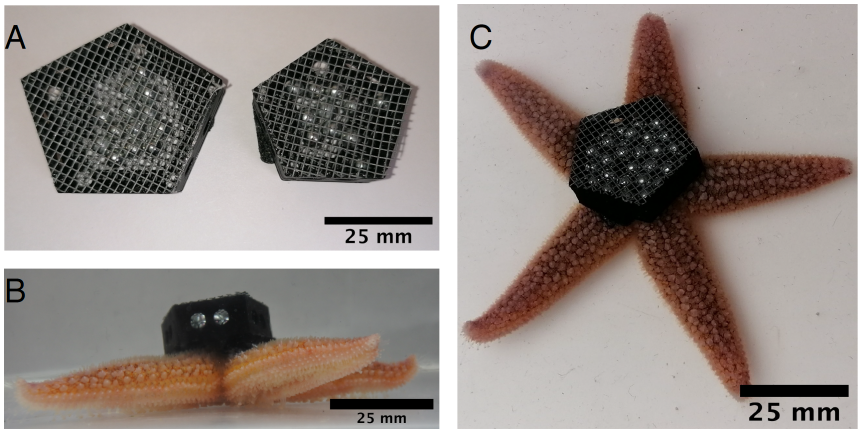

Figure 4.8: *(A) Top view of the backpacks filled with stainless beads. (B) Side view and (C) aboral view of Asterias rubens equipped with the backpack.*

4.4 Detachment trials

To measure detachment forces, we developed a custom setup in which individuals were supported by a 3D-printed harness connected to a traction bench (Zwick Roell) via a nylon string (Fig. 4.9). After a ≈ 10 seconds acclimation, the traction bench pulled at a constant speed of 1 mm/s while forces were continuously recorded, generating force–displacement curves for each trial. These tests were performed on glass substrates, and slate was used only for locomotion speed comparisons.

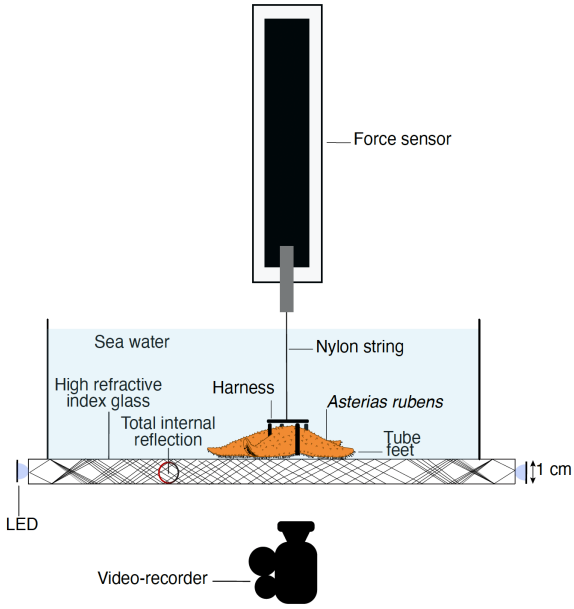

Figure 4.9: *Schematic of the experimental setup used to measure detachment force from a glass surface using a force sensor.*

4.5 Image analysis

4.5.1 Morphological parameters

To quantify sea stars' size and morphological characteristics, high-resolution images of the oral surface were captured in seawater before each experiment. The imaging was performed with a Nikon 1 J5 camera equipped with a 1

NIKKOR 10-30 VR lens. The sea star's average arm length was calculated as the mean of the distances from the central mouth to the tip of each of the five arms. The arms were labeled clockwise as a, b, c, d, and e. We characterized the leading arm labeled "a" as it is the arm oriented with the direction of sea star locomotion. The "a" arm serves as a reference for studying angular arrangements. (Fig. 4.10).

After gently blotting the oral surface to remove excess water [19], each specimen was weighed in seawater using a tared beaker on a digital balance (KERN PCB 3500-2). The submerged mass was read directly on the display with a precision of 0.01 g. No further corrections or calculations were necessary. This method ensures accurate and reproducible values for submerged body mass.

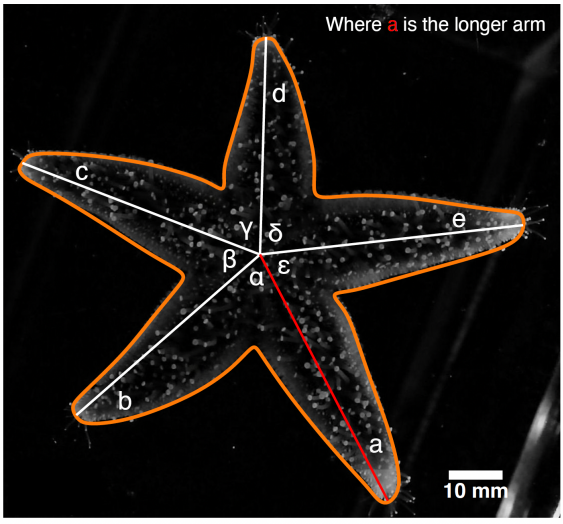

Figure 4.10: *Photograph of the aboral surface of A. rubens showing the labeled assignment of each arm and the corresponding angles. The orange outline is the area of the oral surface (mm^2). The scale bar is 10 mm.*

All images and videos were analyzed in Fiji (https://imagej.nih.gov/ij/, Rasband, W.S., ImageJ, U.S. National Institutes of Health, Bethesda, Maryland, USA, 1997-2018). A ruler with 1-mm graduations was included in the field of view during recordings to establish the reference scale, which was then applied in Fiji to convert pixel distances into millimeters. The calibration uncertainty

is estimated at ±0.5 mm, ensuring reliable morphometric and locomotion measurements.

To assess the number of tube feet per arm, individuals were anaesthetised in a 3.5% magnesium chloride solution in seawater for ten minutes to induce relaxation of the tube feet [20]. Then, three arms were randomly selected, and the number of tube feet was counted to obtain representative data on their distribution. Images were analyzed using Fiji. Relaxation with magnesium chloride is a preferred treatment for specimens to be used for histological analysis or scanning electron microscopy of soft tissues, and is ideal for many echinoderms[21]. Individuals are transferred from seawater directly into a container with a magnesium chloride solution isotonic with seawater. The effect of these chemicals is reversible; individuals recover from anaesthesia when returned to seawater. Care must be taken to ensure that salinity and temperature are the same [22].

4.5.2 High magnification videos

The dynamic of tube feet adhesion was analyzed by recording high magnification videos of the oral surface of *A. rubens* during locomotion. A high magnification video was recorded on the same day and in the same setup to characterize tube feet adhesion (mean adhesion time, mean tube feet contact area). For each sea star, 15 tube feet were examined during locomotion, randomly selected from the oral surface.

These videos were captured using a Nikon D90 camera equipped with an AF-S Nikkor 105 mm lens. For these recordings, tube feet adhesion time, contact area and the circularity index (CI) were precisely measured, providing detailed insights into adhesion dynamics in Fiji. The circularity index is determined as:

$$\mathrm{CI} = 4\pi \times \left(\frac{\mathrm{A}}{P^2}\right) \tag{4.4}$$

Where A is the area of the shape and P is the perimeter. $0 \leq CI \leq 1$

Tube feet were manually tracked in Fiji. Adhesion time was defined as the interval between the first visible contact with the substrate and subsequent

detachment. Videos were recorded at 25 fps, giving a timing precision of ±1 frame, i.e., ≈ ± 0.04 s. This resolution is sufficient to accurately capture the range of adhesion times observed (3–20 s).

Using the Manual Tracking plug-in, which provided (x,y) positions at 0.25 seconds intervals along with the corresponding instantaneous velocities, tube feet detachment speed was calculated directly from these trajectories. The measurement precision is determined by the spatial calibration (≈ ±0.5 mm) and the temporal resolution (0.25 s), ensuring reliable estimates of tube feet velocity.

The lateral-view videos were produced only for illustrative purposes and were not used for quantitative analyses.

4.5.3 Sea star locomotion

The oral surface of sea stars was recorded using a Nikon 1 J5 camera equipped with a 1 NIKKOR 10-30 VR lens positioned beneath the aquarium to capture movement dynamics. Each specimen was carefully placed at the center of the aquarium floor and allowed to acclimate. Once the sea star initiated locomotion, its movement was recorded for around 20 seconds (Fig. 4.11).

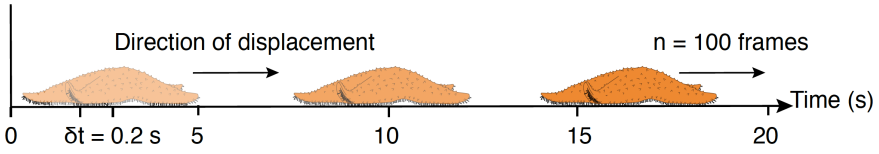

Figure 4.11: *Displacement of sea stars is recorded over 20 seconds, with the number of tube feet in contact and the total contact area measured every 0.2 seconds.*

To evaluate the locomotion performance, the instantaneous locomotion speed was calculated by dividing the displacement D by the time required to move between two successive positions (x_1, y_1) and (x_2, y_2):

$$\sqrt{(x_2 - x_1)^2 + (y_2 - y_1)^2} = D \tag{4.5}$$

We developed a method divided into three main steps for image processing and thresholding (Fig. 4.12) with Fiji to obtain the number of tube feet in contact during locomotion. This method involves processing video frames by enhancing contrast, isolating adhesion sites, and quantifying contact area over time (Fig. 4.12).

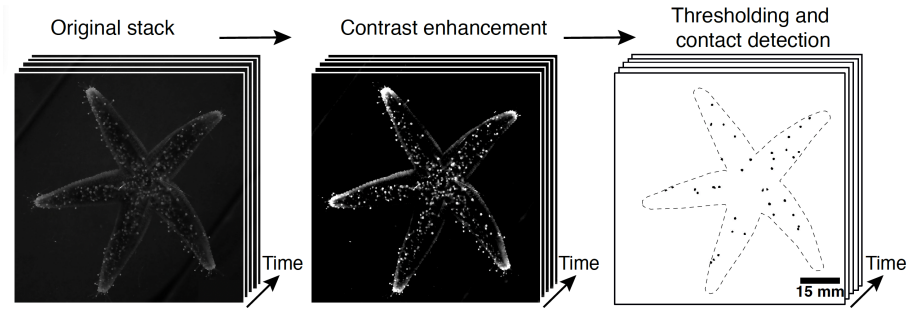

Figure 4.12: *Image analysis pipeline developed in Fiji (ImageJ) to detect tube feet in contact during A. rubens locomotion. From left to right: raw video, contrast-enhanced video, and thresholded video showing detected tube feet as black dots.*

To enhance image contrast, background noise was reduced using a rolling ball algorithm with an optimized radius, followed by manual adjustment of brightness and contrast across the image stack. For the thresholding process, the Intermodes method was employed, and the threshold values were fine-tuned accordingly. Subsequently, contact detection was performed by analyzing the contact area (in mm^2) and the circularity index of tube feet, previously obtained from high magnification video recordings. These parameters were input into the "Analyze Particles" function. By visualizing the resulting binary mask, this approach enabled the quantification of tube feet in contact with the substrate and the corresponding total contact area during locomotion:

$$\text{Total contact area} = \sum(\text{Area of the tube feet in contact}) \tag{4.6}$$

Finally, the percentage of tube feet engaged in substrate contact throughout movement was calculated using the following equation:

$$\text{Percentage of tube feet in contact} = \left(\frac{\text{Number of tube feet in contact}}{\text{Total number of tube feet}}\right) \times 100 \tag{4.7}$$

4.6 Allometric studies

In allometric studies, two key points are essential to consider when analyzing log-log plots. First, if the data form a straight line on a log-log plot, this indicates a power-law relationship between the two variables. Such a relationship can be expressed mathematically as:

$$Y = aX^b, \tag{4.8}$$

where Y is the dependent biological trait, X is the independent variable (often body mass), a is a proportionality constant, and b represents the scaling exponent. The parameter b indicates how Y scales regarding X, and is the key quantity of interest in allometric analyses.

Second, the slope of the linear fit in a log-log plot corresponds to the scaling exponent b. This can be seen by taking the logarithm of both sides of the power-law equation, leading to

$$\log Y = \log a + b \log X, \tag{4.9}$$

In this linearized form, $\log Y$ is plotted against $\log X$, the slope of the line is b, and the intercept is $\log a$. The value of b provides quantitative insight into how one biological trait scales relative to another, forming the basis for interpreting allometric relationships [23, 24, 25, 26].

In this thesis, we investigated two kinds of power-law allometric relationships. First, we analyzed sea star arm length L (mm) as a function of body mass M (g). Assuming that mass scales with volume, we have:

$$M \sim L^3 \tag{4.10}$$

From this, it follows that the arm length scales with mass as:

$$L \sim M^{1/3} \tag{4.11}$$

Taking the logarithm of both variables linearizes the relationship in log-log space (Eq. 4.9), where the slope corresponds to the scaling exponent b, we expect $b = 1/3 \approx 0.33$ under isometric conditions.

Scaling type	Scaling exponent b	Implication
Positive allometry	> 0.33	L increases faster than M
Isometry	~ 0.33	L increases at the same rate as M
Negative allometry	< 0.33	L increases slower than M

Table 4.1: *Scaling types for sea star arm length L as a function of body mass M and their implications.*

The second power-law allometric relationship studied was the mean tube feet contact area A (mm^2) as a function of their mass M (g). Assuming that mass scales with volume, we have :

$$M \sim L^3 \tag{4.12}$$

Considering that the mean tube feet contact area (a 2D trait) scales with a surface, we have:

$$A \sim L^2 \tag{4.13}$$

From this, it follows that the mean tube feet contact area with mass as:

$$A \sim M^{2/3} \tag{4.14}$$

Taking the logarithm of both variables linearizes the relationship in log-log space (Eq. 4.9), where the slope corresponds to the scaling exponent b, we expect $b = 2/3 \approx 0.67$ under isometric conditions.

Scaling type	Scaling exponent b	Implication
Positive allometry	> 0.67	A increases faster than M
Isometry	~ 0.67	A increases at the same rate as M
Negative allometry	< 0.67	A increases slower than M

Table 4.2: *Scaling types for mean tube feet contact area A as a function of their mass M and their implications.*

4.7 Statistical analysis

All significance values were computed statistically and not inferred from graphical representation. Statistical analyses were performed in Prism 10.0 (GraphPad Software, Inc.) using the appropriate tests as specified in the figure legends. Box plots were chosen over bar charts to better represent data distributions, as they display medians, quartiles, spread, and potential outliers, thereby providing a more accurate view of variability [27]. The underlying statistical models, including sample sizes and degrees of freedom, are fully reported, ensuring that replication structure and test validity can be independently verified. Every set of data was tested for normality test using the D'Agostino-Pearson test in Prism 10.0 (GraphPad Software, Inc.), which combines skewness and kurtosis tests to test whether the shape of the data distribution was similar to the shape of a normal distribution. When different populations of sea stars were compared across conditions, independent-sample tests (Mann–Whitney) were appropriate. In contrast, when the same individuals were tested across conditions, a repeated measures one-way ANOVA or a paired t-test was used. Statistical tests are indicated in each figure legend for clarity.

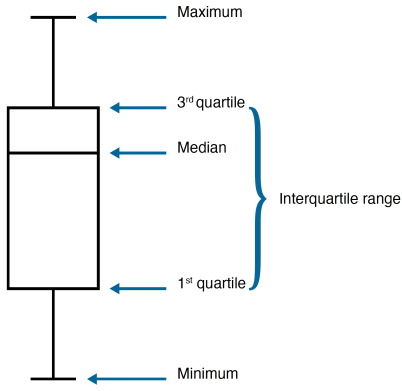

Figure 4.13: *Schematic representation of a box plot diagram with the four different regions.*

Box plot provides a comprehensive overview of the data distribution by illustrating key statistical indicators such as the median, quartiles, and overall range (Fig. 4.13). Although box plots do not reveal the distribution details, they effectively identify asymmetries within the dataset. The distribution is

divided into four equally sized intervals, each representing 25% of the data. The quartile-based diagram facilitates immediate interpretation of the dataset's central tendency, overall spread, and variability.

- The upper (3rd quartile) and lower (1st quartile) quartiles are the ends of the rectangle;
- The interquartile gap (3rd quartile - 1st quartile = interquartile range) corresponds to the rectangle;
- The horizontal line inside the rectangle is the median;
- The minimum and maximum values of the distribution are the two lines located outside the rectangle.

Locomotion was recorded three times per individual on the same day and under identical conditions to compute the mean crawling speed. In addition, a high-magnification video was recorded on the same day and set up to characterize tube foot adhesion (mean adhesion time and contact area). For each sea star, 15 tube feet were analyzed during locomotion, randomly selected from the oral surface. In some cases, locomotion of the same individuals was also recorded on different days. Still, these trials showed no significant difference in crawling speed, indicating that repeated measurements did not bias the results.

Linear regressions were used to analyze allometric scaling, to assess the relationship between average arm length and body mass, and to investigate the relationship between crawling speed and various parameters. Unless otherwise stated, all data are presented as mean ± standard deviation (s.d.). The confidence interval in all experiments was 95%.

A detailed description of statistical parameters is included in all figure captions, with *p $<$ 0.05, **p $<$ 0.01, ***p $<$ 0.001, ****p $<$ 0.0001, and n.s. indicating non-significant results. The p-value is a statistical value that ranges from 0 to 1. It quantifies the probability of obtaining results at least as extreme as those observed, assuming that the null hypothesis (the claim that there's no effect in the population) is true [28].

In other words, it evaluates how compatible the observed data are with the assumption that there is no true effect or difference, for example, that a regression coefficient equals zero or that the means of two groups are identical. A very small p-value indicates that such extreme results would be highly unlikely under the null hypothesis, providing evidence against it [29].

BIBLIOGRAPHY

[1] M. MORIN *et al.* Captivity induces a sweeping and sustained genomic response in a starfish, *Molecular Ecology* **32**, 3541-3556, 2023.

[2] MarLIN. *Asterias rubens.* Accédé le 6 avril 2025.https://www.marlin.ac.uk/species/detail/1194.

[3] CustomPartNet *Fused Deposition Modeling.* Accédé le 6 avril 2025. https://www.custompartnetcom/wu/fused-deposition-modeling.

[4] S. ZHU *et al.* Frustrated total internal reflection: A demonstration and review, *American Journal of Physics* **54**, 601-607, 1986.

[5] M. A. HASHEMI *et al.* Analysis of particle contact using frustrated total internal reflection, *Meccanica* **54**, 653-665, 2019.

[6] K.N. FISH, Total Internal Reflection Fluorescence (TIRF) Microscopy, *Current Protocols in Cytometry* **50**, 12-18, 2009.

[7] F.d FORNEL *et al.* Evanescent Waves: From Newtonian Optics to Atomic Optics, *Springer Science & Business Media* 2001.

[8] I.D.C. HILL *et al.* The biomechanics of tree frogs climbing curved surfaces: a gripping problem, *Journal of Experimental Biology* **221**, jeb.168179, 2018.

[9] E.V. EASON *et al.* Stress distribution and contact area measurements of a gecko toe using a high-resolution tactile sensor, *Bioinspiration & Biomimetics* **10**, 016013, 2015.

[10] J.-H. DIRKS *et al.* Insect tricks: two-phasic foot pad secretion prevents slipping, *Journal of The Royal Society Interface* **7**, 587-593, 2010.

[11] C.J. CLEMENTE *et al.* Jumping without slipping: leafhoppers (Hemiptera: Cicadellidae) possess special tarsal structures for jumping from smooth surfaces, *Journal of The Royal Society Interface* **14**, 20170022, 2017.

[12] C.J. CLEMENTE *et al.* Pushing versus pulling: division of labour between tarsal attachment pads in cockroaches, *Proceedings of the Royal Society B: Biological Sciences* **275**, 1329-1336, 2018.

[13] L.A. THOMAS & C.O HERMANS, ADHESIVE INTERACTIONS BETWEEN THE TUBE FEET OF A STARFISH, LEPTASTERIAS HEXACTIS, AND SUBSTRATA, *The Biological Bulletin* **163**, 675-688, 1985.

[14] C. W. HULL, Method and apparatus for production of three-dimensional objects by stereolithography, *Google Patent*, 1986.

[15] D. LEE *et al.* 3D Microfabrication of Photosensitive Resin Reinforced with Ceramic Nanoparticles Using LCD Microstereolithography, *Journal of Laser Micro/Nanoengineering* **1**, 142-148, 2006.

[16] F. RENGIER *et al.* 3D printing based on imaging data: review of medical applications, *International Journal of Computer Assisted Radiology and Surgery* **5**, 335-341, 2010.

[17] X. WANG *et al.* 3D printing of polymer matrix composites: A review and prospective, *Composites Part B: Engineering* **110**, 442-458, 2017.

[18] A. K. SOOD *et al.* Parametric appraisal of mechanical property of fused deposition modelling processed parts, *Materials & Design* **31**, 287-295, 201O.

[19] E. MONTGOMERY *et al.* Effects of Body Size and Shape on Locomotion in the Bat Star (*Patiria miniata*), *Biological Bulletin* **222**, 222-232, 2012.

[20] C. PUGLIESE *et al.* Effect of Different Formulations of Magnesium Chloride Used As Anesthetic Agents on the Performance of the Isolated Heart of *Octopus vulgaris*, *Frontiers in Physiology* **7**, 610, 2016.

[21] R.S. MCCURLEY & W.M. KIER, The functional morphology of starfish tube feet: the role of a crossed-fiber helical array in movement, *The Biological Bulletin* **188**,197-209, 1995.

[22] G. HENDLER, Collecting, Preserving and Archiving Echinoderms, *Natural History of Los Angeles, Country, Los Angels*, 2004.

[23] T.A. MCMAHON, Size and shape in biology: elastic criteria impose limits on biological proportions, and consequently on metabolic rates, *Science* **179**,1201-1204, 1973.

[24] K. SCHMIDT-NIELSEN, Scaling in biology: the consequences of size, *Journal of Experimental Zoology* **194**,287-307, 1975.

[25] T.A. MCMAHON, On size and life, *New York: Scientific American Library*, 1983.

[26] K. SCHMIDT-NIELSEN, Scaling: why is animal size so important?, *Cambridge university press*, 1984.

[27] M. STREIT & N. GEHLENBORG. Bar charts and box plots, *Nature Methods* **11**, 117-117, 2014.

[28] N.A. LAZAR, The ASA Statement on p-Values: Context, Process, and Purpose, *The American Statistician* **70**,129-133, 2016.

[29] R. HUBBARD & R.M. LINDSAY, Why P Values Are Not a Useful Measure of Evidence in Statistical Significance Testing, *Theory & Psychology* **18**,69-88, 2008.

CHAPTER 5

MORPHOLOGICAL SCALING AND LOCOMOTOR DYNAMICS IN SEA STARS

While the biomechanics of tube feet have been described in echinoderms, the dynamics of their contact formation and breakage during locomotion and the number of tube feet involved in movement have remained largely unexplored. Unlike many animals, sea stars display no straightforward relationship between body mass and crawling speed [1, 2, 3, 4], prompting the need for a deeper examination of the mechanisms underlying their locomotion, especially by focusing on the role of their tube feet [1].

5.1 Scaling in sea stars

First, we focused on the morphology of sea stars of the species *Asterias rubens*, our model species, across a broad size range represented by 24 specimens (Fig. 5.1).

Figure 5.1: *Range of sizes observed in Asterias rubens. The scale bar is 50 mm.*

Looking at morphology, the collected individuals ranged in size from 6 cm to 18 cm in total diameter. The characteristic pentaradial symmetry of *A. rubens* remains consistent across varying sizes (Fig. 5.2), further exemplifying this variability and showcasing the range of sizes analyzed in this thesis.

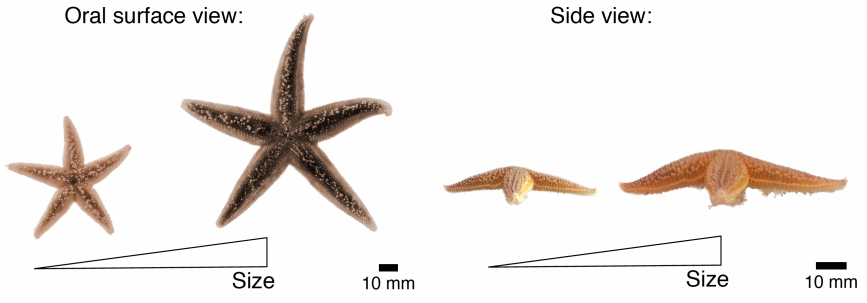

Figure 5.2: *Photographs of the oral and lateral views of two individuals of Asterias rubens illustrating size variability. The scale bar is 10 mm.*

As mentioned in the introduction of this thesis, numerous sea star species exist; therefore, we examined the scaling relationship between body mass and average arm length across eight five-armed sea star species (Fig. 5.3). These measurements were carried out at the Aquariology Department of Nausicaá (Boulogne-sur-Mer, France), thanks to Stéphane Hénard, Renaud Herbert, and Denis Tirmarche, who provided access to various sea star species.

The log-log graph displays a strong positive correlation, supporting the hypothesis that arm length scales predictably with body mass across species[2]. These results also indicate a positive allometry between these two parameters, as the estimated slope was 0.41 ± 0.02 with a 95% confidence interval, indicating that arm length increases at a faster rate than body mass. To reflect isometric growth, arm length should increase in proportion to the expected changes in body mass. Specifically, the expected slope would be 0.33, since length typically scales with the cube root of mass (c.f. Section *"Allometric studies"* in the *Material and Methods*). This observation suggests that smaller species differ in shape from larger species, with the latter possessing disproportionately longer arms.

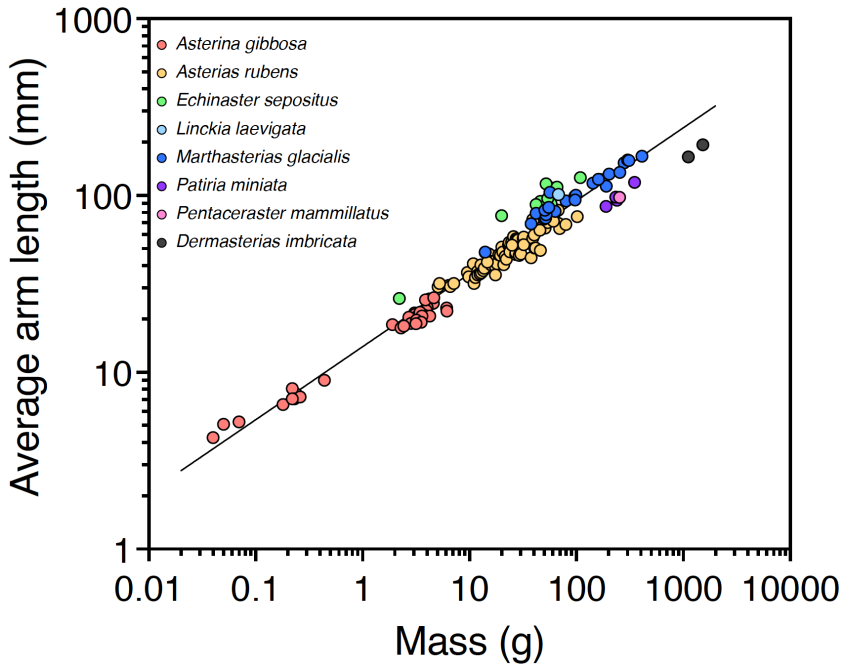

Figure 5.3: *Relationship between the average arm length and the sea star mass across 8 species with 5 five arms: Asterina gibossa (red, n = 37), Echinaster sepositus (green, n=14), Asterias rubens (orange, n=74), Marthasterias glacialis (blue, n=23), Linckia laevigata (light blue, n=2), Patiria miniata (purple, n = 4), Dermasterias imbricata (black, n=2), and Pentaceraster mammillatus (pink, n=1). Each dot corresponds to one individual (n = 157 sea stars,* $R^2 = 0.9541, p < 0.0001$*).*

To assess size-related parameters in *A. rubens*, the average arm length was calculated as the mean of the distances from the central mouth to the tip of each of the five arms. A positive correlation was observed between average arm length and mass of individuals (Fig. 5.4A), indicating that heavier sea stars are predictably larger, consistent with biological scaling principles. The log-log scale (*Supplementary Table 9.1* and *Fig. 9.1A*), indicated an estimated slope of 0.36±0.04 with a 95% confidence interval. This range encompasses the theoretical isometric scaling exponent of 0.33, suggesting that arm length scales approximately isometrically with body mass in *A. rubens*.

We also determined the average number of tube feet per arm across the full range of sea stars with varying masses and showed it increased linearly with size and mass (Fig. 5.4B).

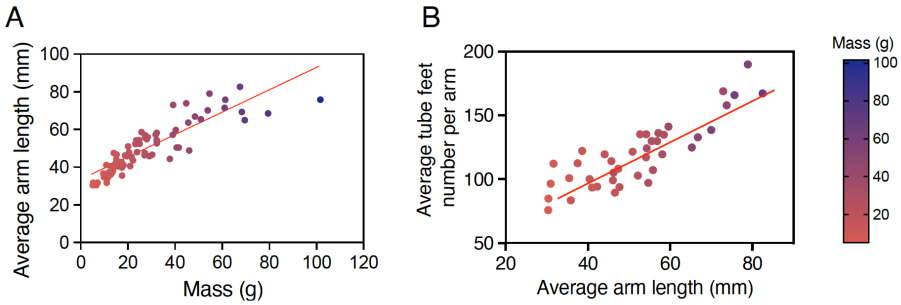

Figure 5.4: *(A) Relationship between the average arm length and mass ($n = 74$, $R^2 = 0.7629, p < 0.0001$). (B) Relationship between the average number of tube feet per arm and the average arm length in individuals of Asterias rubens ($n = 40$, $R^2 = 0.7056, p < 0.0001$). All data are color-coded by individual mass.*

In a comparative approach, we also investigated morphology in another sea star species, *Marthasterias glacialis*, across a broad size range, as the collected specimens ranged in total diameter from 10 cm to 25 cm (Fig. 5.5).

Figure 5.5: *Range of sizes observed in Marthasterias glacialis. The scale bar is 50 mm.*

In the Fig. 5.6, the same positive relationship is observed as in the Fig.5.4 between arm length, body mass, and tube feet number per arm. Concerning the relationship between the arm length and the body mass, the estimated slope in the log-log scale is 0.39±0.04 with a 95% confidence interval (*Supplementary Table 9.1* and *Fig. 9.1B*). This suggests a slightly positive allometric relationship between arm length and body mass in *M. glacialis*. However, the overlapping confidence intervals for the relationships between arm length and body mass in *A. rubens* and *M. glacialis* indicate they exhibit statistically similar scaling laws. It is noteworthy that, when examining the log-log relationship between body mass and arm length across all species (Fig. 5.3), the resulting slope (~ 0.41) indicates positive allometry. In contrast, the species *Asterias rubens* exhibits isometry in this relationship (*Supplementary.A Table 9.1*), with a resulting slope of approximately 0.36. This can reflect a biomechanical constraint in larger species, as they need to maintain similar ranges of motion compared to the smaller ones.

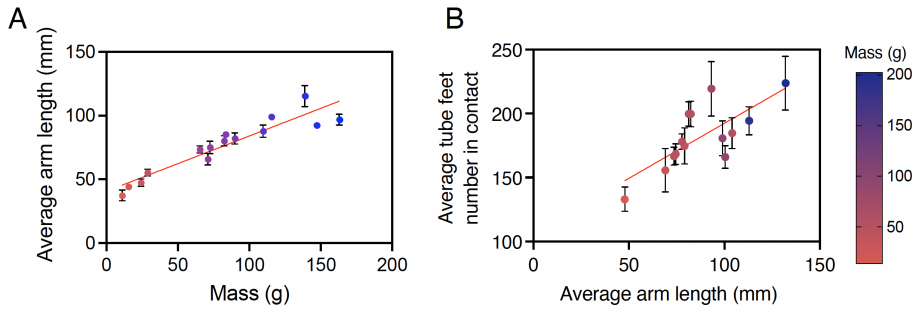

Figure 5.6: *(A)Relationship between the average arm length and mass ($n = 14$, $R^2 = 0.8849$, $p < 0.0001$). (B) Relationship between the average number of tube feet per arm and the average arm length in individuals of Marthasterias glacialis ($n = 14$, $R^2 = 0.4535$, $p < 0.0001$). All data are color-coded by individual mass.*

We next examined whether the pentaradial symmetry in *A. rubens* is maintained during locomotion by labeling the arms in a clockwise manner as a, b, c, d, and e (Fig. 5.7A), using the leading arm "a" as a reference for analyzing angular arrangements.

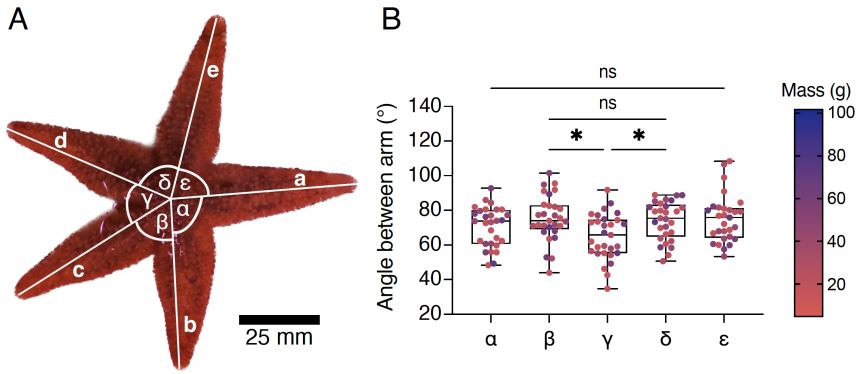

Figure 5.7: *(A) Aboral view of Asterias rubens showing the labeled assignment of arms and the corresponding inter-arm angles. The scale bar is 25 mm. (B) Measurements of inter-arm angles (n = 29 Asterias rubens). All data are color-coded by individual mass. Repeated measures one-way ANOVA were performed, as "each condition" was tested on the same specimens. *p < 0.05, and ns is not significant.*

Interestingly, the angular analysis (Fig. 5.7B) revealed a subtle asymmetry: with the angle (γ) opposite to the leading arm "a" is significantly smaller, 64.9±13.3°, compared to other inter-arm angles. This suggests that although pentaradial symmetry is a defining characteristic of *A. rubens*, minor deviations in arm angles occur and may be functionally associated with locomotion, independently of body size or mass. The observed morphological consistency, along with only minimal angular deviations between arms, may support the activation of tube feet and enhance mechanical stability during movement [5, 6]. Circular statistics are typically used when angles span a wide distribution, ranging from 0° to 360°. In our case, sea star inter-arm angles are constrained around 72±37°. For this reason, we used a repeated-measures one-way ANOVA to compare the experimental results.

5.2 Crawling speed is not correlated with the average number of adherent tube feet

We ensured that glass was a suitable substrate for sea star locomotion essays by performing detachment trials using a force ramp protocol to assess adhesion capabilities. Individuals of *A. rubens* were vertically detached from a glass

surface. The maximum detachment force observed in sea stars (Fig. 5.8) is followed by a sharp decrease, indicating complete detachment from the glass surface. This also means that the sea star was attached strongly beforehand.

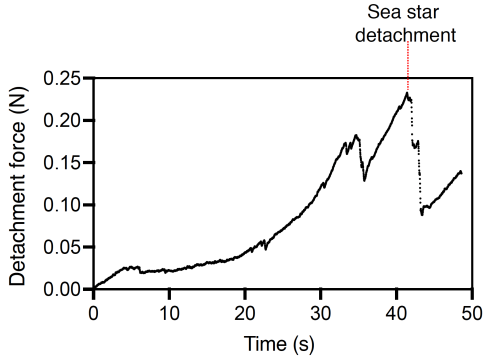

Figure 5.8: *Representative detachment curve showing force as a function of time during the removal of one individual of Asterias rubens from the glass substrate.*

Additionally, we compared locomotion on glass and slate, a rougher, more naturalistic surface for sea stars. Although environmental factors, such as temperature, flow conditions, and substrate inclination, are known to influence echinoderm locomotion [1, 3, 4, 7]. Here, crawling speed did not differ significantly between glass 0.98±0.38 mm/s and slate 1.12±0.22 mm/s surfaces, confirming that glass is an appropriate model surface for studying sea star locomotion (Fig. 5.9).

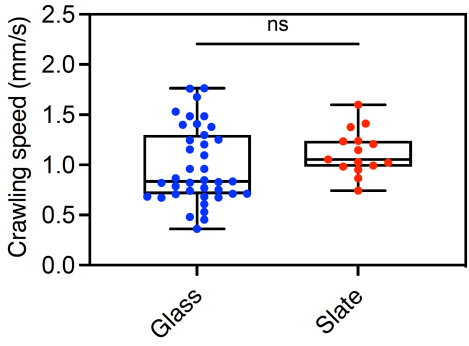

Figure 5.9: *Comparison of crawling speed of Asterias rubens on glass. A Mann–Whitney test was used, since the two groups consisted of different individuals (A. rubens, n = 39 on glass, n = 15 on slate). n.s. not significant.*

As described in the *"Material and methods"*, the locomotion of individual sea stars was recorded over 20 seconds, during which the number of tube feet in contact with the substrate was dynamically monitored as well as the total contact area. These trials revealed that the average number of tube feet in contact (Fig. 5.10A) as well as the total contact area (Fig. 5.10B), two parameters linked together, remained relatively constant during locomotion, with minor fluctuations observed over time. These fluctuations likely reflect the asynchronous and dynamic engagement of tube feet, a characteristic of efficient crawling in echinoderms.

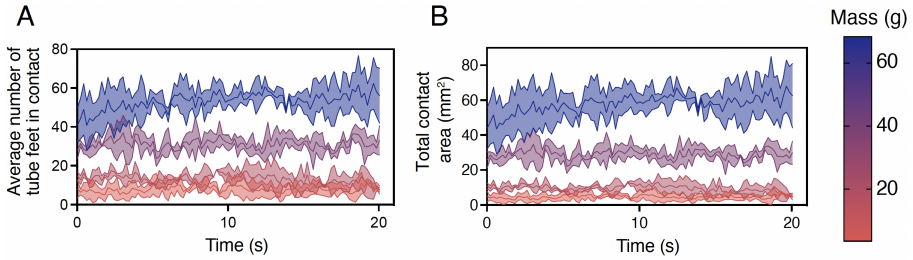

Figure 5.10: *Displacement of Asterias rubens is recorded over 20 seconds, with the average number of tube feet in contact (A) and the total contact area (B) measured every 0.2 seconds (n = 4 Asterias rubens, with their mass from red to blue color: 11.39g, 20.96g, 37.75g and 68.31g).*

A significant finding concerns the linear relationship between the average number of tube feet in contact and body mass, both for *A. rubens* (Fig. 5.11A) and for *M. glacialis* (Fig. 5.12A).

Larger individuals have an increased number of tube feet present on their oral surface, as the radius length scales with body size (Fig. 5.4A). This relationship is consistent with established scaling principles, where morphological traits tend to increase with body mass [1].

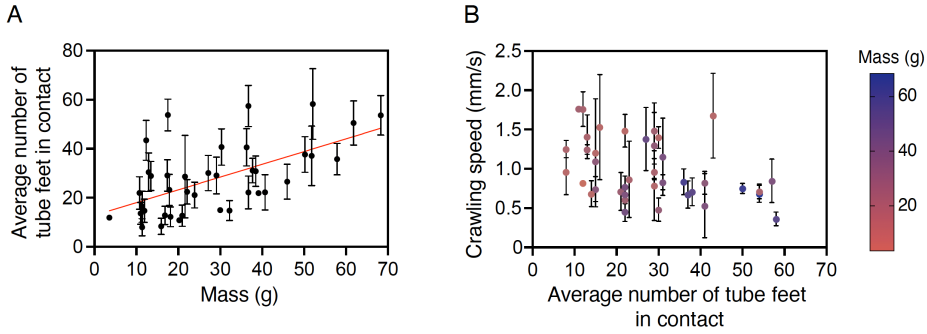

Figure 5.11: *(A) Relationship between the average number of tube feet in contact and mass in Asterias rubens ($n = 39$, $R^2 = 0.3536$, $p < 0.0001$). (B) Evolution of the crawling speed as a function of the average number of tube feet in contact ($n = 39$). All data are presented as mean ± standard deviation (s.d.).*

Interestingly, no significant relationship was found between crawling speed and the average number of tube feet in contact with the substrate in either *A. rubens* (Fig. 5.11B) or *M. glacialis* (Fig. 5.12B), suggesting that sea stars maintain a relatively constant crawling speed regardless of how many tube feet are engaged. Our results show that the average crawling speed of *A. rubens* is 0.98±0.38 mm/s, which is consistent with previous studies 0.8±0.2 mm/s [8]. On the other hand, *M. glacialis* has an average crawling speed of 1.32 ± 0.53 mm/s, which is quite consistent with *A. rubens*.

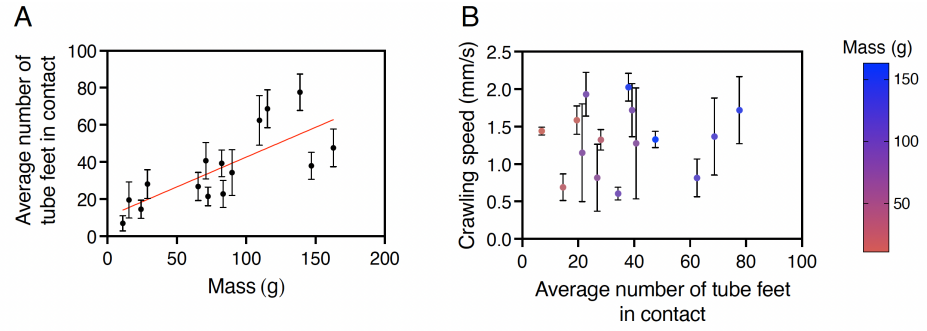

Figure 5.12: *(A) Relationship between the average number of tube feet in contact and mass in M. glacialis ($n = 15$, $R^2 = 0.5711$, $p < 0.0011$). (B) Relationship between the crawling speed and the average number of tube feet in contact during locomotion. All data are presented as mean ± standard deviation (s.d.).*

Despite having a large number of tube feet on their oral surface, only a small fraction of them, typically less than 10% with a slight increase in larger sea stars, is actively used during locomotion (Fig. 5.13A and Fig. 5.14A). This result is consistent with previous observations [9].

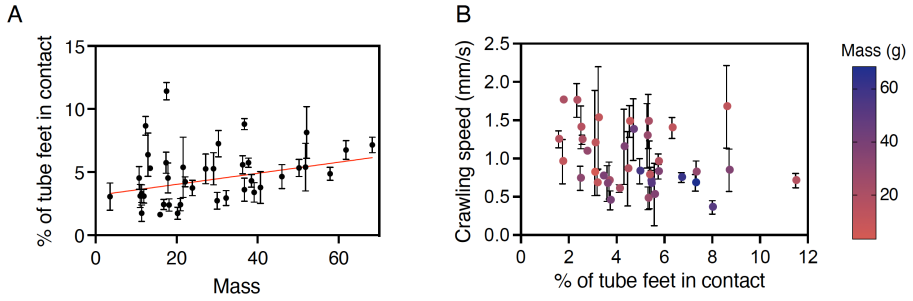

Figure 5.13: *(A) Percentage of tube feet in contact for individuals of Asterias rubens of varying masses ($n = 39$, $R^2 = 0.09263$, $p = 0.0002$). (B) Evolution of the crawling speed as a function of the percentage of tube feet in contact ($n = 39$). All data are presented as mean ± standard deviation (s.d.).*

Furthermore, crawling speed showed no correlation with the percentage of tube feet in contact (Fig. 5.13B and Fig. 5.14B). This apparent constancy may reflect compensatory mechanisms involving tube feet adhesion dynamics, supporting robust locomotion across individuals of varying sizes and species.

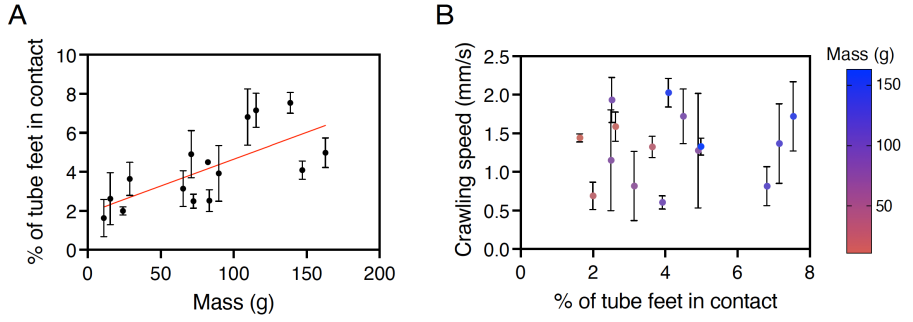

Figure 5.14: *(A) Relationship between the percentage of tube feet in contact and mass in M. glacialis ($n = 15$, $R^2 = 0.4243$, $p < 0.0001$). (B) Relationship between crawling speed and the percentage of tube feet in contact ($n = 15$).*

Surprisingly, we found that crawling speed is not correlated with the percentage or average number of tube feet in contact with the substrate. Even

though larger individuals naturally possess more tube feet, the percentage of them actively engaged in adhesion remains stable across time, suggesting that *A. rubens* uses a constant percentage of its tube feet for locomotion. The lack of dependence on the average number of tube feet in contact further underscores an adaptation that enables sea stars to maintain consistent and efficient locomotion across a variety of surfaces and environmental conditions.

For instance, in *Acanthaster solaris*, locomotion speed is influenced by substrate texture, with slower movement observed on rougher surfaces [4]. In *Patiria miniata*, some individuals possess five or six arms, yet the number of arms has been shown to have no significant effect on crawling speed [1]. Additionally, comparisons across species indicate that sea stars inhabiting tropical environments generally exhibit faster locomotion than those from temperate regions [1], suggesting a significant impact of the environmental conditions on sea stars locomotion.

5.3 Tube feet adhesion time drive adaptive and efficient sea star locomotion

To further investigate adhesion dynamics, high magnification videos of the ambulacral groove and side-view videos were recorded. These recordings provided detailed observations of tube feet dynamics, revealing three distinct stages (Fig. 5.15). The locomotion cycle begins with the attachment stage, during which the tube foot approaches the substrate at an angle, resulting in an elliptical contact shape and a circularity index less than one. This is followed by the adhesion stage, where the tube foot remains firmly attached to the substrate, referred to as the adhesion time, characterized by a circularity index close to one, reflecting a near-perfect circular contact. Finally, in the detachment stage, the tube foot releases from the substrate in preparation for the next movement cycle (Fig. 5.15).

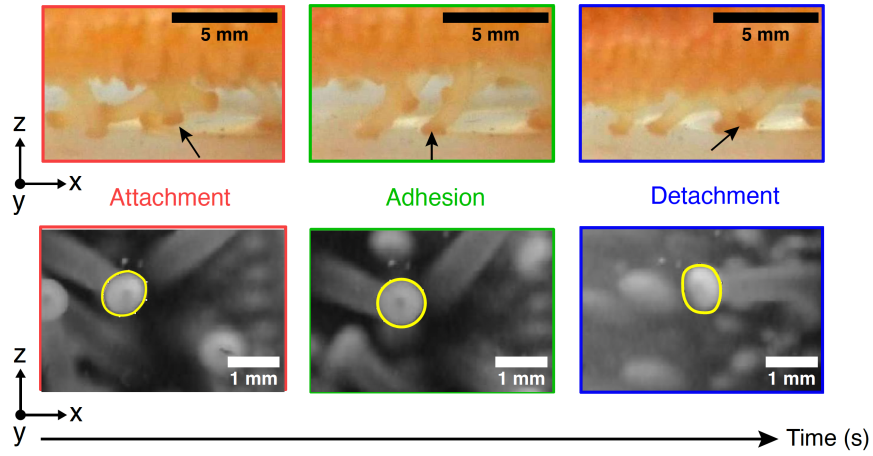

Figure 5.15: *The three stages of tube foot adhesion cycle during locomotion in Asterias rubens, visualized through high magnification videos. The top panels show side views of locomotion, while the bottom panels display views of the ambulacral groove during locomotion. Adhesion time corresponds to the duration of the adhesion stage.*

Temporal variations in the circularity index reveal, therefore, fluctuating patterns that allow precise determination of the period corresponding to the adhesion time of each tube foot (Fig. 5.16).

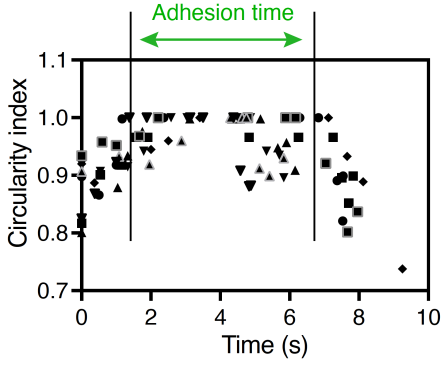

Figure 5.16: *Temporal variation of the tube foot circularity index (n = 10 tube feet). Vertical lines delimit the mean adhesion time for the 10 tube feet.*

Analysis of the mean tube foot contact area during the adhesion stage shows a positive correlation with natural body mass for *Asterias rubens* (Fig. 5.17A) and *Marthasterias glacialis* (Fig. 5.18A). For *A. rubens*, we estimated the slope of the relationship between mean tube foot contact area and mass to 0.42 ± 0.05 with a 95% confidence interval (*Supplementary Table 9.1* and *Fig. 9.2A*). For *Marthasterias glacialis*, the estimated slope was 0.48 ± 0.04 with a 95% confidence interval (*Supplementary Table 9.1* and *Fig. 9.2B*).

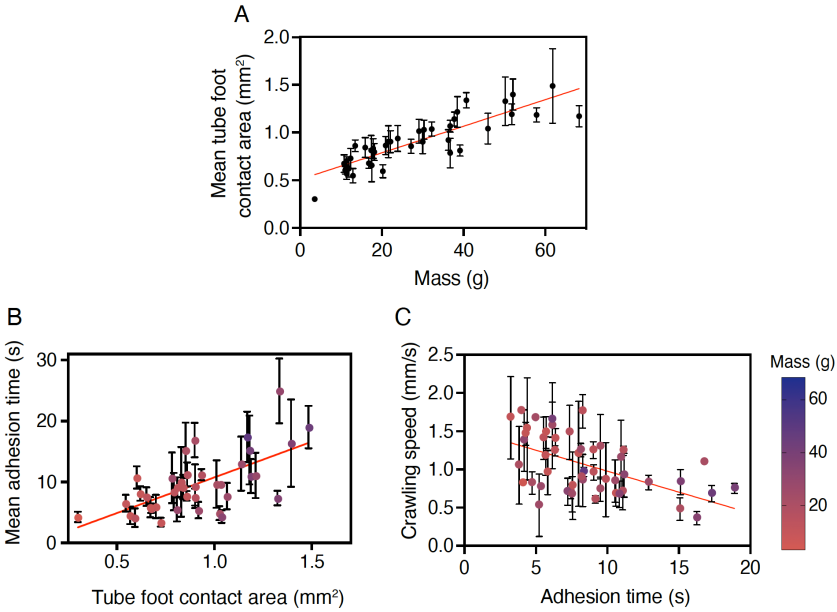

Figure 5.17: *(A) Relationship between the mean tube foot contact area and mass in Asterias rubens($n = 39$, $R^2 = 0.6203$, $p < 0.0001$). (B) Relationship between the mean adhesion time and tube feet contact area ($n = 39$, $R^2 = 0.3088$, $p < 0.0001$). (C) Relationship between crawling speed and tube feet adhesion time ($n = 49$, $R^2 = 0.2115$, $p < 0.0001$). All data are presented as mean ± s.d.*

These results indicate that larger sea stars exhibit negative allometry, meaning that the tube feet contact areas grow more slowly than expected relative to their mass. However, for both sea star species studied, we find that the total contact area shows pronounced extreme positive allometry (*Supplementary Fig.9.3*). Indeed, the estimated slope was approximately 1.03 (*Supplementary Table 9.1*). This indicates that the total contact area of all tube feet together

occupies a proportionally larger fraction of the body surface area in larger individuals. This scaling pattern aligns with findings from other adhesion-based systems, where extreme positive allometry in adhesive pads is understood as a functional adaptation to compensate for the greater mechanical demands placed on larger-bodied organisms [10]. In sea stars, this may reflect a compensatory mechanism to maintain effective attachment capacity as overall body size increases.

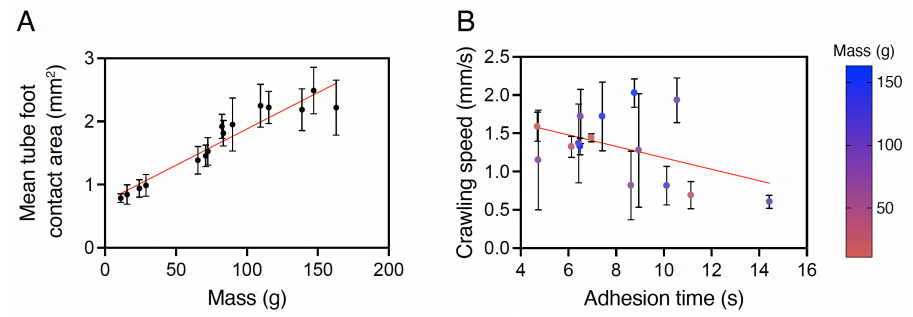

Figure 5.18: *(A) Relationship between the mean tube foot contact area and mass in Marthasterias glacialis($n = 15$, $R^2 = 0.7494$, $p < 0.0001$). (B) Relationship between the crawling speed and the tube feet adhesion time ($n = 15$, $R^2 = 0.1323$, $p < 0.0001$). All data are presented as mean ± standard deviation (s.d.).*

Additionally, a weak but significant positive relationship was observed between adhesion time and mean tube foot contact area (Fig. 5.17B), indicating that larger tube feet require slightly longer contact times. We also found an inverse relationship between crawling speed and adhesion time (Fig. 5.17C and Fig. 5.18B), demonstrating that longer adhesion times are associated with slower locomotion. This indicates that rapid detachment of tube feet after attachment is essential for achieving higher crawling speeds. Notably, adhesion time during locomotion remained below one minute, typically ranging from 3 to 20 s. These observation highlights the importance of tube feet adhesion timing over mere contact number. While larger tube feet and greater contact areas likely enhance adhesion strength, they also lead to increased adhesion time, which in turn reduces crawling speed.

Video recordings at higher resolution revealed that locomotion consists of a cyclic sequence of attachment, adhesion, and detachment phases.

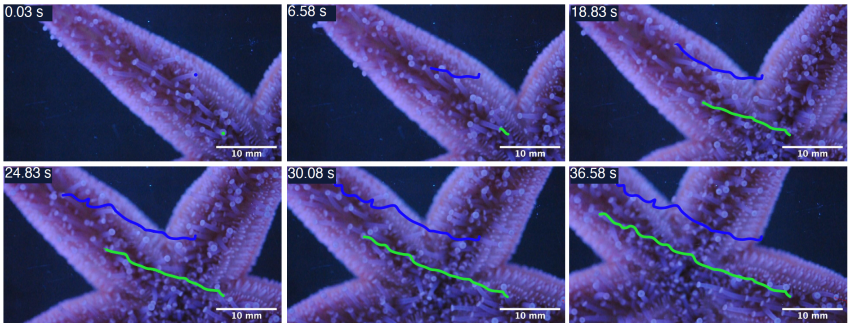

Figure 5.19: *Manual tracking of successive tube feet adhesion across time (Blue and green) during locomotion in Asterias rubens. Scale bar: 10 mm.*

By manually tracking several tube feet (Fig. 5.19), we observed that few of them were reused during locomotion via repetitive detachment and attachment cycles. The time between successive detachment and reattachment stages was referred to as the recovery stroke phase (Fig. 5.20A). We found that this parameter remained relatively constant across individuals of different body masses, with an average duration of 18.6±6.5 seconds (Fig. 5.20B).

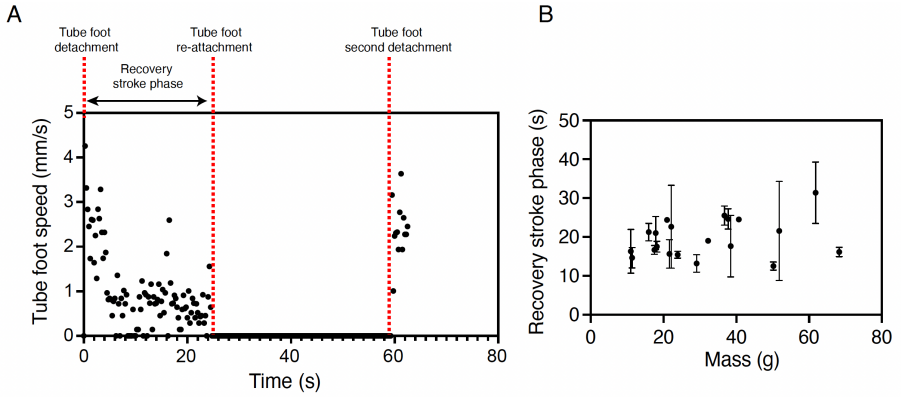

Figure 5.20: *(A) A tube foot speed as a function of the time. A tube foot speed is measured over 60 seconds. (B) Relationship between the recovery stroke phase and Asterias rubens mass (n = 20 individuals). All data are presented as mean ± standard deviation (s.d.).*

Overall, these findings reveal a trade-off between adhesive performance and locomotor efficiency: rapid movement requires shorter adhesion times and thus faster detachment–reattachment cycles [11, 12]. A positive correlation has been observed between stride frequency and maximum speed in several animals that utilize dynamic adhesion for locomotion [12]. Taken together, these findings suggest that the relationship between body mass and crawling speed is mediated through adhesion dynamics. They highlight the pivotal role of tube feet movement and timing in enabling adaptive and efficient locomotion in *A. rubens*.

The relationship between arm length and body mass in *Asterias rubens* has previously been investigated in individuals from the Limfjord (Denmark) [13]. Two main points emerge when comparing our dataset with theirs. First, despite the different collection locations, *A. rubens* morphology follows the same scaling law (Fig. 5.21). Second, while we determined body mass by directly weighing specimens, Burgaard *et al.* estimated it from the volume of displaced seawater upon immersion. Despite these methodological differences, both approaches yield consistent mass–size relationships, underscoring the robustness of this scaling across populations.

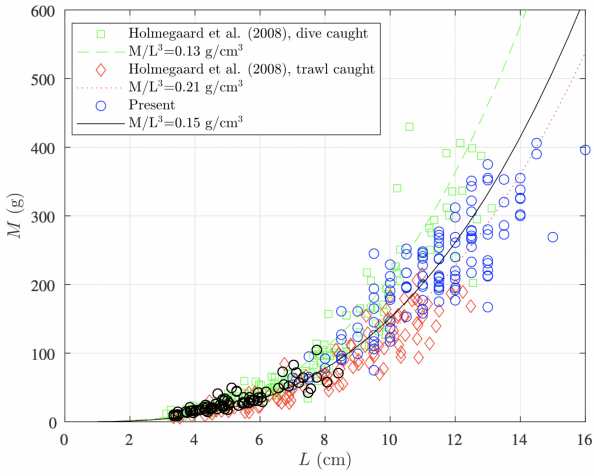

Figure 5.21: *Measured mass of Asterias rubens as a function of their arm length. The graph combines data from Burgaard et al. (2023) [13] with measurements obtained during this thesis (black circles, n = 74).*

Several factors may nevertheless influence sea star locomotion. One of the most important is captivity. Prolonged maintenance in aquaria has been shown to alter gene expression profiles and induce chronic stress in sea stars [14]. Moreover, Flammang *et al.* (1998) demonstrated that the ability of *A. rubens* to produce adhesive footprints declines rapidly in captivity, likely reducing their tenacity [15]. To minimize such effects, we systematically performed locomotion measurements within one month of collection, following a two-week acclimation period. This protocol provided a reasonable balance between allowing animals to adapt to laboratory conditions and preserving their full adhesive capabilities.

The properties of the substrate also represent a potential source of variation in locomotor performance. Surface rugosity has been reported to affect adhesion in echinoderms [16]. In our study, we directly compared locomotion of *A. rubens* on glass and slate, a more naturalistic substrate, and found no significant difference in crawling speed, suggesting that the animals can adapt their locomotion across substrates. However, the presence of biofilms may also play a role. Thomas *et al.* (1985) showed that tube feet adhere more strongly to surfaces covered with a biofilm, which begins to form immediately upon immersion [17]. In our experiments, a strict fill/refill protocol (see *Materials and Methods*) was applied between trials, ensuring the presence of a thin but consistent biofilm on the substrates. This controlled condition minimized potential variability and is therefore not expected to bias our locomotion measurements.

Building on these insights into scaling relationships and the pivotal role of tube feet adhesion time, the next step is to examine how these dynamics respond when sea stars face external challenges. The next chapter examines how sea stars modify their tube feet dynamics in response to altered mechanical and environmental conditions. This shift in focus allows us to probe the mechanisms that underlie their remarkable locomotor versatility.

BIBLIOGRAPHY

[1] E. MONTGOMERY *et al.* Effects of Body Size and Shape on Locomotion in the Bat Star (*Patiria miniata*), *Biological Bulletin* **222**, 222-232, 2012.

[2] E. MONTGOMERY, Predicting crawling speed relative to mass in sea stars, *Journal of Experimental Marine Biology and Ecology* **458**, 27-33, 2014.

[3] B. MUELLER *et al.* Size-specific locomotion rate and movement pattern of four common Indo-Pacific sea stars (Echinodermata; Asteroidea), *Aquatic Biology* **12**, 157-164, 2011.

[4] M.S. PRATCHETT *et al.* Body size and substrate type modulate movement by the western Pacific crown-of-thorns starfish, *Acanthaster solaris*, *PLOS ONE* **12**, 1-14, 2017.

[5] S. HEYDARY *et al.* Sea star inspired crawling and bouncing, *Journal of The Royal Society Interface* **17**, 20190700, 2020.

[6] T. PO *et al.* The directional control of phototaxis in sea stars (*Protoreaster nodosus*), *Journal of Experimental Biology* **228**, jeb249293, 2025.

[7] A.P. ST-PIERRE *et al.* Wave action and starvation modulate intra-annual variation in displacement, microhabitat selection, and ability to contact

prey in the common sea star, *Asterias rubens Linnaeus*, *Journal of Experimental Marine Biology and Ecology* **467**, 95-107, 2015.

[8] P. MAYO *et al.* Studies of avoidance reactions in several species of Predatory British Seastars (Echinodermata: Asteroidea), *Marine Biology* **38**, 41-49, 1976.

[9] G.A. KERKUT, The forces exerted by the tube feet of the starfish during locomotion, *Journal of Experimental Biology* **30**, 575-583, 1953.

[10] D. LABONTE *et al.*Extreme positive allometry of animal adhesive pads and the size limits of adhesion-based climbing, *Proceedings of the National Academy of Sciences* **113**, 1297-1302, 2016.

[11] T.E. HIGHAM, Frictional adhesion of geckos predicts maximum running performance in nature, *Journal of Experimental Biology* **228**, jeb247906, 2025.

[12] W. FEDERLE *et al.* Dynamic biological adhesion: mechanisms for controlling attachment during locomotion, *Philosophical Transactions of the Royal Society B: Biological Sciences* **374**, 20190199, 2019.

[13] K. B. BURGAARD *et al.* Morphology and Settling Velocity of Sea Stars *Asterias rubens*, *Journal of Marine Science and Engineering* **11**, 296, 2023.

[14] M. MORIN *et al.* Captivity induces a sweeping and sustained genomic response in a starfish, *Molecular Ecology* **32**, 3541-3556, 2023.

[15] P. FLAMMANG *et al.* A study of the temporary adhesion of the podia in the sea star *Asterias rubens* (Echinodermata, asteroidea) through their footprints, *Journal of Experimental Biology* **201**, 2383–2395, 1998.

[16] R. SANTOS *et al.* Adhesion of echinoderm tube feet to rough surfaces, *SF Journal of Experimental Biology* **208**, 2555-2567, 2005.

[17] L.A. THOMAS & C.O HERMANS, ADHESIVE INTERACTIONS BETWEEN THE TUBE FEET OF A STARFISH, LEPTASTERIAS HEXACTIS, AND SUBSTRATA, *The Biological Bulletin* **163**, 675-688, 1985.

CHAPTER 6

ADAPTIVE TUBE FOOT DYNAMICS UNDER EXTERNAL PERTURBATIONS

The goal of this chapter is to validate our previous findings on the role of the adhesion dynamics in the sea star locomotion by conducting two different perturbation experiments: (i) artificial mass alteration and (ii) inverted locomotion.

Furthermore, the results of these perturbation experiments have been modeled through numerical simulations based on a mechanistic model in collaboration with Prof. Eva Kanso and Dr. Sina Heydari. This part is not presented in this thesis chapter but is thoroughly discussed in the *Theoretical model* in the supplementary.

6.1 Dynamic adjustments in tube feet contact time in response to mass changes

The goal of this first perturbation experiment is to find a way to modulate the mass of the individuals to observe their adaptation in terms of locomotion. To do so, the individuals were fitted with a 3D-printed backpack carrying additional mass equivalent to 25% or 50% of their body mass during their locomotion (Fig. 6.1).

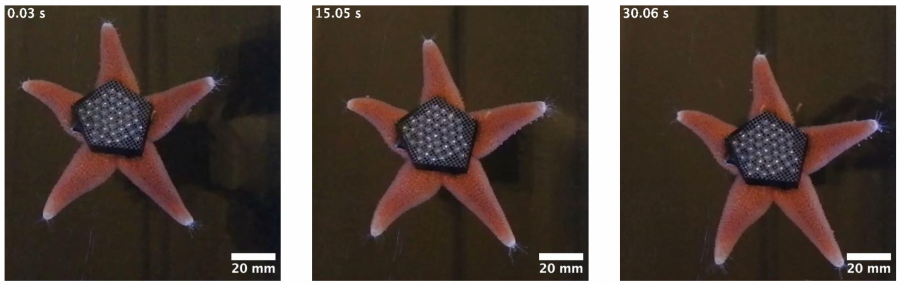

Figure 6.1: *Top view of locomotion for an individual of Asterias rubens equipped with a 3D-printed backpack used in perturbation experiments. Scale bar: 20 mm.*

The mean percentage of tube feet in contact with the substrate slightly increases across conditions with 3.9±2.3% for normal locomotion, 3.6±2.3% for empty backpacks, 3.8±2.3% for +25% mass, and 4.3±2.1% for +50% mass, indicating that *A. rubens* maintains a low level of tube feet engagement re-

gardless of additional load (Fig. 6.2A). This suggests a compensatory strategy to preserve locomotor stability under increased mechanical demand. Even if the tube feet engagement is quite constant, instantaneous crawling speed declined significantly with added mass (Fig. 6.2B), likely due to the greater tube feet force required for tube feet detachment and propulsion [1].

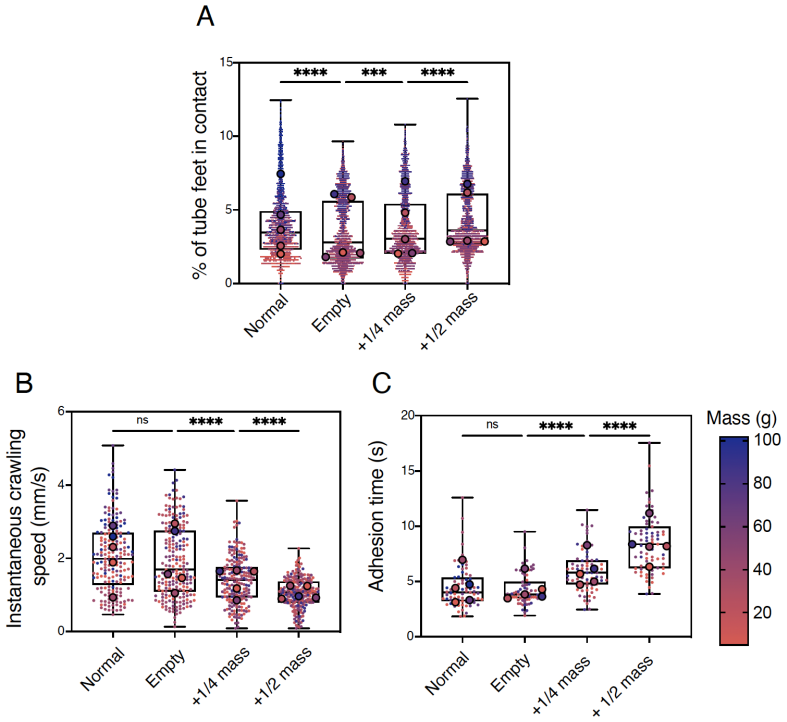

Figure 6.2: *((A) Percentage of tube feet in contact with the substrate, where each small dot corresponds to one tube feet measurement taken every 0.2 s; (B) Instantaneous crawling speed, where each small dot corresponds to the instantaneous crawling measurement taken every 2 s; and (C) tube feet adhesion time, where each small dot correspond to the adhesion time of one tube feet across four conditions: normal locomotion, empty backpack, +25% body mass, and +50% body mass (N = 5 Asterias rubens per condition). Data in all superplots are color-coded by mass; large dots indicate individual averages. Repeated measures one-way ANOVA was employed because the same individuals were tested under four conditions (normal, empty backpack, +25% mass, +50% mass). ***p < 0.001, ****p < 0.0001, ns = not significant.*

Correspondingly, adhesion time increased with mass, from 4.3±1.4 seconds for the empty backpack, to 5.9±1.9 seconds and 8.4±2.6 seconds for +25% and +50% mass, respectively (Fig. 6.2C). This prolongation likely reflects the increased propulsive force required to move the added mass during each locomotor cycle.

Together, these results confirm that crawling speed is inversely related to contact time, which itself is modulated by body mass. This finding highlights the adaptive control of tube feet adhesion dynamics as a key mechanism for maintaining effective locomotion under varying mechanical loads. These perturbation experiments show that *A. rubens* dynamically modulates tube feet contact time in response to added load. Although the number of adhering tube feet remained constant, crawling speed decreased and contact time increased proportionally with the added mass. This suggests that sea stars rely on local mechanical feedback to adaptively tune tube feet dynamics, without requiring changes in movement or overall tube feet engagement.

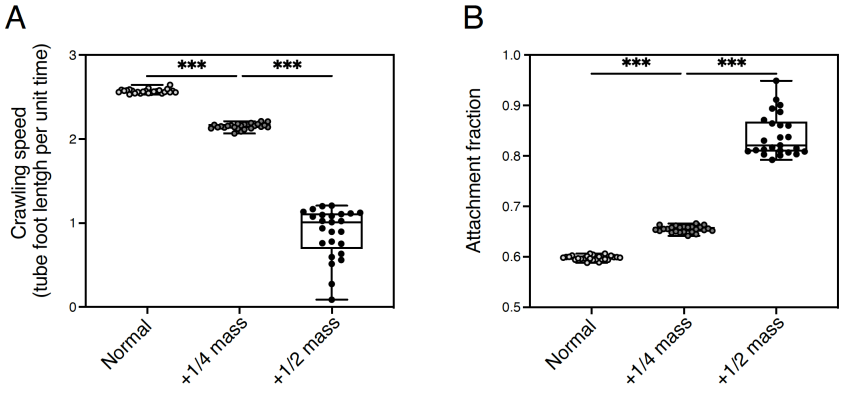

Figure 6.3: *(a) Simulated crawling speed and (b) attachment fraction τ, with $\tau = \sum_{i=1}^{N} T_i^{attached}/NT$, defined as the sum over all tube feet of the time $T_i^{attached}$ each foot spends in attachment, divided by the total simulation time T times the number N of tube feet. Both metrics are shown as a function of sea star weight, increasing from baseline to highest (W = 2, 2.5, 3). The corresponding lengths of detachment for the tube feet are l_{detach} = 0.9, 0.95, and 1, respectively. For each weight condition, 25 simulations were performed with randomized initial foot states. ***p < 0.001, ****p < 0.0001, ns = not significant. From Eva Kanso's work.*

Interestingly, theoretical simulations of crawling speed (Fig. 6.3A) and attachment fraction (Fig. 6.3B) in response to variations in body mass exhibit trends that parallel the experimental observations, namely, a decrease in instantaneous crawling speed (Fig. 6.2B) and a corresponding increase in adhesion time (Fig. 6.2C). These results confirm the validity of the model based on fully decentralized adaptive control of the tube feet. These findings support the hypothesis that sea star locomotion can emerge from local sensing and mechanical feedback at the level of individual tube feet, without requiring centralized control. Moreover, they demonstrate that crawling speed under increased mechanical load can be modulated through local adaptation of detachment timing. In the present study, specimens of *A. rubens* exhibited a reduction in crawling speed without a corresponding increase in the number of tube feet recruited. By contrast, in the 2024 study by Po *et al.* on cooperative transport in sea star locomotion, individuals of *Protoreaster nodosus* increased tube feet recruitment when their mass was artificially increased. Yet, their speed was also reduced [1]. This disparity suggests that cooperative transport may not be a universally employed mechanism among sea star species. An alternative explanation is that the difference arises from gait-specific mechanics, as Po *et al.* investigated the bouncing gait[1], which differs from the crawling locomotion gait examined in the present study.

The 3D-printed harness was attached to the aboral surface of *A. rubens*, covering only a very limited portion of the papular area ($<$1.9 cm^2). These papulae (dermal branchiae) contribute to respiration [2], but the restricted coverage is unlikely to impair physiological function. Moreover, a comparable method of affixing devices to the aboral surface was recently employed by Po *et al.* (2024) [1] without reporting adverse effects. We therefore consider it unlikely that the harness introduced respiratory artefacts or biased the locomotion data.

[1] Coordinated locomotion pattern in sea stars where tube feet operate in synchronized clusters, producing rhythmic vertical oscillations of the body and a pulsed forward motion [3].

6.2 Dynamic adjustments in tube feet adhesion time in inverted setup

In this second perturbation experiment, we placed each specimen upside-down (Fig. 6.4), and then we analyzed inverted locomotion, a condition that mimics the natural challenge of navigating vertical or overhanging surfaces in their environment [1].

This inversion alters the distribution of gravitational forces, effectively increasing the load on the tube foot as they counteract the downward pull, thereby requiring greater adhesive forces and movement to maintain stability and locomotion.

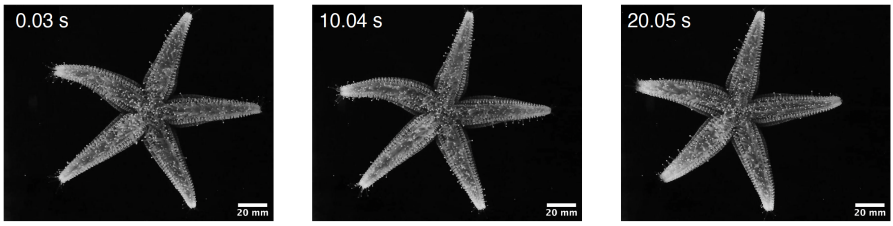

Figure 6.4: *Sequence of an individual of Asterias rubens crawling upside down. Scale bar: 20 mm.*

The mean percentage of tube feet in contact slightly decreased in the inverted position compared to the normal one. We found an average percentage of 4.1±2.1% for the normal locomotion and 2.8±1.5% for the inverted locomotion (Fig. 6.5A), suggesting a compensatory response to counteract the effect of gravity and maintain stability while keeping a low level of tube feet engagement. Interestingly, instantaneous crawling speed was significantly reduced in the inverted condition (Fig. 6.5B), decreasing from 2.1±0.9 mm/s to 0.9±0.5 mm/s, likely due to the higher energy demands associated with this altered posture. Adhesion time was also significantly prolonged during inverted locomotion (Fig. 6.5C), increasing from 4.5±1.8 seconds to 9.1±3.2 seconds, consistent with the need for stronger adhesion to prevent detachment under the influence of gravity [4].

As observed for the first perturbation experiment, results obtained under inverted locomotion showed that, where gravitational forces are altered, the percentage of tube feet in contact decreases slightly. The similarity of behavioral responses across both perturbations, additional mass and inversion, indicates a conserved mechanical strategy to stabilize movement under changing physical conditions.

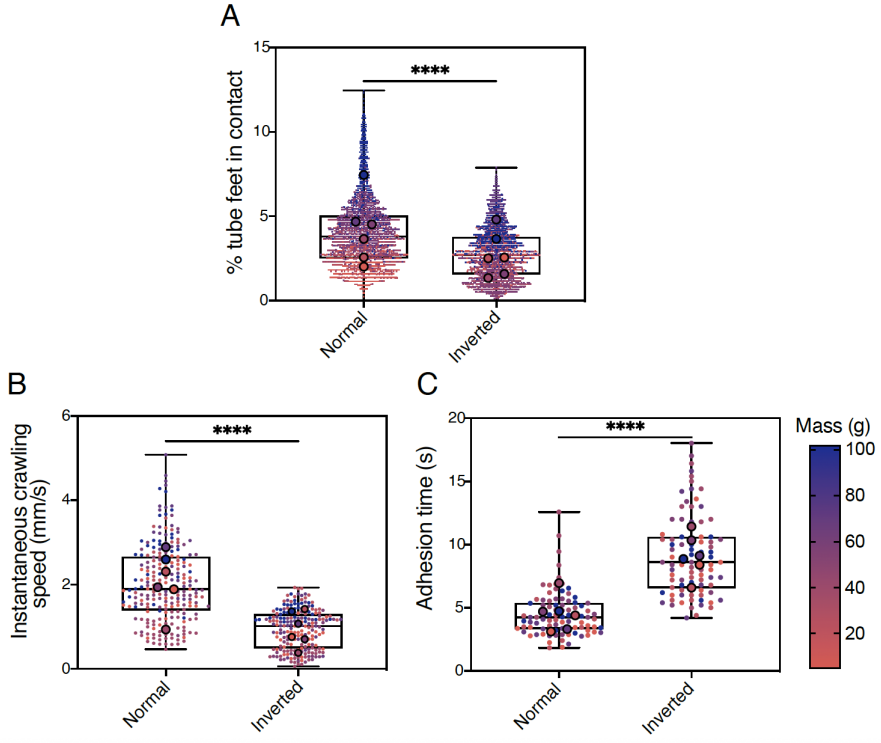

Figure 6.5: *(A) Percentage of tube feet in contact with the substrate, where each small dot corresponds to one tube feet measurement taken every 0.2 s; (B) Instantaneous crawling speed, where each small dot corresponds to the instantaneous crawling measurement taken every 2 s; and (C) tube feet adhesion time, where each small dot correspond to the adhesion time of one tube feet; across the two conditions: normal and inverted locomotion (N = 6 Asterias rubens per condition). Data in all superplots are color-coded by mass; large dots indicate individual averages. A paired t test was applied, as each specimen was tested under both normal and inverted conditions ****$p < 0.0001$.*

The group of Kanso *et al.* compared numerically the sea star locomotion under normal and inverted conditions, with no parameter adjustments, keeping all parameters constant. The simulation results (Fig. 6.6A and B) closely mirror our experimental observations, showing a reduction in instantaneous crawling speed (Fig. 6.5B) accompanied by a corresponding increase in adhesion time (Fig. 6.5C), thereby supporting the validity of the biomechanical approach.

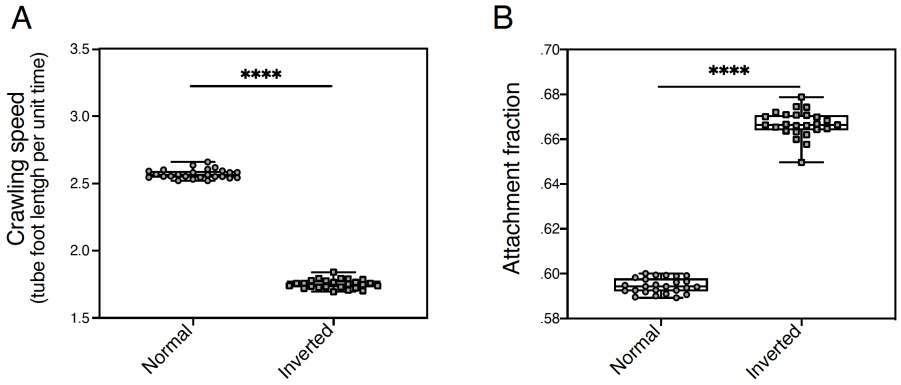

Figure 6.6: *(a) Simulated crawling speed and (b) attachment fraction* $\tau = \sum_{i=1}^{N} T_i^{attached}/NT$*, defined as the sum over all tube feet of the time* $T_i^{attached}$ *each foot spends in attachment, divided by the total simulation time T times the number N of tube feet. Both are shown for the normal and inverted sea stars. For each orientation, 25 random simulations have been performed. Parameter values are N=100, L=40, l=1,* F_{max} *=0.4,* λ *=5, with no parameter adjustment between normal and inverted simulations. ****p < 0.0001. From Eva Kanso's work.*

These numerical simulations based on a biomechanical model of tube feet function replicated the observed trends. By varying body mass and detachment thresholds, the model reproduced the inverse relationship between crawling speed and adhesion time. The simulations further demonstrated that local sensing and adaptive control at the level of individual tube feet are sufficient to generate coherent and efficient crawling behavior, without centralized control. However, a centralized coordination in stepping direction is necessary for efficient locomotion [5, 6]. Together, these perturbation experiments demonstrate that sea stars employ dynamic adjustments in tube feet adhesion time to adapt to increased mechanical demands, whether due to added weight or altered locomotion modes. These experimental findings, combined with the modeling

results, underscore the critical role of tube feet dynamics in stabilizing and adapting sea star locomotion under varying physical constraints.

Overall, our findings identify tube feet contact time (presumably correlating with adhesion time) as a key mass-dependent parameter that governs sea star locomotion. This mechanism provides a flexible strategy to balance stability and speed across individuals and environmental conditions.

BIBLIOGRAPHY

[1] T. PO *et al.* Cooperative transport in sea star locomotion, *Current Biology* **34**, 2551-2557.e4, 2024.

[2] C. P. Hickman *et al. Integrated Principles of Zoology*, 14th ed., McGraw-Hill, 2008.

[3] O. ELLERS *et al.* Kinematics of sea star legged locomotion, *Journal of Experimental Biology* **224**, jeb242813, 2021.

[4] P.-E. MERETTA *et al.* Locomotion and righting behavior of sea stars: a study case on the bat star *Asterina stellifera* (Asterinidae), *Revista de Biología Tropical* **69**, 501-513, 2021.

[5] G.A. KERKYT, The Mechanisms of Coordination of the Starfish Tube Feet, *Behaviour* **6**, 206-232, 1954.

[6] T. PO *et al.* The directional control of phototaxis in sea stars (*Protoreaster nodosus*), *Journal of Experimental Biology* **228**, jeb249293, 2025.

CHAPTER 7

CONCLUSION AND OUTLOOKS

7.1 Conclusion

Sea stars achieve locomotion through the coordinated action of hundreds of small tube feet, despite lacking a central brain. Although the morphology and ultrastructure of echinoderm tube feet have been extensively studied, critical aspects of their dynamics—such as the sequence of contact formation and release, the number of tube feet engaged at any given time, and their direct contribution to propulsion—have remained poorly characterized. Moreover, unlike many other animals, sea stars display a non-linear relationship between body mass and crawling speed, emphasizing the need for a deeper biomechanical understanding of their locomotor strategies.

This thesis investigated the biomechanics and control principles underlying locomotion in *Asterias rubens* and *Marthasterias glacialis*, with particular focus on the dynamics of individual tube feet. By combining frustrated total internal reflection (FTIR) imaging, morphometric scaling, perturbation experiments, and decentralized biomechanical modeling, we revealed how directional movement emerges in the absence of centralized neural control. This distributed strategy contrasts with the centralized regulation seen in most bilaterians and instead resembles other decentralized systems, such as insect ganglia or octopus arms, thereby expanding our comparative understanding of how complex locomotion can arise without a central brain.

We first established that key morphological features, such as arm length and the number of tube feet, scale predictably with body mass. Heavier sea stars possess longer arms and larger contact areas, yet the proportion of tube feet in contact with the substrate remains remarkably low, typically below 10%. Maintaining such a low proportion may facilitate forward motion and prevent excessive drag, particularly in turbulent environments where strong hydrodynamic forces could otherwise impede movement. High magnification imaging further revealed that tube feet are reused cyclically during locomotion, with an average recovery stroke of 20 seconds. Notably, crawling speed was not correlated with the number or proportion of engaged tube feet. This finding contrasts with many models of locomotion, where speed often scales with stride length, limb number, or muscle force output, and highlights the unique biome-

chanical constraints of echinoderm locomotion. Instead, we identified adhesion time—the duration each tube feet remains attached—as the primary determinant of crawling speed, with heavier individuals displaying longer adhesion times. Shorter adhesion times enabled faster crawling, whereas prolonged attachment slowed locomotion. Ecologically, the ability to modulate adhesion time likely allows sea stars to maintain efficiency across diverse environments and substrates, contributing to their success as widespread and resilient benthic predators.

Perturbation experiments confirmed the adaptive nature of this mechanism. When body mass was artificially increased by 25%or 50% using custom 3D-printed backpacks, adhesion times lengthened and crawling speed decreased. Similarly, inverting the animals to alter gravitational orientation produced the same effect. In both cases, the proportion of engaged tube feet remained relatively low, but modulation of adhesion time allowed sea stars to adjust locomotion to changing physical demands. Such adaptability is likely ecologically relevant, as sea stars frequently experience changes in body load during feeding or must recover from overturning in wave-exposed habitats.

These experimental findings were further supported by a biomechanical model based on local control rules derived from shear forces and tube foot deformation. Simulations reproduced the experimental results, showing that both increased load and inverted posture led to longer adhesion times and reduced speeds without requiring centralized control. This theoretical approach reinforces the view that robust, adaptable locomotion in sea stars emerges from local sensing and feedback at the level of individual tube feet. By linking adhesion dynamics with both environmental (inverted locomotion) and physiological (modulation of their body mass) constraints, our work advances the general understanding of decentralized control in biological systems and provides new insights into how sea star locomotion is organized. Beyond biology, these findings identify adhesion time as a tunable parameter that could be exploited in bio-inspired robotics, where decentralized strategies are increasingly recognized as key for building adaptable and resilient machines.

In summary, this work demonstrates that sea stars optimize locomotor performance not by engaging more tube feet, but by fine-tuning the adhesion time of each foot in response to mechanical and environmental conditions. Our demonstration that crawling speed is governed by adhesion timing rather than contact number challenges traditional assumptions in biomechanics and suggests that timing-based control strategies may be more widespread than previously recognized. This decentralized approach enables stable and adaptable movement under a wide range of physical challenges. More broadly, these findings provide insights into the principles of distributed control in biological systems and may inspire the design of autonomous soft robotic systems that operate without centralized coordination. The FTIR platform developed here opens new possibilities for studying locomotion dynamics in echinoderms and other soft-bodied aquatic organisms. Future work comparing tube feet dynamics across echinoderm taxa or testing locomotion under ecologically relevant flow conditions will further clarify how distributed control strategies evolve and how they may inspire the next generation of autonomous soft robots.

7.2 Outlooks

A promising avenue for future research arising from this PhD work concerns the direct measurement of forces during sea star locomotion. Previous assessments of adhesion strength have provided valuable insights into the adhesive capabilities of sea star tube feet, clarifying their mechanical properties, adhesion mechanisms, and force generation capacity [1, 2]. However, these measurements do not quantify the total propulsive force generated during the sea star locomotion, nor do they reveal how these forces are distributed across the animal's arms. Developing a method to measure surface forces in real time during movement is therefore essential to improve our understanding of sea star biomechanics. In this context, we identified large-scale traction force microscopy (TFM) as a promising approach to investigate these mechanisms. Adapting TFM from the cellular to the organismal scale represents a methodological innovation, expanding its application from micro- to macro-biomechanics.

First introduced by the group of Mycah Dembo at Boston University in 1999, TFM has become a key technique for quantifying cellular forces and for elucidating how cells interact with and adapt to their mechanical environment [3]. The method involves culturing cells on an elastic substrate incorporating fiducial markers, commonly fluorescent beads, whose displacement under applied forces is tracked. By imaging the substrate both in a relaxed state and under tension, applying particle image velocimetry (PIV) algorithms (including widely available open-source implementations) [4]. TFM enables quantitative reconstruction of the traction stress field [5, 6]. This approach has been applied not only to single cells but also to multicellular structures [7, 8], and small invertebrates such as terrestrial slugs and centipedes [9, 10] (Fig. 7.1).

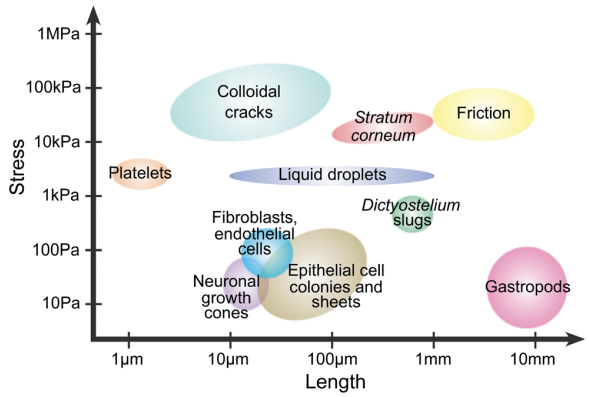

Figure 7.1: *Traction force microscopy across scales. Image from [11].*

In this work, the main challenge was to develop a soft substrate that remains stable in seawater and exhibits high deformability in response to the amount of forces exerted by tube feet. This soft substrate must be transparent and highly elastic to return to its original shape after deformation. To address this challenge, we first tried gelatin-based hydrogels, which are highly hydrophilic, but we did not observe sufficient adhesion with sea stars. We thus decided to use hydrophobic silicon-based elastomers. The polydimethylsiloxane (PDMS) 527 from Dow Corning was selected as a suitable candidate material due to its ability to meet these functional requirements [12]. This development not only enabled sea star experiments but also provides a new tool for studying the biomechanics of other marine invertebrates in situ. This type of PDMS allows

to make transparent elastomers with extremely low Young's moduli [1], down to approximately 0.1 kPa [13] instead of the GPa range usually observed with conventional PDMS 184 elastomers [14].

To prepare the soft elastomer, a mix of 6:5 (w/w) PDMS (Dow Corning Sylgard 527 silicone dielectric gel (Part A and B)) was prepared based on previously published protocols [15]. The mix was stirred for two minutes at 2000 rpm and then defoamed for two minutes at 1500 rpm. The preparation was poured on a flat glass inside of (19 $\times$ 29) cm^2 aquarium to make a 4 mm elastomer layer. The PDMS was allowed to cure for 150 minutes at 50°C. To optically measure the gel deformation, fluorescent blue polyethylene microspheres (UVPMS-BB, Cospheric) of 170 μm in diameter were used as markers. Microbeads were gently dusted on the top of the surface of the elastomer, which was not fully cured, and the elastomer was allowed to cure for 48h at 50°C.

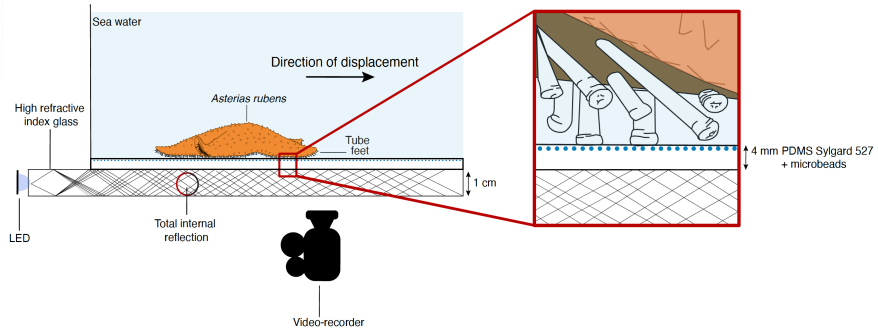

Figure 7.2: *Schematic of our large scale TFM experimental set-up. Sea stars are allowed to crawl, and the movement of their tube feet, as well as of the beads embedded in the substrate, is recorded with a camera placed underneath the aquarium.*

We characterized the mechanical properties of the elastomer with rheological tests. Three 35 mm diameter Petri dishes were filled with 2.55g of PDMS 527 6:5 (w/w). After reticulation, the three samples were characterized by nanoindentation using a CHIARO instrument from Optics 11 equipped with a probe of 0.45 N/m in stiffness and tip of 51.5 μm in radius. The tip was treated for ten minutes with UV ozone and then for ten minutes with Pluronic to prevent

[1] A measure of the material stiffness (in en N/m^2 or Pa, defined as the ratio of applied stress to the resulting strain.

adhesion between the tip and the surface, and the sample was also treated for ten minutes in Pluronic. We determined a Young modulus of 1.7±0.1 kPa.

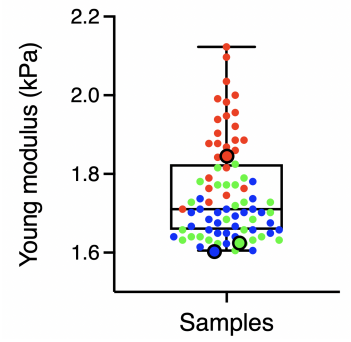

Figure 7.3: *Young modulus measurement of our 3 samples. Each small dot corresponds to one rigidity measurement for the same sample. Data in this superplot are color-coded by sample; large dots indicate the sample average.*

Preliminary tests were conducted on *Marthasterias glacialis*. High-definition videos (3840 × 2160) pixels were recorded at 15 fps. To ensure that the PDMS 527 surface does not introduce artefacts, we determined the sea star crawling speed and compared the results to those obtained on a glass surface (Fig. 7.4).

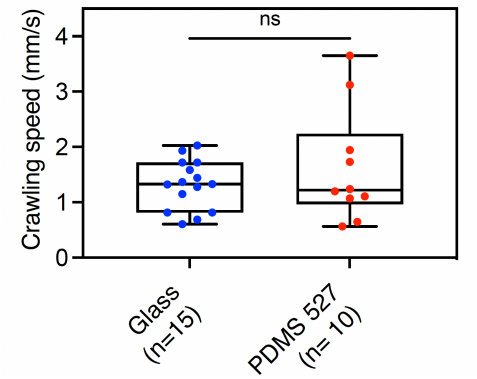

Figure 7.4: *Graph showing the crawling speed of individuals of Marthasterias glacialis when moving on both glass and PDMS 527 surface. A Mann–Whitney test was used, since the two groups consisted of different individuals. n.s. is not significant.*

Interestingly, our results showed that *Marthasterias glacialis* crawling speed did not differ significantly between glass 1.3±0.4 mm/s and PDMS 1.6±1.0

mm/s surfaces, confirming that PDMS can be used for studying sea star traction stress (Fig. 7.4). This validation ensures that behavioral observations remain ecologically relevant and not artifacts of the experimental design.

Large-scale TFM experiments were carried out at UMONS and analyzed in collaboration with Martial Balland and Vladimir Misiak (Microtiss Laboratory, Grenoble Alpes University). Preliminary large-scale TFM measurements suggest that sea stars generate spatially heterogeneous traction forces during locomotion (Fig. 7.5). Initial force maps indicate distinct zones of high traction beneath active arms, potentially corresponding to adherent tube feet. This could demonstrate, for the first time, how propulsive forces are spatially distributed in a radially symmetric marine invertebrate.

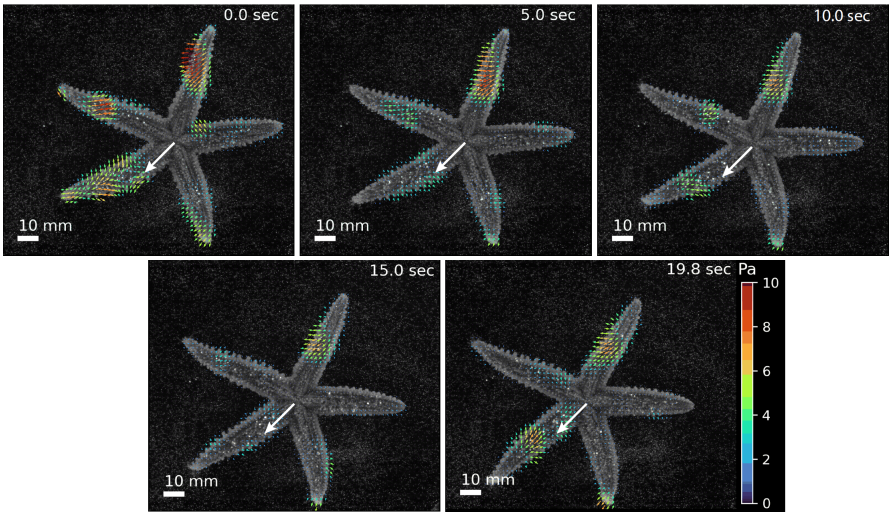

Figure 7.5: *Sequence of traction stress maps of sea star locomotion across time. The color scale indicates traction magnitude in Pascals (Pa), with traction vectors (generated by the TFM program) representing direction and relative magnitude of surface traction. The big white arrows, manually added to the figure, correspond to the direction of locomotion.*

The analysis of the TFM sequences obtained from six specimens of *Marthasterias glacialis* should enable the extraction of key quantitative parameters, such as the total traction stress as a function of time. The total traction stress (Pa) is defined as the sum of all local traction forces exerted by the organism on the substrate, integrated over the contact area at each time point.

While still preliminary, our data suggest rhythmic variations in force production, potentially corresponding to coordinated tube feet activity (Fig. 7.6). Such rhythmicity could reflect decentralized locomotor control, an emerging theme in neurobiology and biomechanics that this work directly informs. Obviously, these data are still highly speculative and will need to be confirmed by robust and reproducible experiments. Moreover, the absolute values of the traction stress are not yet calibrated and should be interpreted qualitatively.

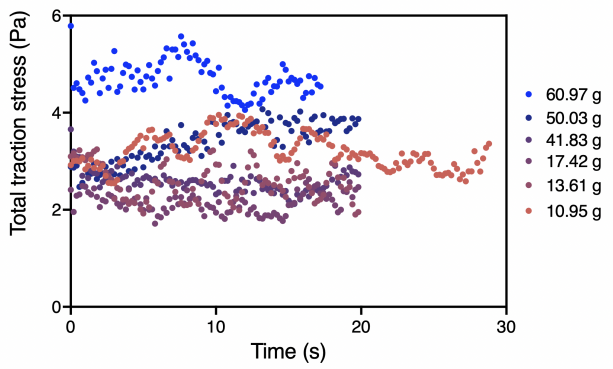

Figure 7.6: *Evolution of the total traction stress (Pa) over time during locomotion. Color code indicates the mass of the different specimens of Marthasterias glacialis (n =6).*

Although these results are still preliminary, they already demonstrate that we can quantitatively determine the forces exerted by sea stars during locomotion. Therefore, these results open new avenues for studying whole-body force integration in radially symmetric animals. In the long term, it would be advisable to repeat these measurements on a larger number of specimens, particularly on the species *Asterias rubens*, to complete the data obtained on the dynamics of tube feet adhesion and to improve statistical robustness. A comparative approach would also clarify whether observed force patterns are species-specific adaptations or conserved echinoderm strategies. It could also be valuable to introduce specific stimuli, such as food cues, to investigate how foraging behavior influences force distribution across sea star arms. Furthermore, particular attention could be given to the bouncing behavior observed at the end of certain locomotor sequences, small, rapid oscillations of the body or arms [16] that may reflect elastic recoil, residual tube feet activity, or postural adjustments. A systematic analysis of these phenomena could reveal additional

biomechanical strategies involved in movement termination and stability control.

In addition, we began collaborating with Artur Ruppel from the Montpellier Cell Biology Research Center, who recently developed a TFM analysis toolbox. This toolbox integrates established TFM algorithms with the advanced visualization capabilities of napari, an open-source, Python-based, multi-dimensional image viewer designed for scientific image analysis (https://napari.org/stable/), and enabling systematic analysis of cell–substrate interactions. Integrating this analysis with tube feet kinematics could link microscopic adhesion events to macroscopic movement, bridging scales of organization. The software supports both single-frame and time-series analysis, making it well-suited for a wide range of experimental configurations, such as large-scale TFM. In future work, combining TFM with high-resolution tracking of tube feet movements could help quantify how individual tube feet mechanics contribute to global movement, which is key to a better understanding of decentralized locomotion control.

From a biological perspective, future research could explore adhesion time as a potential proxy for sea star health. Traditionally, righting time, the time required for an inverted animal to return to its normal orientation, has served as a general health indicator, as it is impaired under adverse conditions such as changes in pH, water temperature, or salinity [17, 18, 19]. With the TIRF-based system developed in this thesis, it may be possible to directly monitor changes in tube feet adhesion time in response to such environmental stress factors. This approach could provide a more localized and sensitive metric for assessing both physiological state and ecological impact. This could provide a valuable biomonitoring tool in the context of global change, where marine invertebrate resilience is increasingly threatened. Furthermore, comparative analyses across a broader range of echinoderm species, particularly those inhabiting different environmental niches or exhibiting distinct morphological traits, could reveal whether modulation of adhesion time is a conserved locomotor strategy or a species-specific adaptation.

From an engineering and biomimetics perspective, our findings contribute to the growing interest in echinoderm-inspired robotic systems. From leveraging sea star tube feet morphology to designing devices capable of underwater gripping and object transport [20, 21], understanding the functional principles of tube feet offers a valuable blueprint for bio-inspired underwater locomotion and adhesion. Notably, the very recent work of Lee *et al.* demonstrates the practical potential of translating tube feet adhesion dynamics into artificial systems [21]. Their design of bio-inspired actuators capable of switchable underwater adhesion reflects the key principles identified in this thesis, namely, that effective adhesion relies on tube feet adhesion dynamics, particularly on the adhesion time. This work thus positions sea star biomechanics as a direct source of inspiration for soft robotics and underwater gripping technologies.

In summary, this thesis provides a foundation for expanding our understanding of biomechanics and decentralized control, both in living organisms and in engineered systems. By elucidating local coordination strategies, we move closer to identifying the fundamental principles that allow complex, adaptive behaviors to emerge from simple, distributed components, such as the tube feet of sea stars. Overall, this thesis not only contributes new methods and data to sea star biology but also establishes a conceptual framework where biomechanics, physiology, and robotics intersect.

BIBLIOGRAPHY

[1] P. FLAMMANG & G. WALKER, Measurement of the Adhesion of the Podia in the Asteroid *Asterias Rubens*(Echinodermata), *Journal of the Marine Biological Association of the United Kingdom* **77**, 1251-1254, 1997.

[2] E. HENNEBERT *et al.* Evaluation of the different forces brought into play during tube foot activities in sea stars, *Journal of Experimental Biology* **213**, 1162-1174, 2010.

[3] M. DEMBO *et al.* Stresses at the Cell-to-Substrate Interface during Locomotion of Fibroblasts, *Biophysical Journal* **76**, 2307-2316, 1999.

[4] W. THIELICKE *et al.* Particle Image Velocimetry for MATLAB: Accuracy and enhanced algorithms in PIVlab, *Journal of Open Research Software* **9**, 12, 2021.

[5] C. BRUYERE *et al.* Actomyosin contractility scales with myoblast elongation and enhances differentiation through YAP nuclear export, *Scientific Reports* **9**, 15565, 2019.

[6] A. KUMARI *et al.* Actomyosin-driven force patterning controls endocytosis at the immune synapse, *Nature Communications* **10**, 2870, 2019.

[7] J.-P. RIEU *et al.* Shell tension forces propel Dictyostelium slugs forward, *Physical Biology* **9**, 066001, 2012.

[8] E. VERCRUYSSE *et al.* Geometry-driven migration efficiency of autonomous epithelial cell clusters, *Nature Physics* **20**, 1492-1500, 2024.

[9] M.W. DENNY *et al.* A Quantitative Model for the Adhesive Locomotion of The Terrestrial Slug, *Ariolimax Columbianus*, *Journal of Experimental Biology* **91**, 195-217, 1981.

[10] J.-P. RIEU *et al.* Dynamics of centipede locomotion revealed by large-scale traction force microscopy, *Journal of The Royal Society Interface* **21**, 20230439, 2024.

[11] W. R. Style *et al.* Traction force microscopy in physics and biology, *Soft Matter* **10**, 4047-4055, 2014.

[12] N. BOSQ *et al.* Melt and glass crystallization of PDMS and PDMS silica nanocomposites, *Physical Chemistry Chemical Physics* **16**, 7830-7840, 2014.

[13] C. MORAES *et al.* Supersoft lithography: candy-based fabrication of soft silicone microstructures, *Lab on a Chip* **15**, 3760-3765, 2015.

[14] R. N. PALCHESKO *et al.* Development of Polydimethylsiloxane Substrates with Tunable Elastic Modulus to Study Cell Mechanobiology in Muscle and Nerve, *PLOS ONE* **7**, e51499, 2012.

[15] M. LEE *et al.* PDMS hydrogel-coated tissue culture plates for studying the impact of substrate stiffness on dendritic cell function, *STAR Protocols* **3**, 101233, 2022.

[16] O. ELLERS *et al.* Kinematics of sea star legged locomotion, *Journal of Experimental Biology* **224**, jeb242813, 2021.

[17] L.M. ARDOR BELLUCCI *et al.* Crawling and righting behavior of the subtropical sea star *Echinaster (Othilia) graminicola*: effects of elevated temperature, *Marine Biology* **166**, 1-9, 2019.

[18] P.-E. MERETTA *et al.* Locomotion and righting behavior of sea stars: a study case on the bat star *Asterina stellifera* (Asterinidae), *Revista de Biología Tropical* **69**, 501-513, 2021.

[19] C.T. SHELLEM *et al.* Salinity has a greater effect on sea star righting time than temperature, New Zealand Journal of Marine and Freshwater Research, 1-15, 2025.

[20] M.A. BELL *et al.*Echinoderm-Inspired Tube Feet for Robust Robot Locomotion and Adhesion, *IEEE Robotics and Automation Letters* **3**, 2222-2228, 2018.

[21] H. LEE *et al.*Starfish-inspired tube feet for temporary and switchable underwater adhesion and transportation, *Science Advances* **11**, eadx3539, 2025.

CHAPTER 8

PROTOCOL

8.1 Thresholding analysis method for locomotion videos

Here is a step-by-step protocol of the thresholding method we conceived to analyse sea star locomotion videos.

Video acquisition and conversion

1. Record videos in monochrome mode at 30 frames per second (fps), with a total duration of approximately 20 seconds (about 600 frames).
2. If needed, convert the video to `.avi` format using **MPEG Streamclip**, compatible with *Fiji* (Rasband, W.S., ImageJ, U.S. National Institutes of Health, Bethesda, Maryland, USA, https://imagej.nih.gov/ij/, 1997-2018).

Image preprocessing

1. Import the video into Fiji.
2. Subsample the video using `Image > Stacks > Tools > Make Substacks`, for example:

   `1-600-6` to retain one frame every six.
3. Convert to 8-bit grayscale: `Image > Type > 8-bit`.
4. Set the scale: `Analyze > Set Scale`
   - Enter known distance and units (e.g., mm).
   - Pixel aspect ratio: 1.0

Background correction and contrast adjustment

1. Subtract background: `Process > Subtract Background`, choose an appropriate rolling ball radius.
2. Adjust brightness/contrast: `Image > Adjust > Brightness/Contrast`, optimize to highlight tube feet contacts, then apply.

Image thresholding and particle analysis

1. Apply threshold: `Image > Adjust > Threshold`
    - Method: **Intermodes**, check `BW`, `Dark Background`, uncheck `Calculate threshold for each image`.
    - Adjust range manually (e.g., 70–180).
2. Set measurement parameters: `Analyze > Set Measurements`, enable:
    - Area, Center of Mass, Perimeter, Stack Position, Limit to Threshold
3. Analyze particles: `Analyze > Analyze Particles`
    - Size: specify range of tube feet contact area (e.g., mm^2) obtained from high-magnification videos of the ambulacral groove
    - Circularity: 0.80 – 1.00
    - Show: `Masks`, check `Display Results` and `Exclude on Edges`
4. Export results to Excel. Add a column called `NUMBER` and populate with 1's.

Pivot table and quantification

1. In Excel, create a pivot table:
    - Rows: `SLICE`
    - Values: `AREA`, `NUMBER`
2. Add a new column for time (in seconds), computed from frame rate.

This process allows the quantification of the number of tube feet in contact, as well as the sticking area (mm^2) during sea star's locomotion.

CHAPTER 9

SUPPLEMENTARY INFORMATION

Here, we present details on the log-log relationships between size-related parameters by comparing *Asterias rubens* and *Marthasterias glacialis*.

Species	Variables	Scaling exponent	95% C.I.	Expected scaling exponent	Allometry
Asterias rubens	AL vs. M	0.36	0.32 to 0.39	0.33	=
	MTA vs. M	0.42	0.37 to 0.47	0.67	-
	SA vs. M	1.03	0.80 to 1.30	0.67	++
Marthasterias glacialis	AL vs. M	0.39	0.35 to 0.43	0.33	+
	MTA vs. M	0.48	0.44 to 0.52	0.67	-
	SA vs. M	1.03	0.99 to 1.07	0.67	++

Table 9.1: *Body-size relations for Asterias rubens and Marthasterias glacialis. Abbreviations: AL, arm length (mm); MTA, mean tube feet contact area (mm^2); SA, sticking area (mm^2); M, mass (g). =, isometry; -, negatively allometry; +, positive allometry; ++, extreme positive allometry.*

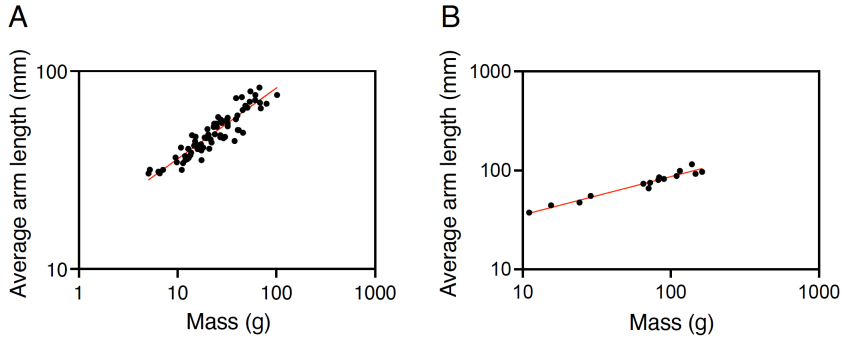

Figure 9.1: *Allometry between the average arm length and the mass in (A) Asterias rubens ($n = 74$, $R^2 = 0.8232$, $p < 0.0001$) and (B) Marthasterias glacialis ($n = 15$, $R^2 = 0.8864$, $p < 0.0001$).*

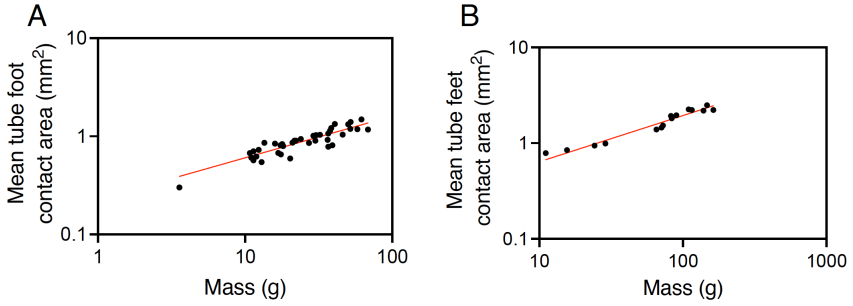

Figure 9.2: *Allometry between the mean tube feet contact area and the mass in (A) Asterias rubens ($n = 39$, $R^2 = 0.652$, $p < 0.0001$) and (B) Marthasterias glacialis ($n = 15$, $R^2 = 0.7685$, $p < 0.0001$).*

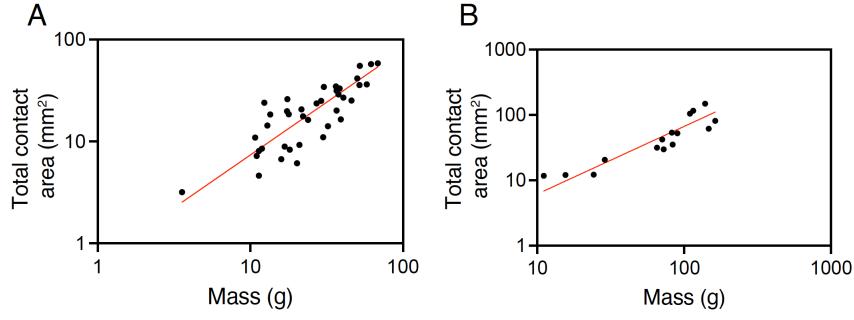

Figure 9.3: *Allometry between the total contact area and the mass in (A) Asterias rubens ($n = 39$, $R^2 = 0.7372$, $p < 0.0001$) and (B) Marthasterias glacialis ($n = 15$, $R^2 = 0.5658$, $p < 0.0001$).*

CHAPTER 10

THEORETICAL MODEL

In this Theoretical model, we provide details on the physical modeling for our perturbation experiments created by Eva Kanso's team. They propose a mathematical model for describing the sea star locomotion driven by the action of hundreds of tube feet. The model was first introduced and developed in [1] and later employed with modifications in [2].

Sea star biomechanics

We modeled the sea star as a rigid body of length L, mass m, and submerged weight W, whose center of mass is located at (x, y) in the vertical plane (Fig. 10.1A). The ventral surface of the sea star is lined with N tube feet, anchored to the body at evenly spaced positions, denoted by the signed distance d_n from the sea star's center of mass, with $d_{n+1} - d_n = d$ and $n \in [1, N]$. We characterized each tube foot by its length ℓ_n and inclination angle θ_n from the vertical y-axis. When engaged with the substrate, a tube foot distal end is located at (x_n, y_n). Consequently, the state (ℓ_n, θ_n) of the tube feet, and the location of its distal end (x_n, y_n) are related to the position (x, y) of the sea

star body via the algebraic constraints

$$x_n + \ell_n \cos\theta_n = x + d_n, \qquad y_n + \ell_n \sin\theta_n = y. \tag{10.1}$$

When attached and engaged with the substrate, a tube foot exerts an active force F_a on the sea star's body, induced by activation of muscle tissues lining either the podium or ampula, and experiences a passive restorative force F_p due to the resistance of connective tissues (Fig. 10.1B) Both active and passive forces act along the length of the tube foot and can either push or pull on the sea star's body [1, 3]. When ampullar muscles are activated, the tube foot extends, applying a pushing force, while when the podium muscles are activated, the tube foot contracts, applying a pulling force. To mathematically model these active forces, we used a piecewise linear force-length constitutive relationship inspired by Hill's muscle model [4, 5] (Fig. 10.1B and C). When actively pushing, F_a is given by

$$F_a(\ell) = \begin{cases} F_{\max}\dfrac{\ell}{\ell_c}, & \ell < \ell_c, \\ F_{\max}\dfrac{(\ell - \ell_{\max})}{(\ell_c - \ell_{\max})}, & \ell_c < \ell < \ell_{\max}, \\ 0, & \text{otherwise.} \end{cases} \tag{10.2}$$

where $F_{\max}$ is a scalar denoting the maximum active force that can be generated by the tube feet. When actively pulling, a similar expression with negative active force can be written. For the passive force F_p, we used a linear spring $F_p = -k_p(\ell_n - \ell_o)$, where ℓ_o is a resting length ℓ_o at which F_p vanishes. That is, a tube foot n engaged with the substrate applies a total force $F_n = F_a + F_p$ on the sea star body; When tube foot n detaches from the substrate and enters its recovery stroke, the force F_n goes to zero.

The sea star body moves under the collective action of all tube feet. Applying Newton's second law, we arrive at the equations governing the horizontal and

vertical displacements (x, y) of the sea star center of mass,

$$\begin{aligned} -c_x\dot{x} - \sum_n F_n \cos\theta_n &= m\ddot{x}, \\ -W - c_y\dot{y} + \sum_n F_n \sin\theta_n &= m\ddot{y}. \end{aligned} \tag{10.3}$$

Here, c_x, and c_y are internal damping parameters that account for all damping forces, including damping from the tube feet. Eqns. (10.1) and (10.3) form a differential-algebraic system of $2 + 2N$ equations for $2 + 2N$ unknowns (x, y, l_n, θ_n) provided control rules for when the tube feet should actively apply pushing or pulling forces on the sea star's body and when they should attach and detach from the substrate.

Non-dimensionalization.

To non-dimensionalise the equations of motion, we use the length of the tube foot $\ell_{\max}$ as our characteristic length scale. The system has two nominal time scales: an inertial time scale $T_g = \sqrt{\ell_{\max}/g}$ obtained from balancing the weight and inertial forces and a relaxation time scale $T_d = c_d/k_p$ obtained from balancing the damping and elastic forces ($c_d\ell_{\max}/T_d \sim k_p\ell_{\max}$). Roughly, T_d is the time it takes for the tube foot to relax to its rest length after being stretched or compressed. Sea stars move slowly and their locomotion is dominated by viscous effects; we thus consider $T_d/T_g \gg 1$, indicating an overdamped regime. Using $\ell_{\max}$ and T_d as our characteristic length and time scales, respectively, we rewrite (10.3) in non-dimensional form, where the non-dimensional mass $\tilde{m}$ is related to the actual mass m via $\tilde{m} = m/\gamma$, where $\gamma = T_d^2/T_g^2 = (c_d^2/k_p^2)/(L/g) \gg 1$.

Feedback control at the tube foot level.

In this model, no direct control of the sea star center of mass is imposed. Tube feet are controlled based on local adaptive feedback mechanisms. Namely, an attached tube foot senses its own state (ℓ_n, θ_n) and responds as follows: depending on θ_n, the tube foot experiences shear either in the same or in the opposite direction to its horizontal motion, and accordingly, it decides to either

push or pull (Fig. 10.1D). When the tube foot is axially stretched beyond a certain length l_{detach}, it detaches. In the detached state, it applies no force on the sea star body. It stays in the detached state for a random duration τ_n, dictated by a probability of reattachment $P_{\text{reattach}} = \lambda\tau_n$, where λ is the rate of reattachment. That is, the longer the duration of the tube foot in the detached state, the higher its probability of reattaching. When a tube foot reattaches, it does so by taking a random step size $\Delta\theta_n$ drawn from a uniform distribution $\Delta\theta_n \sim U(0, \pi/4)$ in the direction of motion of the sea star body, such that, on a flat horizontal terrain, the attachment site (x_n, y_n) satisfies $x_n = x + d_n + y \tan \Delta\theta_n$ and $y_n = 0$.

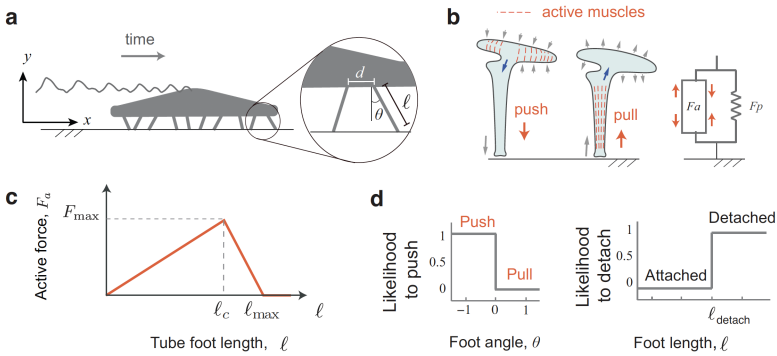

Figure 10.1: *The mathematical sea star model. (a) Locomotion of the sea star model is carried by 10 tube feet. The inset shows the length of a foot (l), its tilt angle (θ), and the distance (d) between two consecutive tube feet. (b) The mathematical model of the tube feet consists of a passive linear spring and an active force profile, which can generate either pushing or pulling forces depending on which set of muscles are activated. (c) Active force profile inspired by Hill's muscle model. (d) Control policies at the tube feet level. The policies indicate the likelihood of transitioning from active pushing to pulling and from attached to detached phase as a function of local sensory cues for each foot. The tube feet transition from detached to attached at length l_{det}.*

Parameter values

Measurements are used in *Asterias rubens* [1, 6] to guide the choice of parameter values in the model. Namely, we set the dimensionless tube foot length to $\ell_{\max} = 1$ and sea star body length to $L = 40$, corresponding in dimensional form to about 2 mm tube feet and 8 cm body diameter. We considered

$N = 100$ tube feet, and we set a base submerged weight to $W = 2$ and chose the maximal active force to be $F_{\max} = 0.4$. With this choice, 10% of the tube feet exerting on average an active force $F_{\max}/2$ are sufficient to carry the sea star weight, consistently with experimental measurements in *Asterias rubens* [1, 6]. We considered overdamped motion with a ratio of relaxation to inertial time scales $\gamma = 50$, and we assumed a rate of reattachment of $\lambda = 5$.

Results

The two scenarios that were explored experimentally in the main manuscript of this thesis: (i) locomotion on a horizontal substrate while increasing the sea star's weight, and (ii) locomotion on horizontal and inverted substrates.

In the first set of simulations, we tested three different weights: $W = 2$, $W = 2.5$, and $W = 3$. As the weight increased, we adjusted the detachment length parameter l_{detach}, from $l_{\text{detach}} = 0.9$, 0.95 and 1, respectively. It examined numerically the sea star locomotion, while keeping all parameters the same, except for the sea star weight and detachment lengthl_{detach}: namely, we increased the sea star weight by 25% and 50% (Fig. 10.2), consistent with our experiments, and correspondingly, increased l_{detach} with increasing the sea star weight. For each weight, we conducted 25 Monte-Carlo simulations, each for a total time duration of $10T_d$.

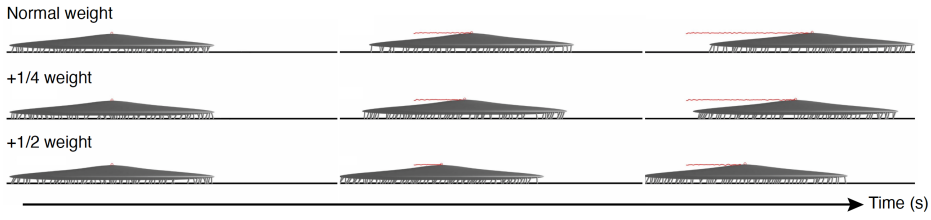

Figure 10.2: *Simulated sea star locomotion in response to a 25% and 50% increase in initial mass, with no parameter adjustment and all parameters held constant.*

In each simulation, we calculated the crawling speed, defined as the total distance traveled by the center of mass divided by the total simulation time. We also calculated the attachment fraction, $\tau = \sum_{i=1}^{N} T_i^{\text{attached}}/NT$, defined

as the sum over all tube feet of the total time each foot spends in attachment T_i^{attached}, divided by the total simulation T times the number N of tube feet. This gives the average proportion of time that a typical tube foot is attached.

In the second set of simulations, the weight and detachment length were kept fixed at $W = 2$ and $\ell_{\text{detach}} = 0.9$. We conducted 25 random simulations for locomotion on a horizontal substrate and 25 for locomotion on an inverted substrate, with no parameter adjustment (Fig. 10.3).

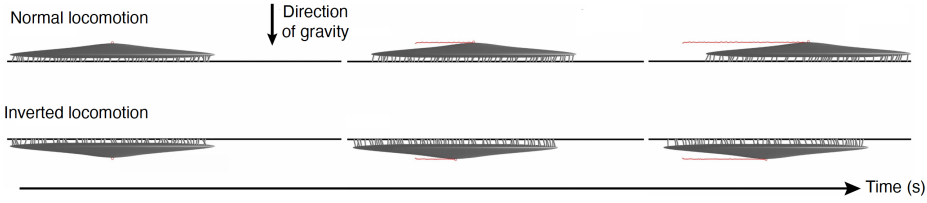

Figure 10.3: *Simulated sea star locomotion under inverted conditions, with no parameter adjustment and all parameters held constant.*

BIBLIOGRAPHY

[1] S. HEYDARY *et al.* Sea star inspired crawling and bouncing, *Journal of The Royal Society Interface* **17**, 20190700, 2020

[2] T. PO *et al.* Cooperative transport in sea star locomotion, *Current Biology* **34**, 2551-2557.e4, 2024.

[3] O. ELLERS *et al.* Soft skeletons transmit force with variable gearing, *Journal of Experimental Biology* **227**, jeb246901, 2024.

[4] A. V. HILL, The heat of shortening and the dynamic constants of muscle, *Proceedings of the Royal Society of London. Series B-Biological Sciences* **126**, 136-195, 1938.

[5] Y.C. FUNG *et al.* Biomechanics. Mechanical Properties of Living Tissues, *Journal of Applied Mechanics* **49**, 464-465, 1982.

[6] G.A. KERKUT, The forces exerted by the tube feet of the starfish during locomotion, *Journal of Experimental Biology* **30**, 575-583, 1953.

CHAPTER 11

PUBLICATIONS AND COMMUNICATIONS

Publications

1. *Appreciating the role of cell shape changes in the mechanobiology of epithelial tissues*, M. Luciano, M. Versaevel, E. Vercruyse, A. Proces, Y. Kalukula, A. Remson, A. Deridoux & S. Gabriele, AIP Biophysics Reviews, 3.(2022)

2. *Tube feet dynamics drive adaptation in sea star locomotion*, A. Deridoux, S. Heydari, S.N. Gorb, E.A. Kanso, P. Flammang & S. Gabriele, PNAS Under review.

Scientific Communications

Poster Presentations

1. GDR AQV Days 2022 — January 2022
   Institut Jacques Monod, Paris (France)

2. Journée de rencontre des jeunes chimistes de la SRC — April 2022
   University of Liege (Belgium)

3. GDR AQV Days 2023 — May 2023
   Oléron (France)

4. ZOOLOGY 2023 — May 2023
   Leiden (Netherlands)

5. 2024 SRC Scientific Day — October 2024
   University of Mons (Belgium)

Oral Presentations

1. Soapbox Science — June 2022
   Place de la Bourse, Brussel (Belgium)

2. 11^{th} European Conference on Echinoderms — October 2023
   University of Lyon (France)

3. GDR AQV Days 2024 — May 2024
   La Vogüe (France): Best oral presentation award

4. 17^{th} International Echinoderm Conference & 2^{nd} International Hemichordate Meeting — July 2024
   Puerto de la Cruz (Tenerife)